A Practical Guide to Tensegrity Design

2nd edition

P.O. Box 426164, Cambridge, MA 02142-0021
USA

For a revision history, see
`http://www.channel1.com/users/bobwb/tenseg/book/revisions.html`.
Your questions or comments are appreciated. Please email them to:
`bobwb@juno.com`
or send them by Postal Service mail to the address above.

Version 2.01
December 17, 2004

To my mother and father

Contents

List of Figures

List of Tables

Preface

This is the second edition of *A Practical Guide to Tensegrity Design*. The first edition was released in spiral-bound format generated from LaTeX source in 1994. Section 1.3 on the early history of tensegrity has been rewritten. New material on realistically modeling the complex details of hubs has been added throughout the book. Illustrations have been clarified and augmented. Two electronic editions have been prepared, one using XHTML and MathML, and the other in PDF format generated from the updated LaTeX source.

The book covers the basics of doing calculations for the design and analysis of tensegrities. Examples with complete data have been provided so you can calibrate your software accordingly. The book presumes you are well versed in linear algebra and differential calculus and are willing to explore their application in diverse ways.

I've found the tools here useful for designing and analyzing tensegrities and hope they prove useful to you. I would be interested in hearing how they work out for you and receiving data you have generated from the design and analysis of tensegrity structures. I'd also appreciate suggestions for improvement and notification of mistakes of any sort including typographic errors.

Bob Burkhardt
Shirley, Massachusetts
September 3, 2004

Acknowledgements

My studies of tensegrity have provided me with an interesting tour of human endeavor. The topic seemed to fit the skills I had and developed them in ways I appreciated. I would summarize these skill areas as mathematics, graphics, computer programming and geometry.

At Los Angeles Harbor Community College, where I started out studying physics but switched to economics, my good-humored physics professor, William Colbert, provided me with computer access even after I had stopped taking physics courses. He helped me get started in computer programming with APL and tolerated my interest in BASIC. I stuck with economics for quite awhile, and fortunately my economics professors encouraged me to get a rigorous background in mathematics. In particular Sheen Kassouf at the University of California at Irvine encouraged me to take rigorous courses in linear algebra and statistics, and Peter Diamond at the Massachusetts Institute of Technology advised me to take a rigorous calculus course. Frank Cannonito and Howard G. Tucker provided my introduction to rigorous mathematical thinking at UCI. Rudiger Dornbusch in the economics department at MIT emphasized the importance of paying attention to units in doing mathematical analysis which has helped me through many a conundrum.

After I left graduate school, I indulged a more serious interest in Buckminster Fuller's work. Gradually that interest focused on tensegrity where it seemed to me there was a dearth of information on designing these structures. Fuller's engineering orientation appealed to me, so I looked into getting more expertise in that vein. After taking a couple night courses in machine shop at Minuteman Tech and investigating vocational-technical schools, I ended up at the Lowell Institute School. There I learned electronics technology mostly, but I took a course in welding too.

At that time the School was located at MIT and being directed by Bruce Wedlock. I was surprised to find myself on the MIT campus again, and took advantage of the continued access to MIT's excellent libraries. I dug up a lot of the books in the references (Appendix C) there. (As far as libraries are concerned, I also found the General, Research and Art Libraries at the Boston Public Library to be very helpful.) Eventually, I landed a job at the School, first as a teaching assistant in electronics technology and then as an instructor teaching computer programming. At one point, Dr. Wedlock kindly let me offer a course on tensegrity through the School though the course finally had to be canceled due to insufficient enrollment.

Teaching at the Lowell Institute School brought me into contact with UNIX and the X Window System. UNIX systems of one sort or another finally provided the development environment for my continuing pursuit of the craft of tensegrity computation. I started out doing computations on a TI-55 programmable pocket calculator and graduated from there to a Commodore 64 and its successors, the 128 and the Amiga. Finally I wound up using Linux with occasional ports to Windows as opportunities arose. The software migrated from the TI's machine language, to BASIC, to C and is now written in C++ . In UNIX environments, the Free Software Foundation's C and C++ compiler and `emacs` editor have proven very useful.

LaTeX provided an avenue where I could easily communicate the mathematical constructs I found useful in working with tensegrity. More recently I've started working with MathML. `mfpic`, which allows diagrams to be developed using LaTeX's METAFONT, has been useful for developing a lot of the illustrations in the book. POV-Ray has been a great visualization tool and has also been used to generate many of the illustrations. HTML and the World Wide Web have been a great avenue for communicating my work more widely. And let's give a cheer for `pdflatex` which puts LaTeX with embedded PNG illustrations into Adobe's PDF format.

Thanks to Buckminster Fuller for the long letter he wrote to me on tensegrity and for bringing the technology to my attention through his books. The variety and insight of the work of Kenneth Snelson and David Georges Emmerich has been a great source of inspiration. Several times I've made "discoveries" only to discover that one of them found the same thing years ago, and I might have saved myself some time by studying their work more closely. Snelson associate Philip Stewart's inquiries about a structure provided the stimulus for developing a lot of the material on complex hubs and vector constraints. Maxim Schrogin's inquiry about maximal strut clearances in prisms prompted the orthogonal tensegrity prism example of Section 7.3.6, and his structures have been the source of much inspiration. Grappling with the structures of Ariel Hanaor and René Motro has also been very instructive.

I thank Chris Fearnley for suggesting I put LaTeX into PDF format and especially for inviting me to talk at the January 25-26, 2003, gathering of the *Synergeticists of the Northeast Corridor* whose participants patiently listened to my presentation of the first four chapters of this book.

In the end, I have no one to blame for all this but myself.

Bob Burkhardt
Shirley, Massachusetts
August 23, 2004

Chapter 1

An Introduction to Tensegrity

1.1 Basic Tensegrity Principles

Anthony Pugh[1] gives the following definition of tensegrity:

> A tensegrity system is established when a set of discontinuous compressive components interacts with a set of continuous tensile components to define a stable volume in space.

Tensegrity structures are distinguished by the way forces are distributed within them. The members of a tensegrity structure are either always in tension or always in compression. In the structures discussed in this book, the tensile members are usually cables or rods, while the compression members are sections of tubing. The tensile members form a continuous network. Thus tensile forces are transmitted throughout the structure. The compression members are discontinuous, so they only do their work very locally. Since the compression members do not have to transmit loads over long distances, they are not subject to the great buckling loads they would be otherwise, and thus they can be made more slender without sacrificing structural integrity.

While the structures discussed in this book aren't commonly seen, tensegrity structures are readily perceptible in the surrounding natural and man-made environment. In the realm of human creation, pneumatic structures are tensegrities. For instance, in a balloon, the skin is the tensile component, while the atoms of air inside the balloon supply the compressive components. The skin of the balloon consists of atoms which are continuously linked to each other, while the atoms of air are highly discontinuous. If the balloon is pushed on with a finger, it doesn't crack; the continuous, flexible netting formed by the balloon's skin distributes this force throughout the structure. And when the external load is removed, the

[1] *Pugh76,* p. 3. See also the last footnote in this chapter which cites *Kanchanasaratool02*'s elegantly succinct definition and the footnote in Section 6.2.3 which cites *Wang98*'s rigorous and descriptive definition.

balloon returns to its original shape. This resilience is another distinguishing characteristic of tensegrity structures.

Another human artifact which exhibits tensegrity qualities is prestressed concrete. A prestressed concrete beam has internal steel tendons which, even without the presence of an external load, are strongly in tension while the concrete is correspondingly in compression. These tendons are located in areas so that, when the beam is subjected to a load, they absorb tensile forces, and the concrete, which is not effective in tension, remains in compression and resists the heavy compressive forces elsewhere in the beam. This quality of prestressed concrete, that forces are present in its components even when no external load is present, is also very characteristic of tensegrity structures.

In the natural realm, the structural framework of non-woody [2] plants relies completely on tensegrity principles. A young plant is completely composed of cells of water which behave much like the balloon described above. The skin of the cell is a flexible inter-linkage of atoms held in tension by the force of the water in the contained cell.[3] As the plant is stretched and bent by the wind, rain and other natural forces, the forces are distributed throughout the plant without a disturbance to its structural integrity. It can spring back to its usual shape even when, in the course of the natural upheavals it undergoes, it finds itself distorted far from that shape. The essential structural use the plant makes of water is especially seen when the plant dries out and therefore wilts.

1.2 Applications of Tensegrity

The qualities of tensegrity structures which make the technology attractive for human use are their resilience and their ability to use materials in a very economical way. These structures very effectively capitalize on the ever increasing tensile performance modern engineering has been able to extract from construction materials. In tensegrity structures, the ethereal (yet strong) tensile members predominate, while the more material-intensive compression members are minimized. Thus, the construction of buildings, bridges and other structures using tensegrity principles could make them highly resilient and very economical at the same time.

In a domical configuration, this technology could allow the fabrication of very large-scale structures. When constructed over cities, these structures could serve as frameworks for environmental control, energy transformation and food production. They could be useful in situations where large-scale electrical or electromagnetic shielding is necessary, or in

[2]The qualification "non-woody" is used to exclude trees. The woody elements of a tree are made to undergo both tension and compression, much as is required of the structural elements of a geodesic dome.

[3]Donald Ingber has pointed out (personal communication, October 8, 2004) that this very simple view of the living cell does not reflect very well the results of modern research in applying tensegrity principles to the analysis of cell structure. No doubt this example would benefit from the attention of a biologist and the details would change as a result. For a look at how tensegrity principles have been applied to the analysis of living cells, see *Ingber98.*

extra-terrestrial situations where micrometeorite protection is necessary. And, they could provide for the exclusion or containment of flying animals over large areas, or contain debris from explosions.

These domes could encompass very large areas with only minimal support at their perimeters. Suspending structures above the earth on such minimal foundations would allow the suspended structures to escape terrestrial confines in areas where this is useful. Examples of such areas are congested or dangerous areas, urban areas and delicate or rugged terrains.

In a spherical configuration, tensegrity designs could be useful in an outer-space context as superstructures for space stations.

Their extreme resilience make tensegrity structures able to withstand large structural shocks like earthquakes. Thus, they could be desirable in areas where earthquakes are a problem.

1.3 Early Tensegrity Research

Key contributions to the early development of tensegrity structures appear to have come from several people. Some historians claim Latvian artist Karl Ioganson exhibited a tensegrity prism in Moscow in 1920-21 though this claim is controversial.[4] Though Ioganson's work was destroyed several years later by the Soviet regime, photographs of the exhibition survived, and French architect David Georges Emmerich cited a different structure by Ioganson as a precedent to his own work.[5] The word "tensegrity" (a contraction of "tensile-integrity") was coined by American entrepreneur Buckminster Fuller.[6] Fuller considered the framing of his 1927 dymaxion house and a 1944 construction to be early examples of the technology.[7]

In December, 1948, after attending lectures by Fuller at Black Mountain College in North Carolina, Kenneth Snelson made a catalytic contribution to the understanding of

[4] *Gough98,* Fig. 13, p. 106, makes this claim. Kenneth Snelson contests this claim and does not believe the sculpture in the old exhibition photo on which the claim is based was a tensegrity prism.

[5] *Emmerich88,* pp. 30-31. The structure Emmerich references is labeled "Gleichgewichtkonstruktion". He states:

> Cette curieuse structure, assemblée de trois barres et de sept tirants, était manipulable à l'aide d'un huitième tirant detendu, l'ensemble étant déformable. Cette configuration labile est très proche de la protoforme autotendante à trois barres et neuf tirants de notre invention.

This apparently means he doesn't recognize Ioganson's invention of the tensegrity prism. *Gough98*'s thorough examination of the exhibition photographs unfortunately doesn't mention Emmerich's work.

[6] See the description for Figure 1 in U.S. Patent No. 3,063,521, "Tensile-Integrity Structures", November 13, 1962. Kenneth Snelson prefers the description "floating compression" to the term tensegrity.

[7] *Fuller73,* Figs. 261, 262 and 263, pp. 164-165.

tensegrity structures when he assembled his X-Piece sculpture.[8] This key construction was followed by further contributions by Fuller, Snelson and others of their circle.[9] Independently, in France, in 1958, Emmerich was exploring tensegrity prisms and combinations of prisms into more complex tensegrity structures, all of which he labeled as "structures tendues et autotendantes" (self-tensioning tensile structures).[10]

Emmerich, Fuller and Snelson came out with patent claims on various aspects of the technology in the 1960's,[11] and all continued developing the technology. Fuller's primary interest was adapting the technology to the development of spherical and domical structures with architectural applications in mind.[12] He also used tensegrity structures to make some philosophical points.[13] As an architect, Emmerich was also interested in architectural applications and designed at least one dome as well.[14] Snelson is primarily interested in the artistic application of tensegrity and has explored the technology in a variety of sculptures.[15] His work in tensegrity also led him to develop a model of the atom.[16] All three developed tower or mast structures which continue to be a source of fascination for tensegrity enthusiasts but only recently have found practical application in the development of deployable structures.[17]

While many tensegrity models were built and achieved quite a fame for themselves, for instance through a notable exhibition of Fuller's work at the Museum of Modern Art in New York, [18] and a retrospective on Snelson's work at the Hirschorn Museum in

[8] See *Lalvani96,* pp. 45-47. Fuller immediately publicized Snelson's invention, but via a variation on Snelson's X-Piece which used tetrahedral radii rather than an X as the compression component (*Fuller73,* Figs. 264-267). Snelson didn't publish until a decade later when he filed his patent (U.S. Patent No. 3,169,611). Emmerich characterizes Fuller's contribution to Snelson's invention as that of a "catalyst" (*Lalvani96,* p. 49).

It seems both Fuller and Snelson catalyzed this tensegrity revolution by bringing together their relevant ideas and experience and fabricating artifacts that stimulated further innovations. Another important step, which either of them could have taken first, was to start using the simple linear compression components which are used to fabricate the structures studied in this book. In 1949, the same year that Fuller found out about Snelson's work, he fabricated the tensegrity icosahedron (Section 2.3) which is an outgrowth of the "jitterbug"/cuboctahedron framework whose dynamics he had been exploring. On the other hand, Snelson fabricated his "tower" (U.S. Patent No. 3,169,611, Fig. 25, or perhaps a two-fold one composed of his "X-Modules" which are made of two tendon-connected linear struts) out of a designer's frustration with Fuller's "mast" design and its complex compression components with their tetrahedral radii.

[9] *Fuller73,* Figs. 264-280, pp. 165-169.

[10] *Lalvani96,* p. 29.

[11] R. Buckminster Fuller, U.S. Patent No. 3,063,521, "Tensile-Integrity Structures", November 13, 1962. David Georges Emmerich, French Patent No. 1,377,290, "Construction de Reseaux Autotendants", September 28, 1964, and French Patent No. 1,377,291, "Structures Linéaires Autotendants", September 28, 1964. Kenneth Snelson, U.S. Patent No. 3,169,611, "Continuous Tension, Discontinuous Compression Structure", February 16, 1965.

[12] *Fuller73,* Figs. 268-280, pp. 165-169. See also *Lalvani96* and *Wong99,* pp. 167-178, for further discussion of the Fuller-Snelson collaboration and controversy.

[13] See *Fuller75,* Fig. 740.21, p. 407, for an example.

[14] *Emmerich88,* pp. 158-159.

[15] See the "Sculpture" section of Snelson's website, `http://www.kennethsnelson.net.`

[16] See "The Atom" section of Snelson's website, `http://www.kennethsnelson.net.`

[17] For example, *Skelton97.*

[18] Geodesic D.E.W. Line Radome, Octe-truss and Tensegrity Mast - one-man, year-long, outdoor garden

Washington, D.C., [19] the bulk of production structures which Fuller and his collaborators produced were geodesic domes rather than tensegrity structures.[20]

It seems probable that part of the reason that tensegrity structures didn't get farther, even in circles where there was a strong interest in practical applications of tensegrity, was the apparent dearth of powerful and accurate tools for carrying out their design. Fuller's basic tensegrity patent has quotations of member lengths, but no indication of how one would compute the lengths.[21] Probably the lengths were computed after the fact by measuring the tendon lengths of a finished structure.

An early exception to this dearth of information on tensegrity calculating was Hugh Kenner's excellent work *Geodesic Math*[22] which went into an exact technique for the very simple tensegrity prism and outlined an approximate technique for dealing with some simple spherical structures. His technique for designing prisms will be presented in Section 2.2 as an introduction to tensegrity calculations since these simple structures are an excellent avenue for developing an intuitive feel for what tensegrity is all about.

First-hand accounts of the early history of tensegrity can be found in *Coplans67*, *Fuller61* and *Lalvani96.*

1.4 Recent Tensegrity Research

Civil engineers have taken an interest in tensegrity design. An issue of the International Journal of Space Structures[23] was devoted to tensegrity structures. In that collection, R. Motro notes in his survey article "Tensegrity Systems: State of the Art":

> ...there has not been much application of the tensegrity principle in the construction field. ...examples...have generally remained at the prototype state for lack of adequate technological design studies.[24]

The primary obstacles to the practical application of tensegrity technology which these researchers have identified are:

---

exhibit, 1959. Also at least one tensegrity was exhibited inside. See *Fuller73,* p. 169, illus. 280.

[19] Kenneth Snelson and Douglas G. Schultz, Kenneth Snelson, an exhibition, Buffalo, New York: Albright-Knox Art Gallery, c1981. The exhibition was in Washington, D.C., June 4 to August 9, 1981.

[20] See Section 1.5 for a comparison of geodesic dome and tensegrity technology.

[21] See Figure 7 in U.S. Patent No. 3,063,521, "Tensile-Integrity Structures", November 13, 1962.

[22] *Kenner76.*

[23] Vol. 7 (1992), No. 2.

[24] *Motro92,* p. 81.

1. Strut congestion - as some designs become larger and the arc length of a strut decreases, the struts start running into each other.[25]

2. Poor load response - "relatively high deflections and low material efficiency, as compared with conventional, geometrically rigid structures."[26]

3. Fabrication complexity - spherical and domical structures are complex which can lead to difficulties in fabrication.[27]

4. Inadequate design tools - as Motro's statement above suggests, lack of design and analysis techniques for these structures has been a hindrance.

Double-layer designs introduced in Motro's and Hanaor's work[28] begin to deal with the first obstacle. Poor load response (the second obstacle) is still a problem in their configurations, and they don't have much advice on fabrication techniques (the third obstacle). They have developed tools to deal with the fourth obstacle. These tools are based on earlier work by J. H. Argyris and D. W. Scharpf analyzing prestressed networks.[29].

In what follows, reference will be made to this work; however, the techniques presented here are somewhat different and take advantage of some special characteristics of tensegrity structures. The civil engineers' work is the source of the "double-layer" terminology used to describe some of the structures presented here. Appendix A discusses relationships between the civil engineers' work and some of the ideas presented here.

1.5 Other Space Frame Technologies

Other space frame technologies can be roughly sorted into three categories. The first category contains those space frame technologies where members are very homogenous. They are typically realized as planar trusses perhaps connected at an angle with other planar trusses. Biosphere 2[30] is an example. Their faceted shape means they contain less space per unit of material than a spherical shape would. *Makowski65* contains a variety of examples.

The second category contains those which are typified by the geodesic domes[31] and Kiewitt domes.[32] Geodesic domes share many qualities of tensegrity domes. The primary difference

[25] *Hanaor87,* p. 35.
[26] *Hanaor87,* p. 42.
[27] *Hanaor87,* p. 44.
[28] See *Hanaor92, Hanaor87, Motro87* and Appendix A.
[29] *Argyris72.*
[30] *Kelly92,* p. 90.
[31] *Fuller73,* pp. 182-230.
[32] *Makowski65.*

is the requirement of these technologies that all components be able to sustain both tensile and compressive forces.

The third category is typified by the circus tent. Here a tensile network (the tent fabric) is supported at various locations by large poles. Anchors and supporting cables usually also play a role. These structures can almost be considered a sort of tensegrity since elements of the structure are either in tension all the time or compression all the time. Their compressive elements are much fewer and much more massive than in the usual sort of tensegrity. Many times these poles disrupt the internal space of the structure substantially. The tensile network has a catenary shape to it between the compressive supports. This means it encloses less space than it would if it were supported as in the usual spherical tensegrity with many struts embedded in the network. For a variety of examples of structures in this category, see *Otto73.*

1.6 Book Scope and Outline

The discussion here will center on tensegrity structures of a particular type. They are composed of discrete linear members: the tensile members can be thought of as cables which pull two points together, while the compression members can be thought of as sections of rigid tubing which maintain the separation of two points. The tensile members are continuously connected to each other and to the ends of the compression members while the compression members are only connected to tensile members and not to other compression members.[33] The primary motivation for this work is to outline mathematical methods which can be applied to the design and analysis of this sort of tensegrity.

Also some new classes of tensegrity structures are presented. In particular, highly-triangulated methods of tensegrity trussing will be discussed which can be applied to domical, spherical and more general tensegrity designing. These double-layer tensegrities are designed to be effective in larger structures where trussing is needed.

While a lot of the discussion will center around highly symmetric, spherical structures, the derivation and analysis of truncated structures like domes are also fully treated. The development of techniques for these less symmetric applications makes tensegrity a much more likely tool for addressing practical structural problems.

Finally, sections on analyzing member forces and clearances in tensegrity structures are included. This analysis is a large element of concern in any engineering endeavor and also

[33]These structures would be described as Class 1 tensegrity structures using the definition cited in *Kanchanasaratool02.* That definition is:

> A tensegrity system is a stable connection of axially-loaded members. A Class k tensegrity structure is one in which at most k compressive members are connected to any node.

"Connection" doesn't seem like quite the right word here and could be a typographical error. Substituting "continuously-connected collection" yields a better description. "node" is synonymous with "hub".

of interest to anyone who seeks an understanding of the behavior of tensegrity structures.

Chapter 2

Basic Tensegrity Structures

2.1 Basic Tensegrity Structures: Introduction

This section presents some simple tensegrity structures. In this form, the basic features of tensegrity structures are most readily grasped. In the context of these structures, various mathematical tools are illustrated which can be applied to tensegrity design. Some of these structures are simple enough that the member lengths can be expressed in algebraic formulas. But even with these simple structures, sometimes the help of the computer, and the powerful numerical calculation tools it provides, is needed.

These simple structures permit some mathematical approaches which are intuitively appealing but which are difficult to apply to more complex structures. The intuitive approaches deal explicitly with angular measures. The alternative Cartesian approach involves no angles, only points and distances between them. For computations, the Cartesian approach is simple and powerful, but the physical reality of the structure is less apparent in the mathematics, and the approach needs to be supplemented with other tools when structure visualization is necessary.

2.2 T-Prism: The Simplest Tensegrity

2.2.1 T-Prism Intuition

The t-prism is illustrated in Figure 2.1. It is the simplest and therefore one of the most instructive members of the tensegrity family. Some art historians believe it was first exhibited by the Latvian artist Karl Ioganson in Moscow in 1920-21 though this claim is

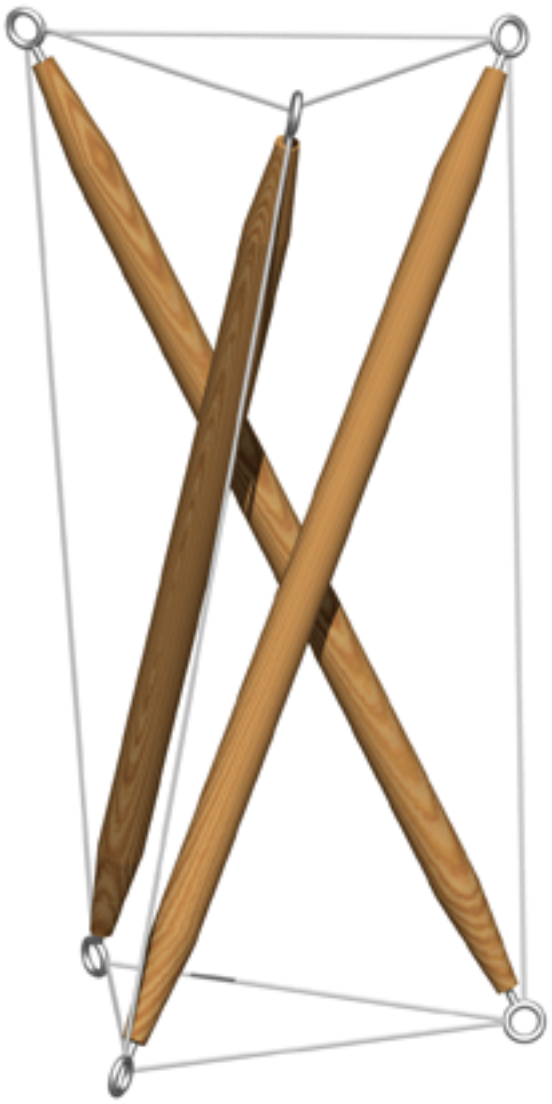

Figure 2.1: Tensegrity Prism

controversial.[1]

A model can be easily constructed using 5/16-inch-diameter (8 mm) dowel, some small screw eyes,[2] and some braided Dacron or nylon fishing line. The dowel should be cut into three seven-inch (178 mm) lengths and an eye screwed into either end of each length. Both eyes on a dowel should face the same direction. Then, using the fishing line, the three dowels are tied together by connecting one end of each of them to one end of each of the others so that there is a three-inch (76 mm) length of line between each pair of dowels.[3] The result should be an equilateral triangle of tendons, each three inches (76 mm) long, connecting the three struts together. Next the opposite ends of the struts are tied together in a similar manner. These two sets of tendons are the end tendons. At this point, the result should be a triangular prism whose side edges are marked out by the struts and whose triangular ends are made of fishing lines (see Figure 2.2).

The structure can be held up with a thumb and two fingers from each hand so that it can be viewed as a prism. When one end of the prism is twisted relative to the other, the rectangular sides of the prism lose their rectangularity and become non-planar quadrilaterals. Two opposite angles of each quadrilateral become obtuse (greater than 90°), and two opposite angles become acute (less than 90°). The structure is completed by connecting the vertices of each quadrilateral corresponding to the two obtuse angles with a tendon made of fishing line.

The length of these final three tendons (one for each side of the prism – the side tendons) has to be chosen carefully; otherwise, the structure will turn out to be a loose jumble of sticks and fishing line. As the two ends of the prism are twisted relative to each other, the vertices corresponding to the opposite obtuse angles initially grow closer to each other. As the twisting continues, there comes a point where they start to move apart again. If the side tendons are tied with a length of fishing line which corresponds to the minimum length reached at this point (which comes when the two ends are twisted 150° relative to each other), the structure is stable since it can't move away from that configuration except by lengthening the distance between those two points, and that is prevented by the minimum-length tendon. This is the "trick" which underlies all the tensegrity design methods explored here.

---

[1] *Gough98,* Fig. 13, p. 106, shows a tensegrity prism which claims to be a modern reconstruction of Ioganson's sculpture which was destroyed in the mid-1920's by the Soviet regime. Snelson contests this reconstruction and does not believe the sculpture in the old exhibition photo on which it is based was a tensegrity prism. As was noted in Chapter 1, the tensegrity prism was the first tensegrity structure assembled by Emmerich. Snelson also claimed it in his patent (see U.S. Patent No. 3,169,611, Fig. 22b).

[2] Small screw eyes, 7-8 mm in diameter, work the best. Likely candidates can be found in hardware stores or picture framing shops. Anthony Pugh (*Pugh76,* p. 72) favors nails instead of screw eyes. Nails have the advantage that *ad hoc* adjustments of the member lengths don't have to be made to accommodate the dimensions of the attachment point. Pugh's detailed information on tensegrity model construction is recommended reading.

[3] A stunsail tack bend (used in sailing) is an effective knot in this application. If problems are encountered tying the fishing line to the right length, thin gauge wire can be used. This doesn't have to be knotted but merely twisted at the right length. The sharp wire ends can be a hazard.

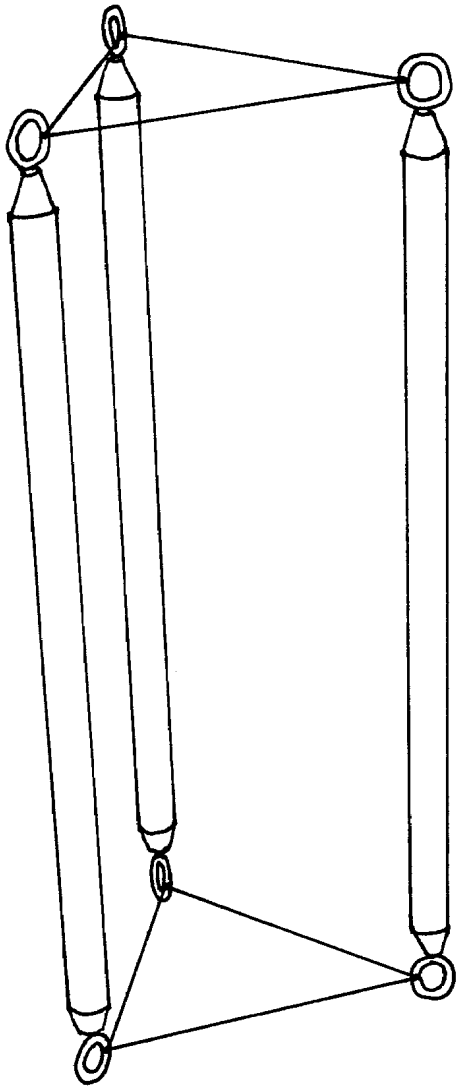

Figure 2.2: T-Prism Construction: Triangular Prism Stage

	Coordinates		
Point	z	radius	angle
A	0	r	0
B	0	r	$\frac{2\pi}{3}$
C	0	r	$-\frac{2\pi}{3}$
A'	h	r	θ
B'	h	r	$\theta + \frac{2\pi}{3}$
C'	h	r	$\theta - \frac{2\pi}{3}$

Table 2.1: T-Prism: Polar Coordinates

So next the computation of the length of this minimum-length tendon is explored.

2.2.2 T-Prism Mathematics: Cylindrical Coordinates

[A lot of the analysis presented in this section is derived from *Kenner76,* pp. 8-10. The analysis presented there is a more general one.]

For the t-prism, the most intuitive and convenient coordinate system for mathematical analysis is the cylindrical coordinate system.[4] Figure 2.3 outlines how the t-prism is oriented in this system. The z axis of the system coincides with the axis of the t-prism ($\overline{OO'}$) and therefore pierces the centers of two triangular ends. The center of one of these ends (O) coincides with the origin, while the other center (O') lies on the positive z axis. The points which make up the triangle about the origin are marked with the labels A, B, and C. The z coordinate of all these points is 0. This position will be held constant in the mathematical analysis. On the other triangle, the corresponding points are marked A', B' and C'. The z coordinate of these points is h, the height of the t-prism. This height is a variable in the mathematical analysis.

Since the z axis goes through the centers of both triangles, their vertices are equidistant from the z axis. The measure of this distance, denoted r, represents the radial portion of their coordinate representation. This value will also be held constant for the purposes of the mathematical analysis. Besides the z axis, the figure also contains the reference axis labeled x. This axis serves as the reference for the value of the angular coordinate.[5] The value of this coordinate for A' is the variable θ, while the value of this coordinate for A is fixed at 0. The value of θ (which is measured in radians) measures the twist of the two triangular ends with respect to each other. Since A', B', and C' lie on the same triangle, the angular component for B' is $\theta + \frac{2\pi}{3}$ and that for C' is $\theta - \frac{2\pi}{3}$. Table 2.1 summarizes the coordinate values for the six points.

[4] A presentation of this system can be found in most calculus texts, for instance *Leithold72,* p. 863.

[5] The value can be expressed in radians or degrees. Here (for mathematical convenience) radians are primarily used.

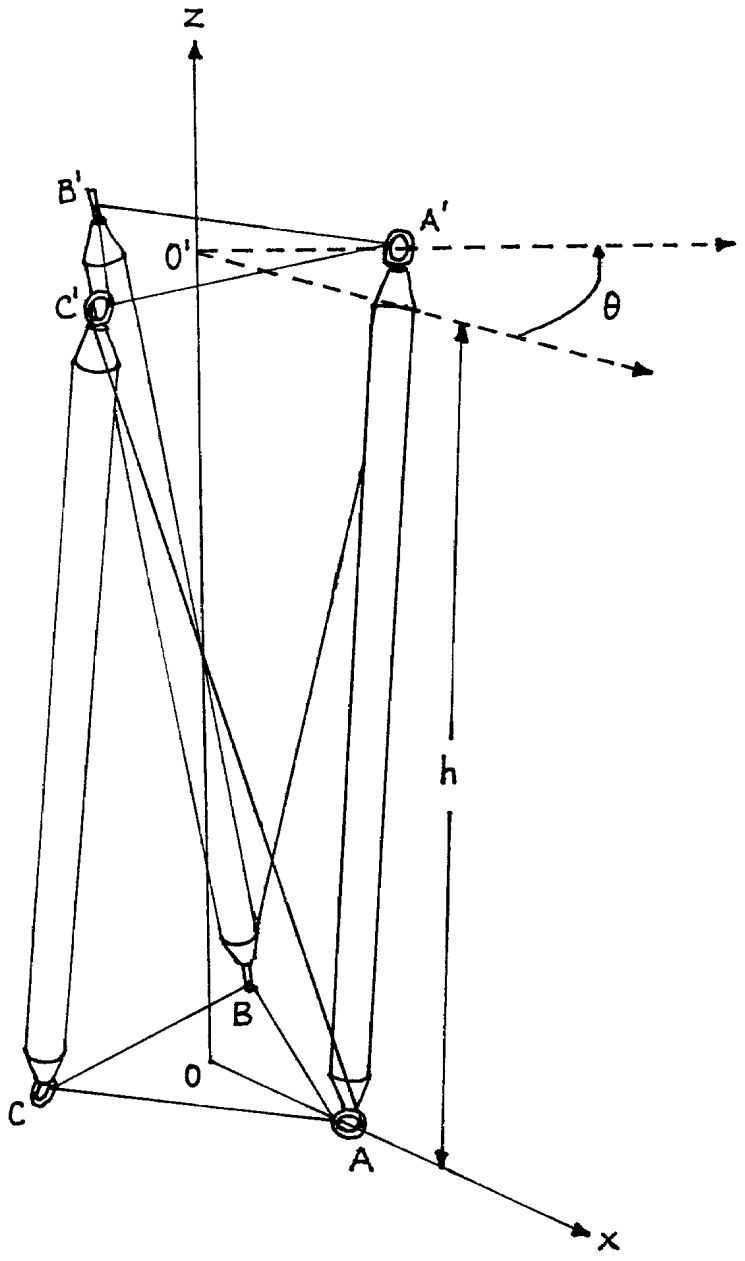

Figure 2.3: T-Prism: Cylindrical Coordinates

Now the struts (the compressive component of the structure) can be inserted into the model. These will correspond to the line segments $\overline{AA'}, \overline{BB'}$ and $\overline{CC'}$. Next the side tendons are specified which link up the two tendon triangles which in turn make up the ends of the prism. Starting from point A, the side tendon can be connected to either B' or C'. Either decision would result in a viable structure provided the connections are made consistently around the structure. One of these structures would be the mirror image of the other. Here the side tendon is connected to C', so the side tendons correspond to the line segments $\overline{AC'}, \overline{BA'}$ and $\overline{CB'}$.

Now the essence of the problem is reached: how long should each member (each tendon and each strut) be? By fixing the value of r (the radius of the prism's triangular ends), the length of each end tendon (call this value u) has been fixed via the equation $u = 2r \sin \frac{\pi}{3}$. For the other members, there are two choices. The side tendon lengths $\overline{AC'}$ etc. can be specified and then $\overline{AA'}$ etc. chosen to be the **maximum** length struts compatible with the specified tendon lengths; or, the strut lengths $\overline{AA'}$ etc. can be specified and then $\overline{AC'}$ etc. chosen to be the **minimum** length side tendons compatible with the specified strut lengths. Here the strut lengths are fixed and the side tendon lengths minimized.[6] The choice is arbitrary here and there is no real benefit to doing it one way or the other. In more complex structures, however, specifying the struts a priori allows the designer to specify them all to be equal in length. This uniformity eases the manufacture of the struts since only one length of strut needs to be made.

So the problem is:

Using the variables h and θ, minimize side tendon length $t = |\overline{AC'}|$ keeping in mind the following constraints:

- Fixed triangle radius $\overline{r}$
- Fixed strut length $\overline{s} = s = |\overline{AA'}|$
- Strut symmetry constraints: $|\overline{AA'}| = |\overline{BB'}| = |\overline{CC'}|$
- Side tendon symmetry constraints: $|\overline{AC'}| = |\overline{BA'}| = |\overline{CB'}|$

The symmetry constraints stem from the fact that this tensegrity is based on a triangular prism which has a three-fold symmetry about its axis. Symmetrical struts are chosen to be equal for convenience. They could just as well be specified to all have different lengths. The side tendon lengths are chosen to be equal for convenience also. Here more care needs to be taken since the side tendon lengths, $|\overline{AC'}|$ etc., are variables of the problem, and artificial constraints here could invalidate the mathematical model of the structure. There is nothing in the geometry of the structure which says these tendons must be equal, and

[6] This is implicitly the solution sought in the experiment with the t-prism carried out above. The struts were fixed in length and the t-prism was twisted until the opposite rectangle ends were as close together as possible.

actually a valid structure could be constructed with these tendons unequal; but, as it turns out, when the structure otherwise exhibits a rotational symmetry, imposing this symmetry on the solution results in a viable structure, and, as important, it whittles down the size of the problem considerably.

To get mathematical formulas for the different lengths, the formula for the length of a chord on a cylinder is needed. It is:

$$l^2 = (\Delta z)^2 + 2r^2 - 2r^2 \cos(\Delta\theta)$$

where

l = length of the chord
Δz = difference in z coordinate between the two points
$\Delta\theta$ = difference in angular coordinate between the two points

Notice that the formula is expressed in terms of the second power of the length. The second root of this expression would also yield a formula for the length; but, it is just as valid,[7] and, more importantly, mathematically easier, to work in second powers. In virtually every tensegrity problem examined in these notes, working with second powers of lengths makes the problem more tractable.

All this considered, the final mathematical form for the problem is:

$$\begin{aligned} \underset{\theta,\, h}{\text{minimize}} \quad & t^2 = |\overline{AC'}|^2 = h^2 + 2r^2 - 2r^2 \cos(\tfrac{2\pi}{3} - \theta) \\ \text{subject to} \quad & \overline{s}^2 = s^2 = |\overline{AA'}|^2 = h^2 + 2r^2 - 2r^2 \cos\theta \\ & \overline{r} = r \end{aligned}$$

This constrained optimization problem can be turned into an easier unconstrained one by solving the constraint for $h^2 + 2r^2$ and substituting this into the objective function. Doing this, the equivalent unconstrained problem is obtained:

$$\underset{\theta}{\text{minimize}} \quad \overline{s}^2 + 2\overline{r}^2 \cos\theta - 2\overline{r}^2 \cos(\tfrac{2\pi}{3} - \theta)$$

Taking the derivative with respect to θ and equating the result to 0 yields:[8]

[7] For example, instead of constraining the strut length to be a certain value, the second power of the strut length can be constrained to the the second power of that certain value, and the effect of the constraint will be the same.

[8] Here an important mathematical advantage of expressing the angular measures in terms of radians is realized: the derivative of cos is simply $-\sin$. The result is equated to 0 since that is a necessary first order condition for a minimum.

$$-2\overline{r}^2 \sin\theta - 2\overline{r}^2 \sin(\frac{2\pi}{3} - \theta) = 0$$

or

$$\sin\theta = -\sin(\frac{2\pi}{3} - \theta) = \sin(\theta - \frac{2\pi}{3}).$$

The sines of two angles can be equal only if either their **difference** is an **even** multiple of π, or their **sum** is an **odd** multiple of π. In this case only the latter is a possibility.[9]

The first alternative is that that the sum is just π, i.e. that:

$$\theta + (\theta - \frac{2\pi}{3}) = \pi$$

which means a solution to the problem is

$$\theta = \frac{5\pi}{6} = 150^\circ.$$

Substitution of this value for θ into the modified objective function above yields:

$$t^2 = |\overline{AC'}|^2 = \overline{s}^2 + 2\overline{r}^2 \cos(\frac{5\pi}{6}) - 2\overline{r}^2 \cos(\frac{-\pi}{6}).$$

In the experiment above, the fixed strut length, $\overline{s}$, was 7 and the fixed end tendon length, $\overline{u}$, was 3. Hence:

$$\begin{aligned} \overline{s}^2 &= 7^2 = 49 \\ \overline{r}^2 &= (\frac{\overline{u}}{2\sin(\frac{\pi}{3})})^2 = (\frac{3}{2\sin(\frac{\pi}{3})})^2 = 3 \end{aligned}$$

and therefore:

$$t^2 = |\overline{AC'}|^2 = 49 + 2\cdot 3(\frac{-\sqrt{3}}{2} - \frac{\sqrt{3}}{2}) = 49 - 2\cdot 3\sqrt{3} = 38.6077$$

So $t = |\overline{AC'}| = 6.2135$ inches (158 mm).

[9]The difference between the two angles in question is $\theta - (\theta - \frac{2\pi}{3}) = \frac{2\pi}{3}$ which is not an even multiple of π.

The next alternative is that the sum is $-\pi$, i.e. that

$$\theta + (\theta - \frac{2\pi}{3}) = -\pi.$$

This alternative yields the solution

$$\theta = \frac{-\pi}{6}.$$

This solution corresponds to a **maximum** value of the objective function rather than a minimum. Mathematically, this alternative could be eliminated by examining the second order conditions for a minimum. The previous solution would fulfill them; this solution would not. For now, such care need not be taken since it is also known that θ needs to be positive. However, as the models get more complex, these issues will need to be dealt with. This latter solution **would** be a valid tensegrity solution if the strut length were being maximized with respect to a fixed-length side tendon.

All other alternatives[10] are equivalent to the two examined since the other alternatives can be reduced to one of the solutions examined plus an even multiple of π.

2.2.3 T-Prism Mathematics: Cartesian Coordinates

As an introduction to the material presented in succeeding chapters, the triangular t-prism is re-examined from the vantage point of Cartesian coordinates. The three-fold symmetry of the triangular prism make this analysis much simpler as compared with prisms of higher symmetry.

Now each vertex of the prism is expressed as a point in xyz-space. The three-fold symmetry constrains the coordinates of the three points within each triangle to be permutations of each other. A and A' are arbitrarily chosen to be the basic points. The other points are called symmetry points since they can be generated from the basic points. These coordinate values are summarized in Table 2.2 and illustrated in Figure 2.4.

With Cartesian coordinates, it is no longer convenient to deal with the parameter r, and instead the common length of each end tendon, u, is used directly. The constraints imposed by the specification of fixed lengths for the sides of the triangles formed by the end tendons must now be explicitly written out for each triangle:

[10] These would involve substituting other odd multiples of π besides π and $-\pi$ into the equations above.

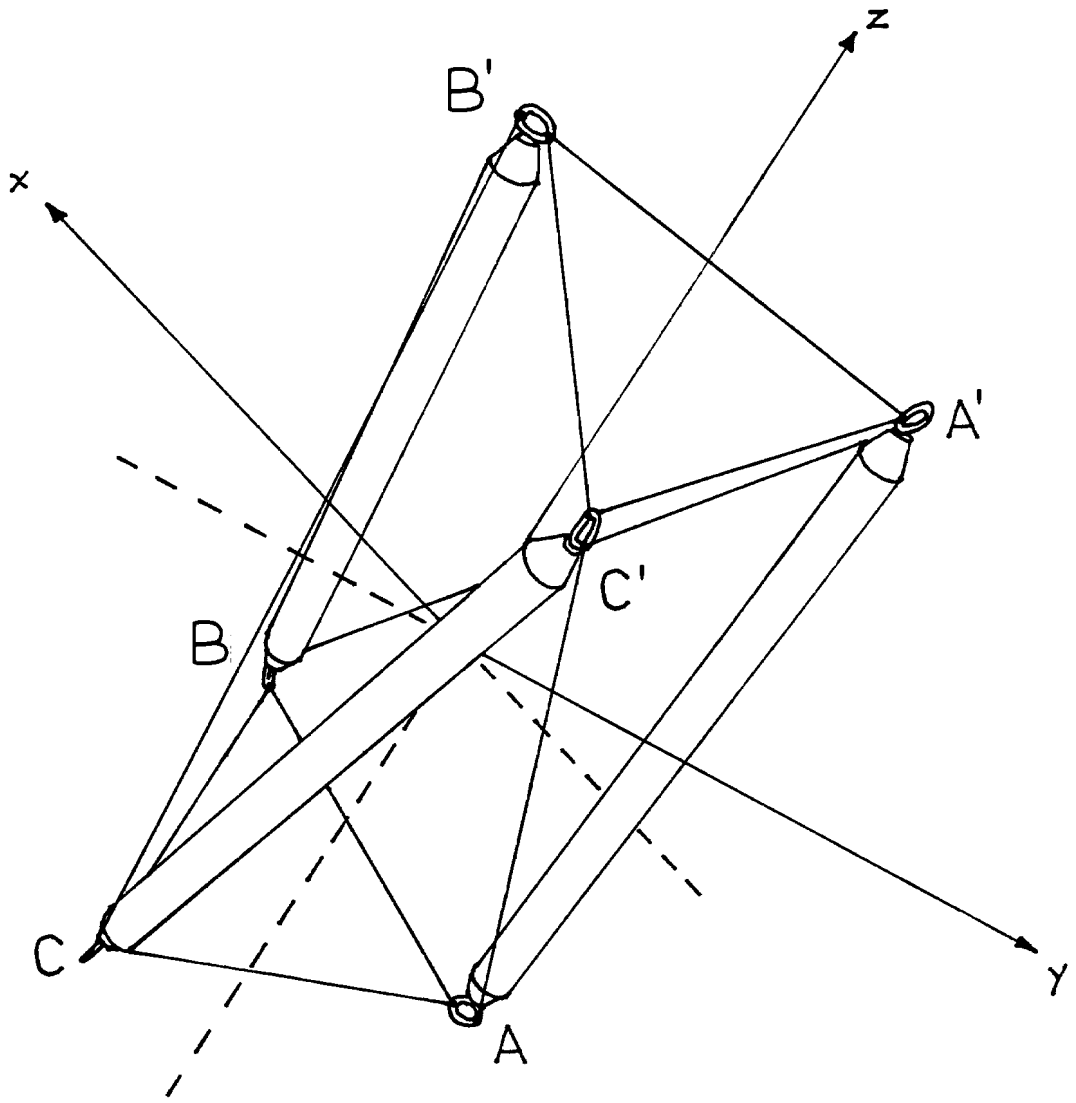

Figure 2.4: T-Prism: Cartesian Coordinates

	Coordinates		
Point	x	y	z
A	x_A	y_A	z_A
B	z_A	x_A	y_A
C	y_A	z_A	x_A
A'	$x_{A'}$	$y_{A'}$	$z_{A'}$
B'	$z_{A'}$	$x_{A'}$	$y_{A'}$
C'	$y_{A'}$	$z_{A'}$	$x_{A'}$

Table 2.2: T-Prism: Cartesian Coordinates

$$\begin{array}{rcrcrcl} \overline{u}^2 & = & u^2 & = & |\overline{AB}|^2 & = & (x_A - x_B)^2 + (y_A - y_B)^2 + (z_A - z_B)^2 \\ & & & & & = & (x_A - z_A)^2 + (y_A - x_A)^2 + (z_A - y_A)^2 \\ \overline{u}^2 & = & u^2 & = & |\overline{A'B'}|^2 & = & (x_{A'} - z_{A'})^2 + (y_{A'} - x_{A'})^2 + (z_{A'} - y_{A'})^2 \end{array}$$

Only the constraint for one side of each triangle is written out since the symmetry of the structure (which is subsumed in the coordinate representation) ensures that if the constraint is met for one side of the triangle, the other sides will satisfy the constraint also. The constraint imposed by the strut length appears as:

$$\overline{s}^2 = s^2 = |\overline{AA'}|^2 = (x_A - x_{A'})^2 + (y_A - y_{A'})^2 + (z_A - z_{A'})^2$$

Again, this equation is not written out for all three struts since the structure's symmetry ensures that if the constraint is met for one strut, it will be met for the others.

Taking all this into consideration, the mathematical representation of the problem now appears as:

$$\begin{array}{lrcrcrcl} \text{minimize} & & & t^2 & = & |\overline{AC'}|^2 & = & (x_A - y_{A'})^2 + (y_A - z_{A'})^2 + (z_A - x_{A'})^2 \\ x_A, y_A, z_A & & & & & & & \\ x_{A'}, y_{A'}, z_{A'} & & & & & & & \\ \text{subject to} & \overline{u}^2 & = & u^2 & = & |\overline{AB}|^2 & = & (x_A - z_A)^2 + (y_A - x_A)^2 + (z_A - y_A)^2 \\ & \overline{u}^2 & = & u^2 & = & |\overline{A'B'}|^2 & = & (x_{A'} - z_{A'})^2 + (y_{A'} - x_{A'})^2 + (z_{A'} - y_{A'})^2 \\ & \overline{s}^2 & = & s^2 & = & |\overline{AA'}|^2 & = & (x_A - x_{A'})^2 + (y_A - y_{A'})^2 + (z_A - z_{A'})^2 \\ & & & 0 & = & & & x_A + y_A + z_A + x_{A'} + y_{A'} + z_{A'} \\ & & & 0 & = & & & x_A - y_A \end{array}$$

The final two constraints are added for computational reasons. Without these constraints, the problem has infinitely many solutions.[11]

These equations don't lend themselves to the easy substitutions that the previous set up did, and, in this problem, certainly the previous approach is to be preferred since it is so simple to solve. The problem with the earlier approach is that it doesn't generalize as easily to more complex problems as this Cartesian approach does.

Given the complexities involved in solving a system like this, the discussion of how the solution is obtained will be deferred until later when the problems absolutely require it.

[11]The fourth constraint centers the t-prism about the origin. The fifth constraint fixes it with respect to rotations about its central axis.

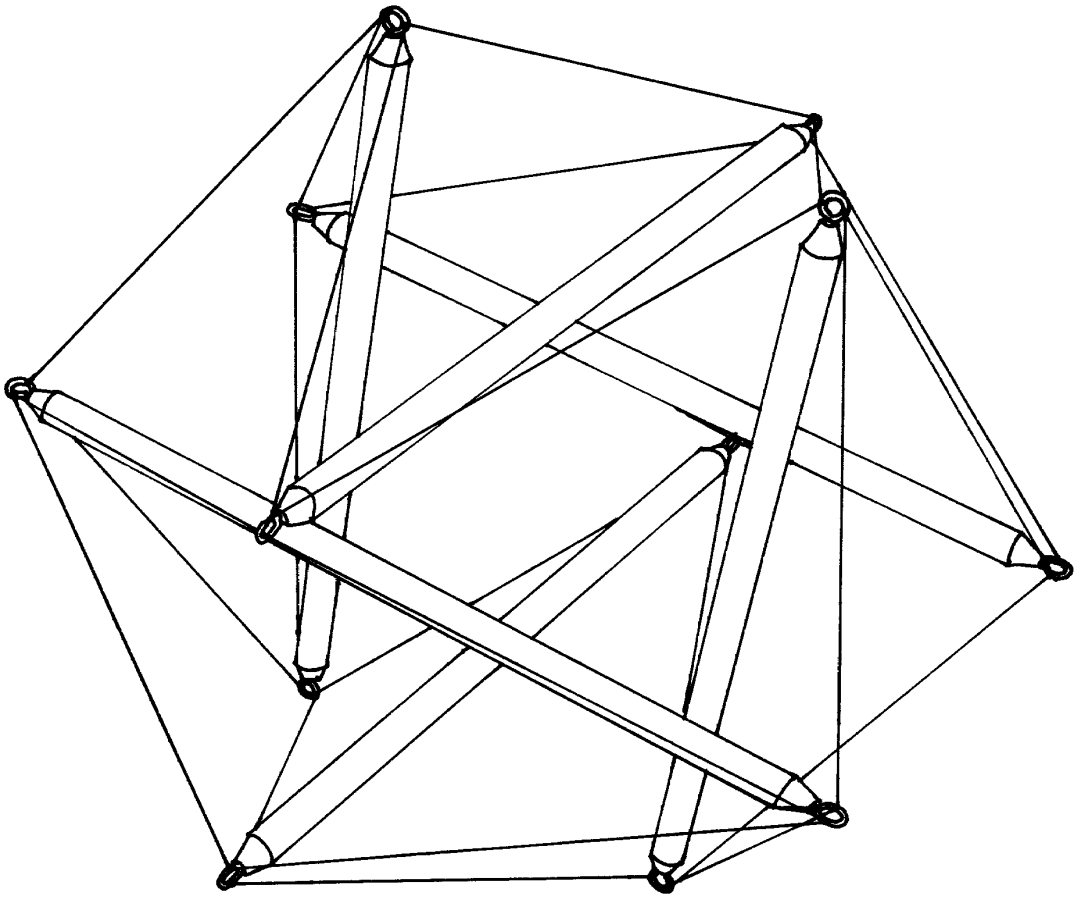

Figure 2.5: Tensegrity Icosahedron

2.2.4 T-Prism Mathematics: Further Generalizations

Kenner76 shows how the formulae of Section 2.2.2 can be generalized to handle four-fold and higher-symmetry prisms and cases where the radii of the ends differ. For the higher-symmetry prisms, it is also not necessary that the side tendon be restricted to connecting adjacent struts: it can skip over one or more struts in its trip from one end of the prism to the other. Although *Kenner76* doesn't explore this possibility, it is easy enough to generalize his formulae to handle it.

2.3 T-Icosahedron: A Diamond Tensegrity

The t-icosahedron is illustrated in Figure 2.5. It was first exhibited by Buckminster Fuller at Black Mountain College in 1949.[12] It is one of the few tensegrities which exhibit mirror

[12] *Fuller73,* Fig. 270.

symmetry. Its network of tendons would mark out a cuboctahedron if the (non-planar) quadrilaterals in which the struts are nested were changed to squares. The struts are inserted as the diagonals of these squares so each strut is parallel to the strut in the opposite square and so no strut shares a vertex with another strut. This tensegrity is classified as a "diamond" type because each strut is surrounded by a diamond of four tendons by which it is seemingly supported by two adjacent struts. This type contrasts with the "zig-zag" type which is described in Section 2.4.

The octahedral symmetry of the t-icosahedron gives the Cartesian coordinate system a real advantage in analyzing this structure since the Cartesian coordinate axes exhibit exactly the same symmetry. As a contrast to the approach taken with the t-prism, the member lengths for this structure will be derived by maximizing the length of the struts with respect to a fixed length for the tendons.

Figure 2.6 shows how the system of tendons can vary from a doubled-up octahedral arrangement to a cuboctahedron and then all the way back down to an octahedron. The place where a typical strut will go is marked by a pair of small outward-pointing arrows. These small arrows also indicate the direction of movement of this pair of opposite points of the quadrilateral as the tendon system goes through its transformations. An inward-pointing pair of small arrows indicates how the other pair of points in the quadrilateral moves during the transformations. Just past the middle of the transformations, the distance between the points indicated by the outward-pointing arrows reaches a maximum. By inserting the struts into the tendon system at this stage, the structure can be stabilized since any other stage in the transformations cannot accommodate a strut of this length.

As mentioned, this family of tensegrities is exceptionally easy to model with Cartesian coordinates. Figure 2.7 presents the model used here. The family is extremely simple in that at every stage each point is symmetric to all of the others.[13] (In addition all the tendons are symmetric to each other, as are all the struts.) So when the coordinates for one point are known, the symmetry transformations of the tensegrity can be applied to find the coordinates of any other point.

The coincidence of the symmetry of the tensegrity with that of the coordinate system is most readily exploitable if the first point, A, is chosen to lie in the positive quadrant of the xy plane. Its coordinates are x_A, y_A and 0. To do a mathematical analysis, two other points, B and C, are needed. They will be used to express the equations for the length of a strut (which is being maximized) and the length of a tendon (which represents a constraint). A glance at Figure 2.7 shows that B is obtained from A by rotating the figure about the axis through origin and the point (1.0, 1.0, 1.0) by 120°.[14] The corresponding rotation of the coordinate axes takes the x axis into the y axis, the y axis into the z axis

[13]This means that, given one point on the structure and any other point on the structure, the structure can be rotated so the given point is positioned where the other point used to be and the structure will appear to be unmoved.

[14]This axis is not shown in the figure, since would point straight out at the viewer from the origin and thus only be visible as a point.

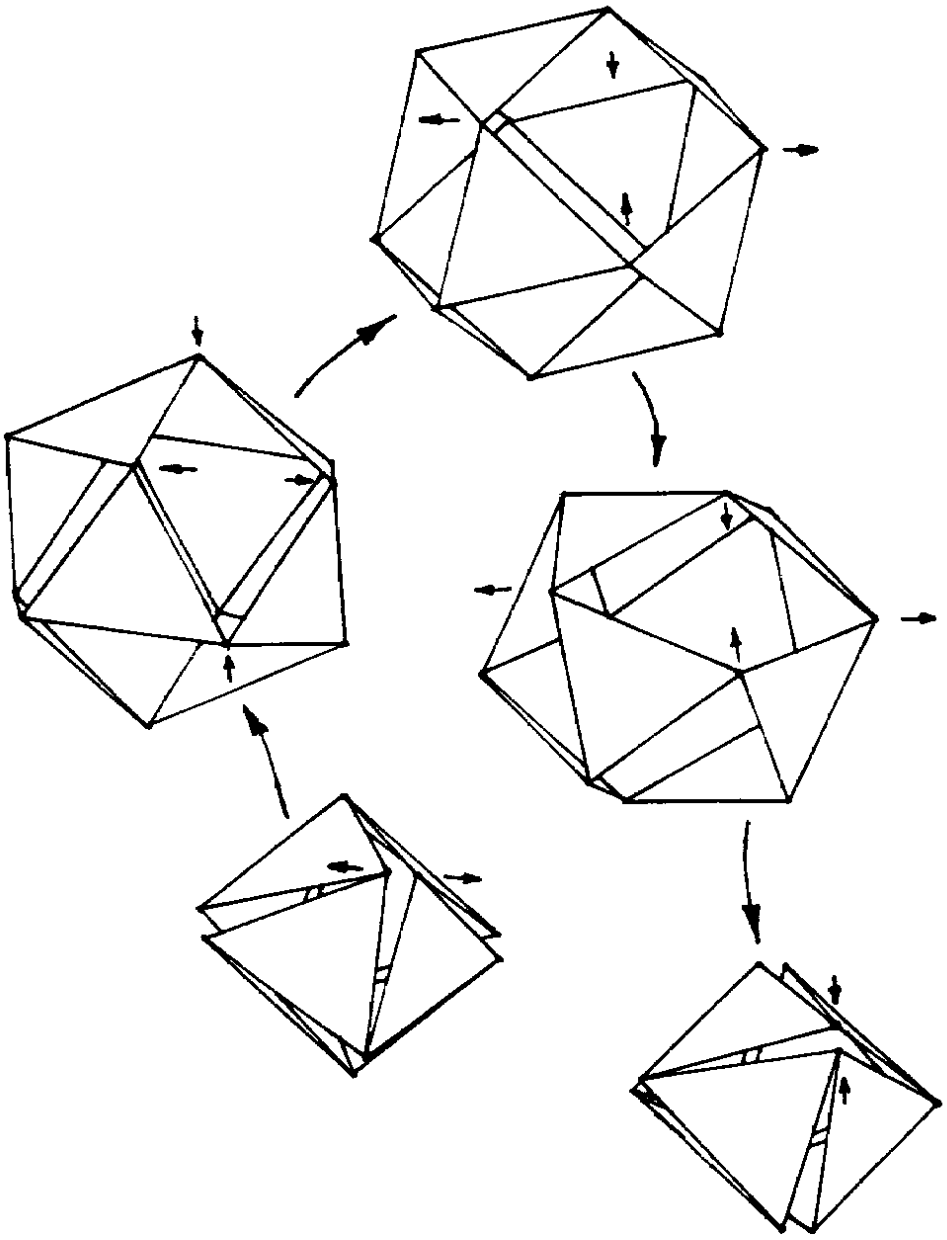

Figure 2.6: T-Icosahedron: Transformations

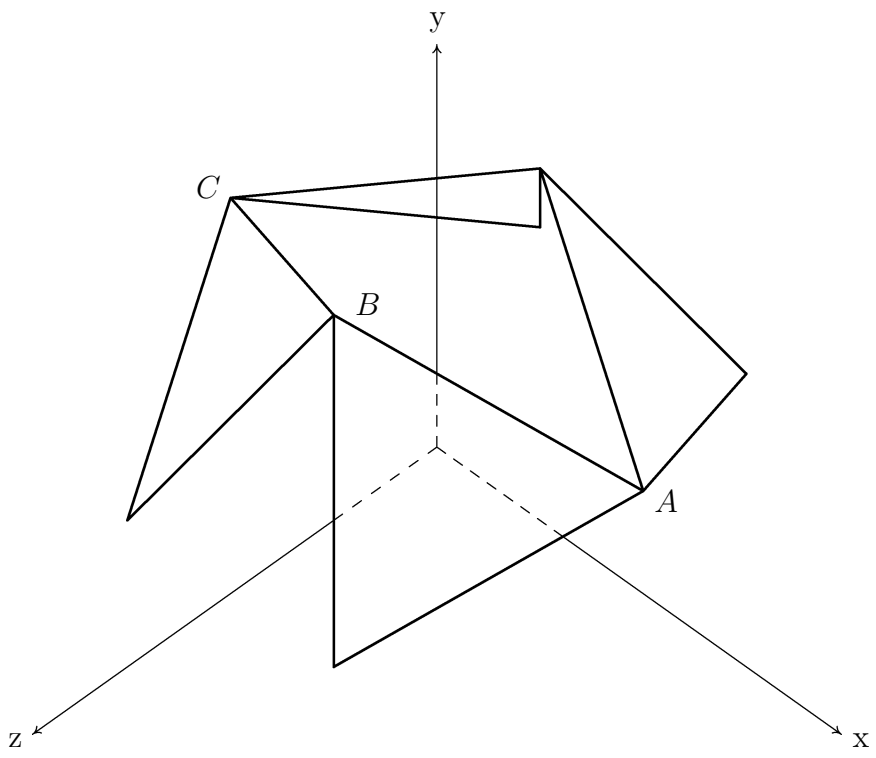

Figure 2.7: T-Icosahedron: Cartesian Coordinates

and the z axis into the x axis. This means the coordinates of B are $x_B = z_A = 0$, $y_B = x_A$ and $z_B = y_A$. C is obtained from A by a 180° rotation about the y axis. So $x_C = -x_A$, $y_C = y_A$ and $z_C = -z_A = 0$.

Thus, the problem can be expressed as follows:

$$\begin{aligned} \underset{x_A, y_A}{\text{maximize}} \quad s^2 &= |\overline{AC}|^2 \\ \text{subject to} \quad 1 &= |\overline{AB}|^2 \end{aligned}$$

The value for the fixed lengths of the tendons has been chosen as 1. Substituting using the standard Pythagorean length formula yields:

$$\begin{aligned} \underset{x_A, y_A}{\text{maximize}} \quad & (2x_A)^2 \\ \text{subject to} \quad 1 &= x_A^2 + (y_A - x_A)^2 + y_A^2 \end{aligned}$$

This problem can be solved using the method of Lagrange.[15] The adjoined objective function

$$(2x_A)^2 + \lambda(x_A^2 + (y_A - x_A)^2 + y_A^2 - 1)$$

is differentiated by x_A, y_A and λ and the resultant equations set to zero obtaining:

$$\begin{aligned} 0 &= 8x_A + \lambda(4x_A - 2y_A) \\ 0 &= \lambda(4y_A - 2x_A) \\ 0 &= x_A^2 + (y_A - x_A)^2 + y_A^2 - 1 \end{aligned}$$

The second equation says $x_A = 2y_A$. Substituting that result into the third equation gives:

$$0 = 4y_A^2 + y_A^2 + y_A^2 - 1$$

So $y_A = \sqrt{\frac{1}{6}}$, $x_A = 2\sqrt{\frac{1}{6}}$ and the strut length is $4\sqrt{\frac{1}{6}} = 1.63299$.

The Theorem of Pythagoras and the symmetry of the Cartesian coordinate system combined to make the work very easy here. Expressing points as symmetry

[15] See any calculus text, for example *Leithold72,* pp. 951-954.

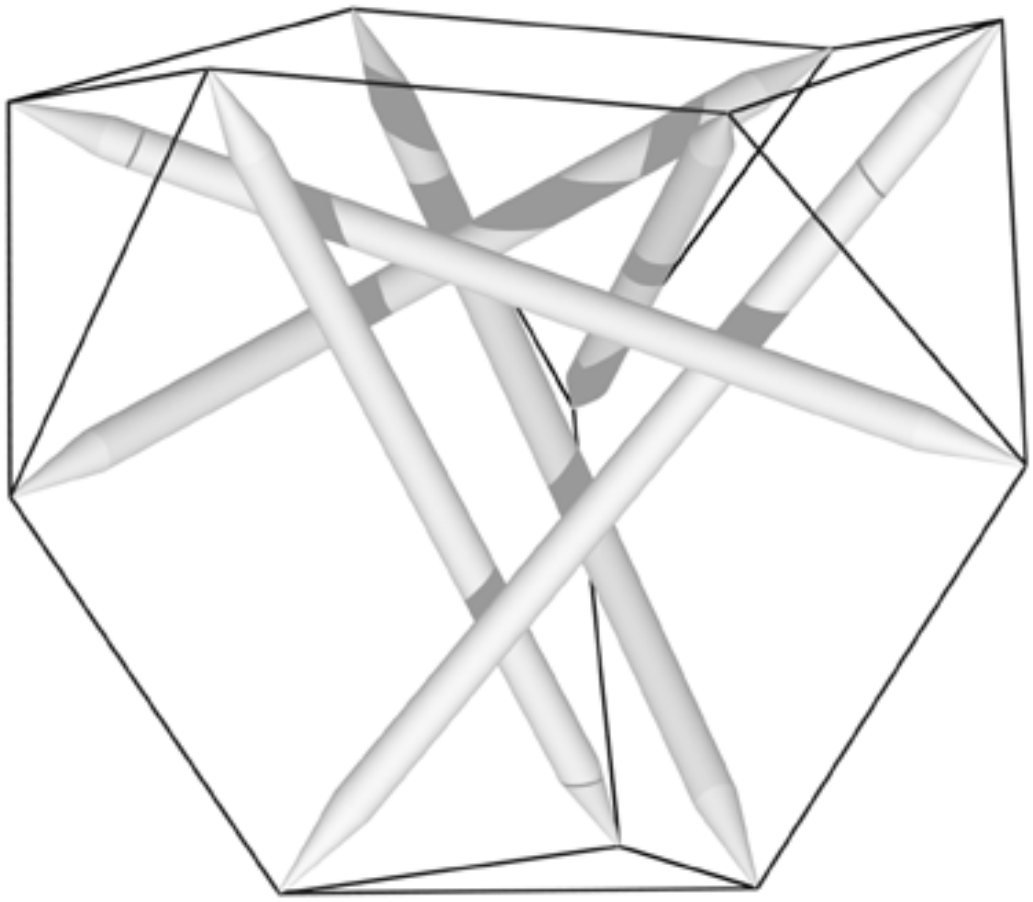

Figure 2.8: Tensegrity Tetrahedron

transformations of other points can be quite a mess, the general case involving a matrix multiplication, but here a few permutations sufficed.

So working with structures with octahedral symmetry is very desirable just from a computational point of view. In later sections some spherical tensegrity trusses are studied where the use of octahedral symmetry is a practical necessity just from a geometric point of view. This being the case, computational complexities are kept to a minimum if Cartesian coordinates are used.

2.4 T-Tetrahedron: A Zig-Zag Tensegrity

The t-tetrahedron is illustrated in Figure 2.8. It was first exhibited by Francesco della Sala at the University of Michigan in 1952.[16] It is called a "zig-zag" tensegrity because each

[16] *Fuller73,* Fig. 268.

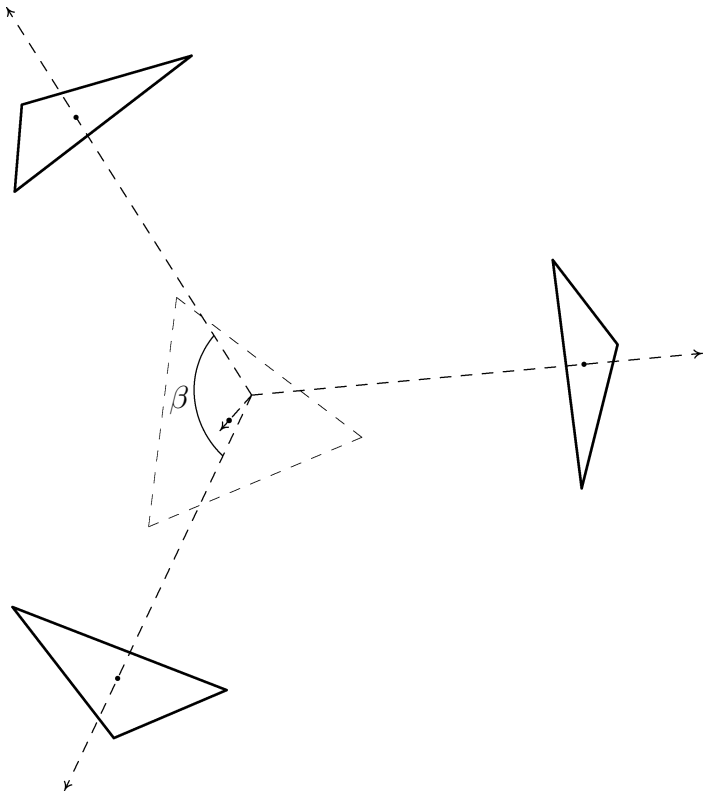

Figure 2.9: T-Tetrahedron: Mathematical Model

strut is held out by two struts tied into a zig-zag of three tendons spanning the strut. The t-tetrahedron is the zig-zag counterpart of the diamond t-icosahedron examined in Section 2.3. Both structures have six struts. The t-tetrahedron has four tendon triangles, whereas the t-icosahedron has eight.

Closer examination of these two structures yields another way the diamond and zig-zag forms can be contrasted. Four non-adjacent triangles of the t-icosahedron can be chosen to correspond to those of the t-tetrahedron. Each of these four triangles is connected to its three partners by two tendons (see Figure 2.5). The "nose" of each of the triangles is connected to the "ear" of the other (assuming the two triangles are looking at each other). This contrasts with the t-tetrahedron where each triangle is connected to each of its neighbors with a single tendon connecting the "noses" of the two triangles. With fewer tendons, the t-tetrahedron is simpler and less rigid than its diamond counterpart. In general, due to the use of fewer tendons, zig-zag structures are simpler and less rigid than their diamond counterparts.

The mathematical model for this structure is based on the structure itself and doesn't refer to any 3D coordinate systems. The mathematical analysis relies heavily on results from spherical trigonometry.[17]

[17]See *Hogben65,* pp. 367-382 for an intuitive look at this subject, and *Kells42,* Chapters 3, 5 and 8 for a more thorough and technical look.

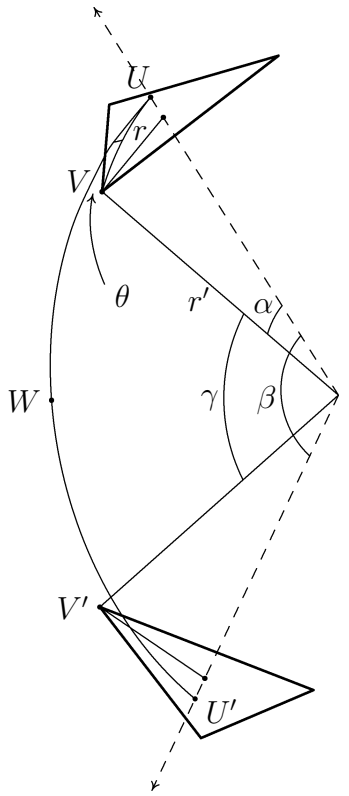

Figure 2.10: T-Tetrahedron: Detail

Figure 2.9 illustrates the model for analyzing the t-tetrahedron. The t-tetrahedron can be conceived of as four triangles mounted on four rays extending from the center of the tetrahedron. The angle between any two of these rays is denoted by β. The main interest here will be in $\frac{\beta}{2}$ which is approximately 54.736° ($\cos(\frac{\beta}{2}) = \sqrt{\frac{1}{3}}$; $\sin(\frac{\beta}{2}) = \sqrt{\frac{2}{3}}$). Two of these rays and the corresponding triangles have been included in Figure 2.10.

All four triangles are symmetrical with respect to each other and have radius r. This symmetry allows only two methods of transforming a triangle: moving it in and out along its ray and rotating it about that ray. This symmetry also dictates that if one triangle rotates counter-clockwise,[18] the other triangles rotate correspondingly. It is assumed that initially the triangles are oriented so they are all pointing at each other. The rotation angle is denoted by θ.

As mentioned, each pair of triangles is connected by a tendon (whose length will be minimized) and a strut as well (whose length represents a constraint). It is assumed that the tendon runs between the two triangle vertices which are initially pointing at each other and that the strut runs between the two vertices 120° ($= \frac{2\pi}{3}$) counter-clockwise from the vertices attached to the tendon.

[18] In speaking of triangle rotation, it is always assumed the structure is being viewed from outside. Counter-clockwise in this case amounts to a right-handed rotation of the triangle about its axis since the axis points out from the origin. From inside the structure, this would appear to be **clockwise** rotation.

Since both triangles are orthogonal to their corresponding rays, all their vertices are the same distance from the center of the tetrahedron. This distance is denoted r'. Thus all the vertices can be conceived of as being located on a circumscribing sphere of radius r'. Two symmetrical instances of these vertices are labeled V and V'. Other important points on this sphere are where the rays intersect it. These are labeled U and U'.

The arc corresponding to the tendon ($\widehat{VV'}$), the arc connecting the center points of the two triangles ($\widehat{UU'}$), and the arcs corresponding to the radii of the two triangles ($\widehat{UV}$ and $\widehat{U'V'}$) define two spherical triangles. These two triangles touch each other at the point where $\widehat{UU'}$ and $\widehat{VV'}$ intersect. This point is labeled W. The symmetry of the structure dictates that the corresponding parts of these two triangles must be equal. (In particular the structure could be rotated 180°, exchanging U with U', and the structure should appear to be unchanged.) This means that the arcs $\widehat{UW}$ and $\widehat{U'W}$ are equal and their common measure is $\frac{\beta}{2}$. Also $\widehat{VW} = \widehat{V'W} = \frac{\widehat{VV'}}{2}$.

The angular measure of $\widehat{VV'}$ is denoted γ. It is useful to know how γ changes as a function of the twist angle θ, the triangle radius r and the sphere radius r'. This length can be computed using the Law of Cosines of Spherical Trigonometry. That law yields:

$$\cos(\frac{\gamma}{2}) = \cos(\frac{\beta}{2})\cos\alpha + \sin(\frac{\beta}{2})\sin\alpha\cos\theta$$

where α denotes the arc length of $\widehat{UV}$ which equals the arc length of $\widehat{U'V'}$. By inspection, it can be seen that $\sin\alpha = \frac{r}{r'}$ and therefore $\cos\alpha = \sqrt{1 - \frac{r^2}{r'^2}}$ so:

$$\begin{aligned}\cos(\frac{\gamma}{2}) &= \frac{\cos(\frac{\beta}{2})\sqrt{r'^2 - r^2} + \sin(\frac{\beta}{2})r\cos\theta}{r'^2} \\ &= \frac{g(\theta, r')}{r'^2}\end{aligned}$$

For convenience, the functional notation

$$g(\theta, r') \equiv \cos(\frac{\beta}{2})\sqrt{r'^2 - r^2} + \sin(\frac{\beta}{2})r\cos\theta$$

denotes part of this expression. Note that only values which will be variables in the analysis appear explicitly as arguments in this function.

From this cosine value, the length of the tendon connecting the two triangles (denoted t) and its second power can be derived as follows:

$$\begin{aligned} \frac{t}{2} &= r' \sin(\frac{\gamma}{2}) \\ t^2 &= 4r'^2(1 - \cos^2(\frac{\gamma}{2})) \\ t^2 &= 4(r'^2 - g^2(\theta, r')) \\ t^2 &= f(\theta, r') \end{aligned}$$

Again, for convenience the functional notation

$$f(\theta, r') \equiv 4(r'^2 - g^2(\theta, r'))$$

is used. $f_1(\theta, r')$ and $f_2(\theta, r')$ refer to the partial derivatives of this function with respect to its first and second arguments.

$$\begin{aligned} f_1(\theta, r') &= 8g(\theta, r') \sin(\frac{\beta}{2}) r \sin(\theta) \\ f_2(\theta, r') &= 8(r' - g(\theta, r') r' \frac{\cos(\frac{\beta}{2})}{\sqrt{r'^2 - r^2}}) \end{aligned}$$

Now only a formula for the strut length need be derived before the analysis moves on to the specification of the minimization problem. Strut length, denoted by s, is simply specified by the formula:

$$s^2 = f(\theta + \frac{2\pi}{3}, r')$$

This follows since, as noted above, the strut vertices are located $\frac{2\pi}{3}$ radians counter-clockwise from the tendon vertices on the same two triangles.

So the minimization problem is simply:

$$\begin{aligned} \underset{\theta, r'}{\text{minimize}} \quad t^2 &= f(\theta, r') \\ \text{subject to} \quad s^2 &= f(\theta + \tfrac{2\pi}{3}, r') \end{aligned}$$

Assuming the constraint can be solved for r' in terms of θ, this can be respecified as the unconstrained minimization problem:

$$\underset{\theta}{\text{minimize}} \quad t^2 = f(\theta, r'); r' = r'(\theta)$$

The first order condition for a minimum is:

$$0 = f_1(\theta, r') + f_2(\theta, r')\frac{dr'}{d\theta}.$$

$\frac{dr'}{d\theta}$ is obtained by implicitly differentiating the constraint:

$$\begin{aligned} 0 &= f_1(\theta + \frac{2\pi}{3}, r') + f_2(\theta + \frac{2\pi}{3}, r')\frac{dr'}{d\theta} \\ \frac{dr'}{d\theta} &= -\frac{f_1(\theta + \frac{2\pi}{3}, r')}{f_2(\theta + \frac{2\pi}{3}, r')} \end{aligned}$$

Substituting this expression into the original first order condition yields:

$$0 = f_1(\theta, r') - f_2(\theta, r')\frac{f_1(\theta + \frac{2\pi}{3}, r')}{f_2(\theta + \frac{2\pi}{3}, r')}$$

This equation is solved simultaneously with the constraint equation to get the minimizing value of θ and (incidentally) the corresponding value for r'. While the mathematical programming problems examined in previous sections could be solved completely using mathematical formulas, this problem requires numerical tools to reach a final solution.

The procedure for numerically deriving a solution to these equations, and thus to the mathematical programming problem, is as follows:

Step 1 Set $\theta = 0$.

Step 2 Given θ, solve the constraint for r'.

Step 3 Given r', solve the first order condition for θ.

Step 4 Repeat the process from **Step 2** until θ converges.

To find equation solutions, a simple binary algorithm for finding zeros of functions was used. This involved specifying a search interval for each equation[19] and then evaluating the equation at each endpoint. One of the values should be greater than zero and one less than

[19]For the constraint, r and s were used as the bounds for r'. For the first order condition, $\frac{-\pi}{2}$ and $\frac{\pi}{2}$ were used as the bounds for θ.

Iteration #	Solution Values r'	θ
1	2.10683424	0.124151607
2	2.07636415	0.120243860
3	2.07719872	0.120351753
4	2.07717557	0.120348762
5	2.07717622	0.120348845
6	2.07717620	0.120348842

Table 2.3: T-Tetrahedron: Solution

zero. The equation is then evaluated at the midpoint of the interval and a search interval specified which is bounded by the midpoint and the endpoint which differs from it in sign. In this manner, the search interval is halved at each iteration. When the search interval is less than twice the tolerance specified for a solution, the midpoint of the search interval is taken as the solution. This technique works remarkably well given how simple it is.

The triangle radius was chosen to be 1 (which implies a length of $\sqrt{3}$ for its tendons) and the strut length s to be 4. Applying the above technique, the sequence of values shown in Table 2.3 was obtained.

The final solution was $\theta = 0.120348842$ radians. The length of the tendon is obtained by substituting the final values for θ and r' into the equation for tendon length. This yields a tendon length of 1.84242715.

2.5 Basic Tensegrity Structures: Conclusions

In this chapter, several simple tensegrity structures were examined and some methods presented for designing them. Future chapters will build on this foundation as the design of more and more complex structures is explored. Cartesian methods will be emphasized more and more and spherical trigonometry will pretty much disappear from the scene as the most complex structures are analyzed. The nature of the problems seem to require this.

Chapter 3

General Tensegrity Structures

3.1 General Programming Problem

3.1.1 General Programming Problem: Introduction

An inventory of the components of a tensegrity structure can start out with sub-systems called hubs. These hubs are the areas in the tensegrity where members meet and are fastened together. Members are interactions between pairs of hubs and can be further broken down into struts (compression members which keep pairs of hubs apart) and tendons (tensile members which pull pairs of hubs together). There may be constraints relating to member lengths, symmetry and geometrical determinacy.

In initial design stages, it may be easier to treat the hubs as undifferentiated systems where members all meet at a point. This was the strategy used in Chapter 2. In many real applications though, tendons are attached to the hub at multiple points. In these cases, the design either has to formally model the hub as composed of multiple attachment points or adopt some ad hoc way of relating the model's geometry to that of the physical structure. When the hub is formally modeled as a collection of separate attachment points, one or more vectors will indicate how these attachment points are positioned with respect to each other and relative to a single basic point associated with the hub. Additional constraints will be necessary to determine each vector's length and direction.

As Chapter 2 showed, an effective tensegrity design strategy involves minimizing or maximizing the lengths of one set of members while the other members are constrained to have various fixed lengths. So, the general problem is set out as:

$$\begin{array}{ccccc} \underset{P_1,...,P_{n_h},V_1,...,V_{n_v}}{\text{minimize}} & & \text{o} & \equiv & \overline{w}_1 l_1^2 + \cdots + \overline{w}_{n_o} l_{n_o}^2 \\ \text{subject to} & & \text{Member constraints:} & & \\ & & \pm\bar{l}_{n_o+1}^2 & \geq & \pm l_{n_o+1}^2 \\ & & & \cdots & \\ & & \pm\bar{l}_{n_m}^2 & \geq & \pm l_{n_m}^2 \\ & & \text{Symmetry constraints:} & & \\ & & \overline{s}_1 & = & s_1(\cdots) \\ & & & \cdots & \\ & & \overline{s}_{n_s} & = & s_{n_s}(\cdots) \\ & & \text{Point constraints:} & & \\ & & \overline{d}_1 & = & \overline{W}_1 \cdot P_{d_1} \\ & & & \cdots & \\ & & \overline{d}_{n_d} & = & \overline{W}_{n_d} \cdot P_{d_{n_d}} \\ & & \text{Vector constraints:} & & \\ & & \overline{c}_1 & = & c_1(\cdots) \\ & & & \cdots & \\ & & \overline{c}_{n_c} & = & c_{n_c}(\cdots) \end{array}$$

where:

n_h = number of hubs = number of basic points
n_v = number of vectors
n_o = number of members in the objective function
n_m = number of members in the model
$n_{\bar{o}} = n_m - n_o$ = number of constrained members
n_s = number of symmetry constraints
n_d = number of point constraints
n_c = number of vector constraints

The expression $P_1, ..., P_{n_h}, V_1, ..., V_{n_v}$ appearing under "minimize" indicates that the coordinate values of the basic points and vectors are the control variables of the minimization problem. These are the values which are changed (in accordance with the constraints) to find a minimum value for o.

In the objective function, $\overline{w}_{i_o}$ is a positive constant value if the corresponding member is a tendon and negative if the member is a strut where $i_o \in \{1, \ldots, n_o\}$.

In the objective function and member constraints, l_{i_m} stands for the length of member i_m where $i_m \in \{1, \ldots, n_m\}$.

In the member constraints, $\overline{l}_{i_{\tilde{o}}}$ is a positive constant value. "+" precedes $\overline{l}_{i_{\tilde{o}}}$ and $l_{i_{\tilde{o}}}$ if the corresponding member is a tendon, and "-" precedes them if the member is a strut where $i_{\tilde{o}} \in \{n_o + 1, \ldots, n_m\}$.

In the other constraints, $s_{i_s}(\cdots)$ and $c_{i_c}(\cdots)$ are functions of the coordinate values, and $\overline{s}_{i_s}$, $\overline{d}_{i_d}$ and $\overline{c}_{i_c}$ are constant values where $i_s \in \{1, \ldots, n_s\}$, $i_d \in \{1, \ldots, n_d\}$ and $i_c \in \{1, \ldots, n_c\}$.

In the point constraints, $\overline{W}_{i_d}$ is a triplet of fixed values which is applied to $P_{d_{i_d}}$ using a dot product where for any value of i_d, $d_{i_d} \in \{1, \ldots, n_h\}$.

So, the examination of this problem is divided into five sections: the objective function, the member constraints, the symmetry constraints, the point constraints and the vector constraints.[1]

3.1.2 General Programming Problem: Objective Function

In the basic tensegrity structures of Chapter 2, the objective functions consisted of the second power of the length of one member. If this member was a tendon, the quantity was minimized. If this member was a strut, the quantity was maximized. For these simple structures, including just one instance of a **symmetrical** class of members in the objective function worked fine, but, for more complex structures, this procedure leads to a lopsided structure having one tendon much shorter than its comparable companions. So, in complex structures, the lengths of several instances of **non-symmetrical** classes of members are minimized (for tendons) or maximized (for struts).

How can this be done? A mathematical programming problem can't have more than one objective function; so, a different objective function for the length of each non-symmetrical instance is not a possibility. What can be done is minimize a **weighted sum of the second powers** of these lengths. Positive weights are used for tendon lengths. If a strut is included in the objective function, it is included with a negative weight since minimizing the additive inverse of a quantity is the same as maximizing the quantity. This approach results in a valid tensegrity since, in the final solution, each of the member lengths will be minimized (for tendons) or maximized (for struts) with respect to the others. If this weren't the case, the length of one member could be reduced (for a tendon) or increased (for a strut) while maintaining the lengths of the others. This would result in a weighted sum less than the minimum which cannot be if the problem was solved correctly. So, the general form for the objective function is:

$$\mathrm{o} \equiv \overline{w}_1 l_1^2 + \cdots + \overline{w}_{n_o} l_{n_o}^2$$

[1] *Roth81* contains a highly-technical mathematical look at this problem.

Besides allowing tendons to be minimized and struts to be maximized in the same objective function, the weights give the designer control over the relative lengths of the members which appear in the objective function. The weights can be chosen as desired subject only to the requirement that the weight for a tendon must be positive (since tendon lengths are **minimized**) and the weight for a strut must be negative (since strut lengths are **maximized**). In Section 7.2.6 it is shown that any valid tensegrity configuration can be viewed as the solution to a mathematical programming problem of this form with an appropriate selection of weights. This fact gives this weighted-sum approach complete generality as a tool for tensegrity design.

3.1.3 General Programming Problem: Member Constraints

The member lengths which don't appear in the objective function appear in the constraints. The constraint function is the second power of member length in the case of a tendon and minus the second power of length in the case of a strut. This value is constrained to be **less than** or **equal to** $\pm\bar{l}_{i_{\tilde{o}}}^2$ where again the member type determines the sign used.

In the general model, these constraints are inequalities since tendons are members which can pull points together but can't push them apart, and struts are members which can push points apart but can't pull points together. Practically, the strut may be made of materials which are capable of sustaining a very substantial tensile load (though certainly the struts may be fabricated so they can stand no tensile load at all), but in a final design, they should not be sustaining such a load since they are not designed for this. So, even for struts, an inequality is called for in the constraints.

Since, for uniformity, the equations are organized so that the constrained value is always less than or equal to some fixed value, the second power of strut lengths and the corresponding $\bar{l}_{i_{\tilde{o}}}^2$ constants are negated in the strut constraint equations. In practice (see Section 3.2), all the constraints are treated as equalities.

3.1.4 General Programming Problem: Symmetry Constraints

In the simple tensegrities examined in Chapter 2, symmetry constraints were mentioned, but were dealt with implicitly in the mathematical programming problems by doing substitutions. The simplicity of the symmetry transformations and the coordinate systems used allowed the coordinates of one point to be expressed as a simple signed permutation of the coordinates of another point.

In the general problem, the very real possibility exists that some symmetry constraints cannot be so simply accounted for. In general, a symmetry-transformed coordinate is a linear combination of all three coordinates of another point. However, for most of the models discussed in this book, though some of them are rather complex, the symmetry

constraints are of the simpler type so that they do not appear in the programming problem explicitly, but only appear implicitly as coordinate permutations. This is because most of the models have octahedral symmetries. When other symmetries are used, for example the icosahedral symmetry of the model discussed in Section 5.4, symmetry constraints may need to be introduced explicitly. This introduction creates no real mathematical problems other than slowing down the computations due to the larger system.

$\overline{s}_{i_s}$ is always 0, but it is convenient to keep the label for symbolic manipulations later.

3.1.5 General Programming Problem: Point Constraints

This type of constraint appeared explicitly as the last two constraints in the Cartesian-coordinate model for the t-prism in Section 2.2.3. It appeared implicitly in the cylindrical-coordinate model of the t-prism in Section 2.2.2 where the z coordinates of points A, B and C were fixed at 0. In general, for cylindrical (e.g. masts) or truncated (e.g. domes) structures point constraints need to be introduced to make the mathematical model of the structure determinant. For structures with spherical symmetries, the member, symmetry and vector constraints are sufficient for determining the structure. Point constraints are linear equalities restricting a point to lie in a specific plane. In Cartesian coordinates, the format of a point constraint is a dot product of a point with a triplet of fixed values. The dot product is constrained to be a particular value. The triplet of fixed values is referred to as the determining vector of the point constraint, and the point lies in a plane orthogonal to this vector when it conforms to the constraint. Point constraints don't seem to be necessary when using conjugate direction methods to solve a mathematical programming problem, but can be necessary when using Newton's method to improve a solution's accuracy.

3.1.6 General Programming Problem: Vector Constraints

Vector constraints fill in the details about the geometry of complex hubs. The use of these constraints, and the list of vectors they affect, $V_1, ..., V_{n_v}$, represents a move away from the initial gross analysis of a tensegrity structure where the details of strut-tendon connections are omitted for simplicity's sake, to a more detailed analysis of the structure where the struts and tendons are no longer assumed to meet at a point. This includes situations where a tendon is attached to a point away from the ends of the strut, i.e. between the ends somewhere, or off the centerline of the strut, or both. A vector is a difference between two points and is necessary to model the offset from the strut end point to the point where the tendon is attached.

In general, the tendon attachment points will still be clustered in two areas on the strut in proximity to the locations which were modeled as simple strut end points in the gross analysis. Each cluster of points is defined with respect to the basic point which corresponds

to the hub they represent, or in some cases they are defined with respect to a convex combination of the basic points corresponding to the two hubs a strut connects. Especially in the latter case, the center of the hub will not necessarily coincide with the location of the corresponding basic point.

As an example of what vector constraints are like, consider the case where, instead of assuming the tendon is connected on the center line of the strut, it is more realistically assumed that the tendon connects to the surface of the strut and thus the attachment point falls off the center line of the strut. For this example, the strut is assumed to be a simple cylinder.

The first step is to introduce a single vector which represents the offset to the tendon attachment point from a reference point lying on the center line of the strut. This reference point may be one of the basic points corresponding to the two hubs the strut connects or perhaps a point on a line through the basic points of those two hubs. A vector constraint is then introduced which indicates how far from the reference point the tendon is to be connected. In this case, that distance would correspond to the radius of the strut. This constraint would restrict the tendon's attachment point to lie on a sphere about the point. A second constraint is then introduced to restrict the vector to be orthogonal to the center line of the strut. The attachment point is thus constrained to lie on a plane through the reference point and orthogonal to the strut's center line. This second constraint makes sure the tendon is attached to the surface of the strut rather than at an interior point.

An example using vector constraints appears in Section 7.3.6.

3.2 Solving the Problem

What follows are some methods for solving this general problem. The problem can be characterized as a mathematical programming problem in which both the objective function and the constraints are non-linear in the control variables. The constraint region is not convex[2], so the simpler algorithms admissible in that case cannot be used. The non-linearity of the objective functions and constraints is a simple one. They are both quadratic in the control variables. This simplifies taking their derivatives.

The first simplification made is to assume all the constraints hold with equality. This is fairly innocuous and makes solving the problem easier. The final solution must be checked however to make sure tendons and struts have appropriate member forces.

Two formulations allow unconstrained mathematical programming techniques to be applied to this problem. The first formulation is referred to as the penalty formulation and uses penalty[3] methods. In this formulation, the constraints are recast as deviations from

[2]The non-convexity is due to the strut constraints. For a proof, see Appendix B.
[3]*Luenberger73,* pp. 278-280.

zero and the sum of the second powers of these deviations is incorporated into the the objective function with a large positive coefficient. This formulation is especially useful in the initial stages of solving a problem since it easily handles large deviations from the constraint requirements.

The second formulation is referred to as the exact formulation. It divides the coordinates into dependent and independent sets and solves the constraints for the dependent set in terms of the independent set. The number of coordinates in the dependent set will equal the number of constraint equations. Once this is done, the programming problem can then be treated as an unconstrained problem with the independent coordinates as the control variables. The non-linearity of the constraint system means Newton's method[4] must be used to solve the equations. This method may not work if the initial coordinate values imply large deviations from the constraint requirements. This formulation allows the programming problem to be solved to a high degree of accuracy.

In using Newton's method in conjunction with the exact formulation, both the constraint deviation and its partial derivative with respect to the members of the dependent coordinate set must be computed. Since the constraints are quadratic in the coordinate values, the partial derivatives are linear in the coordinate values. This means it is easy to compute them using formulas. It is also possible to compute the partial derivatives using numerical techniques; however, this may yield less accurate results.

A requirement for the exact formulation to work is a method for reliably dividing the coordinates into a dependent and an independent set since not every partitioning results in a solvable system. This can be done as follows. A $n_{\tilde{o}} + n_c + n_s + n_d$ by $3(n_h + n_v)$ matrix is set up. Call this matrix $\mathbf{A}$. The ijth element of this matrix, a_{ij}, represents the partial derivative of the ith constraint with respect to the jth coordinate value. Gaussian elimination is applied to the matrix with pivoting both over rows and **columns**.[5] At the end of this process, the coordinates corresponding to the $n_{\tilde{o}} + n_c + n_s + n_d$ left-most columns are selected as the dependent set. The remaining coordinates compose the independent set. If coordinate values change a great amount, it may be advisable to recompute this partitioning to maintain the best possible partitioning.

Once one of these strategies is selected, a method must be picked for solving the unconstrained problem. Two effective methods are Parallel Tangents (also called PARTAN)[6] and Fletcher-Reeves.[7] These two methods recommend themselves especially in conjunction with the penalty formulation since they are immune to the problems posed by the asymmetric eigenvalues of the objective function which results from that formulation. Other conjugate direction methods may work as well and will enjoy the same immunity.

[4] *Luenberger73,* pp. 155-158.

[5] This is referred to as "complete" or "total" pivoting. This only gets a footnote in most treatments of Gaussian elimination since for most applications "partial" pivoting (pivoting over rows only) is sufficient. For example, see *Johnston82,* p. 31.

[6] *Luenberger73,* pp. 184-186.

[7] *Luenberger73,* pp. 182-183.

Both of these methods require a method for doing a line search for finding which point in a given direction minimizes the objective function. One method is outlined below. It assumes the value of the objective function for the current coordinate values has already been computed.

1. An initial step size is selected and the point in the given direction found whose distance from the initial point matches this step size. The value of the objective function is computed at this new point.[8]

2. If the objective function value is larger at the new point, the step size is halved until a decrease is obtained, and halving continues until no more improvement (i.e. no more decrease in the objective function) is obtained. If the objective function value is smaller at the new point, the step size is doubled until no further decreases are obtained. In this second case, if the first doubling of the step size doesn't result in an additional decrease, the original step size is halved to see if that results in a decrease. If it does, halving continues until no further decrease is realized.

3. A quadratic technique is used to fine tune the step size. Three points are selected from the doubling/halving process above (the initial point, the best point and the point selected after the best point). A quadratic curve is fitted to the step sizes and objective function values corresponding to these three points. Using this curve, the step size corresponding to the minimum value for the objective function is computed. The actual value for the objective function for this step size is computed. This procedure is repeated, substituting the new point generated for one of the old points. Repetition is terminated when no further improvement to the actual value of the objective function is obtained. The formula for computing the new step size is:

$$s_n = \frac{(s_1^2 - s_2^2)o_1 + (s_2^2 - s_0^2)o_2 + (s_0^2 - s_1^2)o_3}{2((s_1 - s_2)o_1 + (s_2 - s_0)o_2 + (s_0 - s_1)o_3)}$$

   where s_n is the new step size, s_1, s_2, s_3 are the step sizes corresponding to the three points and o_1, o_2, o_3 are the three objective function values.

The final fine-tuning step is important since both PARTAN and Fletcher-Reeves count on the point being an accurate minimizing point in the direction chosen. Once a solution to the unconstrained problem has been reached using conjugate direction methods, Newton's method can be applied to the unconstrained problem to improve the accuracy of the result.

[8] If the exact formulation is being used, it is possible that this step will generate constraint deviations large enough that Newton's method doesn't converge. If this happens, the step size should be halved.

Chapter 4

Higher Frequency Spheres

4.1 Higher Frequency Spheres: Introduction

Now some concrete applications of the methods discussed in Chapter 3 can be made. They will be applied to "higher frequency" versions of the simple spherical structures discussed in Chapter 2. "Higher frequency" in this context means that the spherical structures are composed of a greater number of members. If the members used are about the same size as before, this means the sphere will grow in size. If instead the radius of the sphere stays the same size, the surface now has a finer texture.

As in the model for the t-tetrahedron, the tensegrities will be considered to be a collection of tendon triangles lying approximately on a sphere interconnected with adjacent tendon triangles via struts and tendons. The lengths of the struts as well as of the lengths of the tendons making up the tendon triangles will be considered as fixed, and thus appear as parameters in the mathematical programming problem, while the (second powers of) the lengths of the tendons interconnecting adjacent tendon triangles will appear in the objective function and will be collectively minimized.

Although at least one member's length must appear as a constraint for the problem to be mathematically determinant, there is nothing hard and fast about the classification of members as minimands or constraints. For different applications, different classifications might be useful. The classification selected here is convenient because it allows a good number of the tendon and strut lengths to be constrained, and still enough degrees of freedom are left in the minimization process that tendons of the same class aren't wildly asymmetric. Having a good number of the member lengths constrained is convenient because it means their lengths can be specified precisely; all the tendons or struts of a certain class can be constrained to have the same lengths.

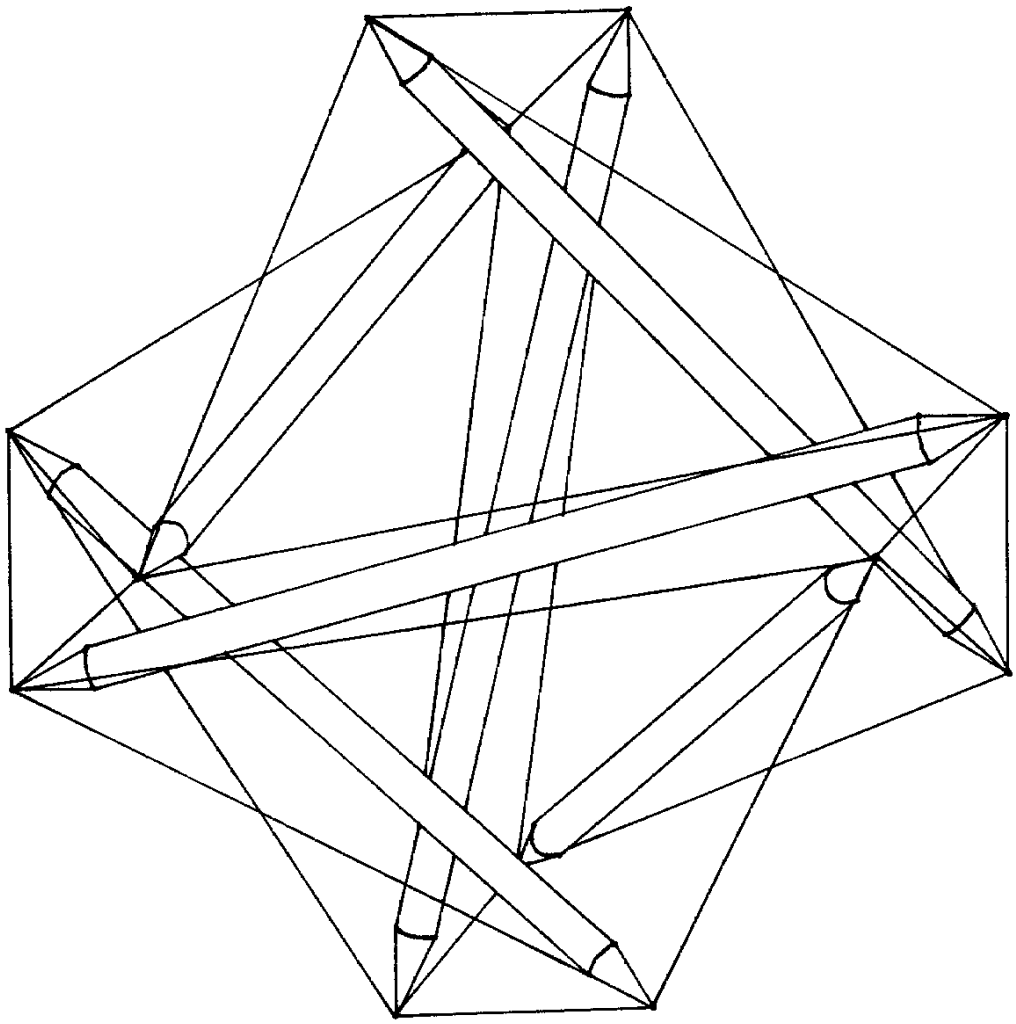

Figure 4.1: 2ν Diamond T-Tetrahedron

4.2 Diamond Structures

4.2.1 Diamond Structures: Descriptive Geometry

As mentioned in Section 2.3, diamond structures are characterized by the fact that each tendon triangle is connected to adjacent tendon triangles via one strut and two interconnecting tendons. This section will examine a diamond configuration of the tensegrity tetrahedron. The zig-zag configuration of the 2ν[1] t-tetrahedron was examined in Section 2.4. The diamond configuration of the 2ν t-tetrahedron is illustrated in Figure 4.1. It is topologically identical to the t-icosahedron (Figure 2.5 of Section 2.3). The only

[1]The qualifier "2ν" is explained below.

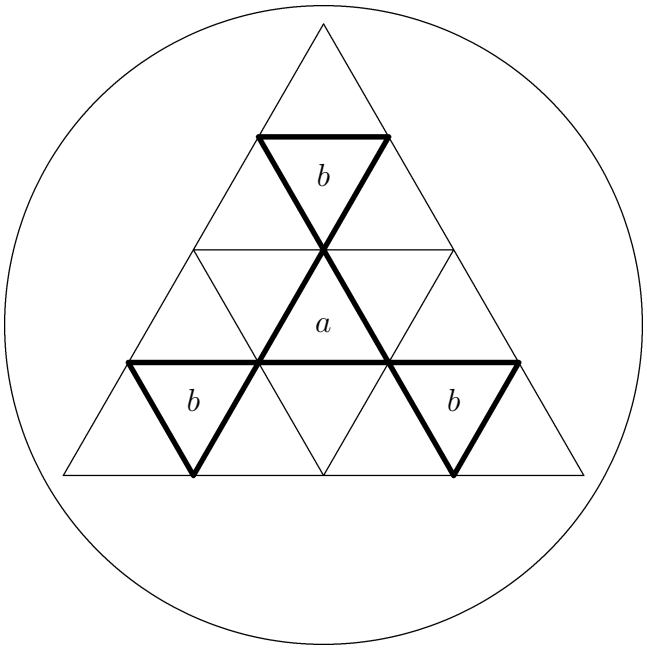

Figure 4.2: 4ν Breakdown of Tetrahedron Face Triangle

difference is that the tendon triangles of the 2ν diamond t-tetrahedron are two different sizes. The t-icosahedron is actually a special case of the 2ν diamond t-tetrahedron with all tendons the same length.

To review the contrast between the diamond and zig-zag configurations presented in Section 2.4, it is most productive to focus on the group of four small triangles from the 2ν diamond t-tetrahedron. These correspond to the 2ν zig-zag t-tetrahedron's four tendon triangles. If two tendon triangles from this group are considered to be facing each other nose-to-nose, the strut can be seen to connect the right ear of one triangle with the right ear of the other triangle as it did in the zig-zag t-tetrahedron. However, there are now two tendons interconnecting the two tendon triangles instead of just one. Each connects the right ear of one tendon triangle with the nose of the other.

These two tendons are symmetrical to each other, so the problem still consists of minimizing one length as it did in the original zig-zag problem, and even the same geometrical model as was used to solve that problem could be used here. However, the general case is more complex than this and is not amenable to treatment with models such as were used to examine the simple 2ν zig-zag t-tetrahedron. So, to illustrate the general procedure, calculations are done for a frequency-four (or 4ν for short) diamond t-tetrahedron.

It is called a 4ν structure because its geometry derives from the 4ν geodesic subdivision of the tetrahedron.[2] Only even-frequency subdivisions are used in tensegrity designs. Figure 4.2 shows a 4ν breakdown of a triangle (in this case, the face of a tetrahedron). The

[2] *Kenner76,* Chapter 5.

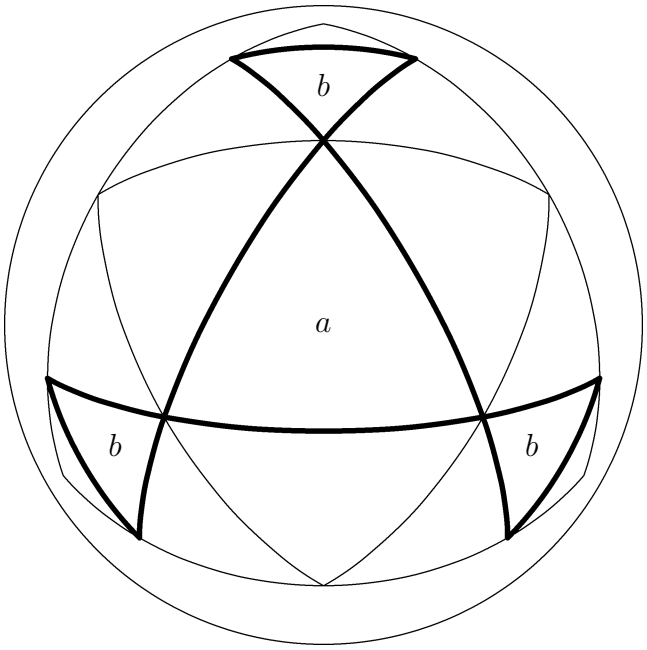

Figure 4.3: 4ν Tetrahedron Face Triangle Projected on to a Sphere

labels a and b indicate which triangles are symmetrically equivalent. The heavy lines represent the lines of the geodesic breakdown used in the tensegrity design. Kenner's procedure is followed and these triangles are projected onto a sphere circumscribing the tetrahedron (see Figure 4.3). Notice that, considering symmetry transformations, there are two types of tendon triangles composing the system, an equilateral tendon triangle and an isosceles one.

Next the interconnecting struts and tendons are introduced. Figure 4.4 shows representative examples of the interconnecting struts. There are two types of strut. One type connects adjacent isosceles triangles, the other type connects isosceles with equilateral triangles. Figure 4.5 shows the corresponding interconnecting tendons. There are a pair of tendons corresponding to each strut type. Note that in both the figures, the triangles have been skewed toward their final positions for clarity's sake. In the tensegrity programming problem, the sum of second powers of the lengths of the four diamond tendons will be minimized, while the lengths of the struts and other tendons will be considered constraints.

4.2.2 Diamond Structures: Mathematical Model

Figures 4.6 and 4.7 show a tetrahedron inscribed within Cartesian coordinate space in a convenient orientation. With this orientation, any symmetry transformation of the tetrahedron can be accomplished merely by permuting the coordinate axes. On the tetrahedral face which falls in the positive quadrant (but extends into three others as well), the elements of the 4ν geodesic subdivisioning relevant to tensegrities have been inscribed. On this triangle, there are four points labeled P_1, P_2, P_3 and P_4. P_1, P_2 and P_3 represent

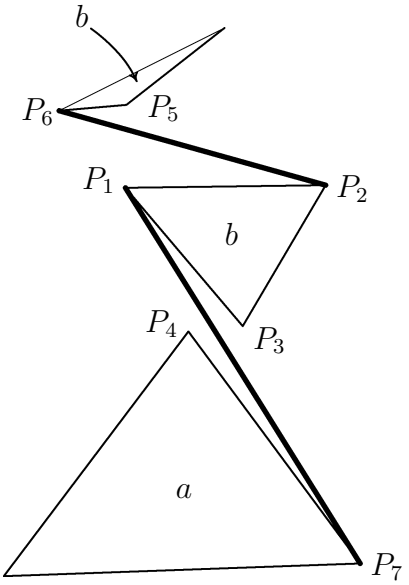

Figure 4.4: 4ν Diamond T-Tetrahedron: Representative Struts

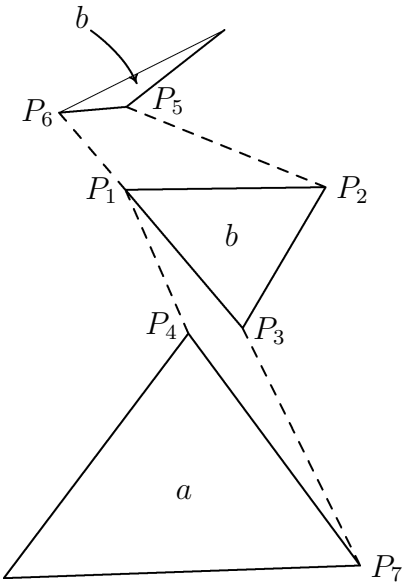

Figure 4.5: 4ν Diamond T-Tetrahedron: Representative Tendons

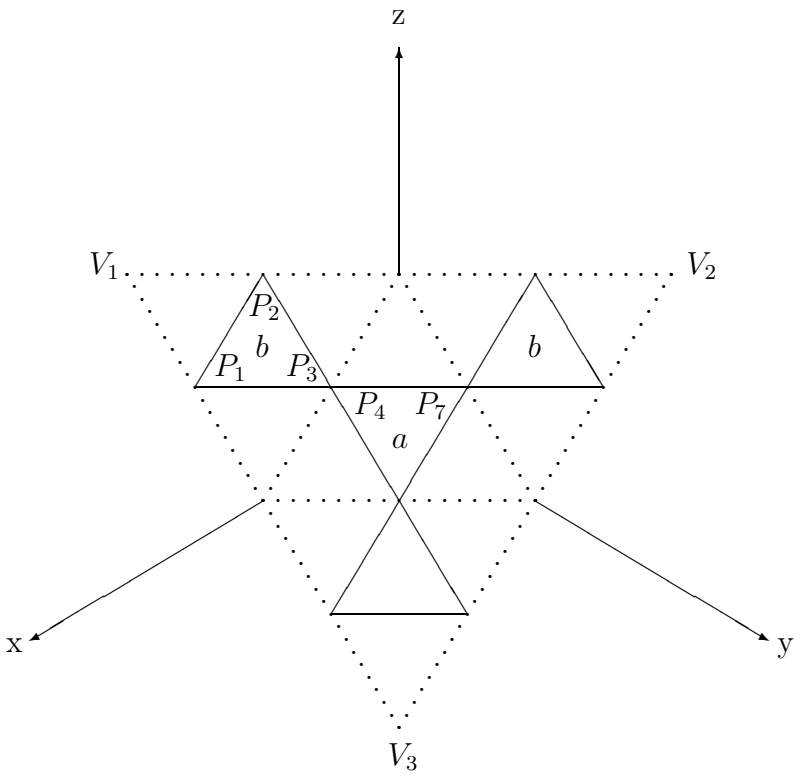

Figure 4.6: 4ν Diamond T-Tetrahedron: Coordinate Model (Face View)

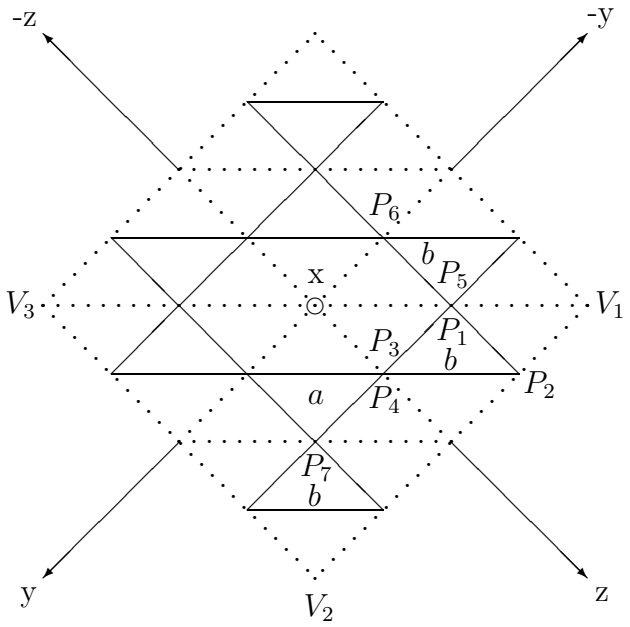

Figure 4.7: 4ν Diamond T-Tetrahedron: Coordinate Model (Edge View)

Vertex	Coordinates x	y	z
V_1	1.0	-1.0	1.0
V_2	-1.0	1.0	1.0
V_3	1.0	1.0	-1.0

Table 4.1: 4ν Diamond T-Tetrahedron: Reference Vertex Coordinates

Point	Coordinates x	y	z
P_1	1.0	-0.5	0.5
P_2	0.5	-0.5	1.0
P_3	0.5	0.0	0.5
P_4	0.5	0.0	0.5

Table 4.2: 4ν Diamond T-Tetrahedron: Point Coordinates

the vertices of the isosceles triangle (or at least it will be isosceles when these points are projected onto a sphere); P_4 is a point on the equilateral triangle.

With these four points, all of the other points of the 4ν subdivisioning can be generated by using the symmetry transforms of the tetrahedron. Notice that, although geodesic structures exhibit mirror symmetry frequently, tensegrity structures generally do not. So P_2 cannot be generated from P_1 using a mirroring operation. Also, initially P_3 and P_4 coincide since initially the vertices of the isosceles and the equilateral triangle are in contact. When the computations start though, they will part company.

The four points, P_1, P_2, P_3 and P_4, can be generated from the three vertex points, V_1, V_2 and V_3, of the triangular tetrahedron face as follows:

$$
\begin{aligned}
P_1 &= \tfrac{3}{4}V_1 + \tfrac{0}{4}V_2 + \tfrac{1}{4}V_3 \\
P_2 &= \tfrac{3}{4}V_1 + \tfrac{1}{4}V_2 + \tfrac{0}{4}V_3 \\
P_3 &= \tfrac{2}{4}V_1 + \tfrac{1}{4}V_2 + \tfrac{1}{4}V_3 \\
P_4 &= \tfrac{2}{4}V_1 + \tfrac{1}{4}V_2 + \tfrac{1}{4}V_3
\end{aligned}
$$

Thus, the coordinates of V_1, V_2 and V_3 summarized in Table 4.1 imply the coordinate values of P_1, P_2, P_3 and P_4 summarized in Table 4.2.

When the values for P_1, P_2, P_3 and P_4 are projected onto the unit sphere, Table 4.3 is

Point	Coordinates x	y	z
P_1	$\sqrt{\frac{2}{3}}$	$-\sqrt{\frac{1}{6}}$	$\sqrt{\frac{1}{6}}$
P_2	$\sqrt{\frac{1}{6}}$	$-\sqrt{\frac{1}{6}}$	$\sqrt{\frac{2}{3}}$
P_3	$\sqrt{\frac{1}{2}}$	0	$\sqrt{\frac{1}{2}}$
P_4	$\sqrt{\frac{1}{2}}$	0	$\sqrt{\frac{1}{2}}$

Table 4.3: 4ν Diamond T-Tetrahedron: Projected Point Coordinates

obtained. These coordinates will serve as the initial values for the computation process. From them the initial values of all member lengths will be computed.

In order to express all the members of the tensegrity, three more points are needed, P_5, P_6 and P_7. These points are symmetry transforms of P_2, P_3 and P_4 respectively. P_5 and P_6 are obtained from P_2 and P_3 by a 120° left-hand rotation of the tetrahedron about the vector from the origin to V_1. In this coordinate system, this is achieved by taking the x axis into the $-y$ axis, the $-y$ axis into the z axis, and the z axis into the x axis, so that P_5 and P_6 can be expressed respectively as $(z_2, -x_2, -y_2)$ and $(z_3, -x_3, -y_3)$.[3] P_7 is obtained from P_4 by a 120° left-hand rotation of the tetrahedron about the vector from the origin to the point $(1.0,\ 1.0,\ 1.0)$. This is achieved by taking the x axis into the z axis, the y axis into the x axis, and the z axis into the y axis, so that P_7 can be expressed as (y_4, z_4, x_4).

So whenever coordinates for P_5, P_6 or P_7 are required, these transformed versions of P_2, P_3 or P_4 will be used. Thus the symmetry constraints of the programming problem are implicitly subsumed in these expressions for P_5, P_6 and P_7. The variables of the programming problem are still limited to the xyz coordinates of the original four points, and no new constraints need to be added to take into account symmetry.

Table 4.4 summarizes the initial lengths for the constrained members obtained using these coordinate values. The relevant mathematical programming problem is:

[3] x_n, y_n and z_n represent the Cartesian coordinates of P_n.

Member #	ID	End Points		Length	Comments
1	t_{12}	P_1	P_2	0.577350	Constraint
2	t_{13}	P_1	P_3	0.517638	Constraint
3	t_{23}	P_2	P_3	0.517638	Constraint
4	t_{47}	P_4	P_7	1.0	Constraint
5	s_{ab}	P_1	P_7	1.414214	Constraint
6	s_{bb}	P_2	P_6	0.919401	Constraint
7	t_{ab1}	P_3	P_7	1.0	To be minimized
8	t_{ab2}	P_1	P_4	0.517638	To be minimized
9	t_{bb1}	P_1	P_6	0.517638	To be minimized
10	t_{bb2}	P_2	P_5	0.577350	To be minimized

Table 4.4: 4ν Diamond T-Tetrahedron: Initial Member Lengths

$$\underset{P_1,P_2,P_3,P_4}{\text{minimize}} \quad o \equiv |P_3-P_7|^2+|P_1-P_4|^2 + |P_1-P_6|^2+|P_2-P_5|^2$$

subject to Tendon constraints:

$$\begin{aligned} \tfrac{1}{3} &\geq |P_1-P_2|^2 \\ \tan\left(\tfrac{\pi}{12}\right) &\geq |P_1-P_3|^2 \\ \tan\left(\tfrac{\pi}{12}\right) &\geq |P_2-P_3|^2 \\ 1 &\geq |P_4-P_7|^2 \end{aligned}$$

Strut constraints:

$$\begin{aligned} -2 &\geq -|P_1-P_7|^2 \\ -0.84529946 &\geq -|P_2-P_6|^2 \end{aligned}$$

This completely specifies the problem. Again, only the coordinates of P_1, P_2, P_3 and P_4 are variables in the minimization process since the coordinates of P_5, P_6 and P_7 are specified to be symmetry transforms of the coordinates of these points.

This is a very formal statement of the problem, and, as stated in Section 3.2, to solve it the inequality constraints are assumed to be met with equality.

4.2.3 Diamond Structures: Solution

As mentioned in Section 3.2, the partials of the constraint equations can be conceived as a matrix, **A**, which has as many rows as their are constraints (6 in this case) and as many columns as there are coordinate values (12 in this case). The ijth element of this matrix,

Variable	Derivative
x_1	-0.875117
x_2	-0.160155
x_3	1.38037
z_3	0.345092
x_4	-0.345093
z_4	0.597720

Table 4.5: 4ν Diamond T-Tetrahedron: Initial Objective Function Derivatives

a_{ij}, is the derivative of the ith member with respect to the jth coordinate value. The coordinate values are numbered in the order they appear, so for example, $a_{4,11}$ is the partial derivative of the second power of the length of the t_{47} tendon with respect to y_4. Its value is $2(y_4 - x_4) + 2(y_4 - z_4)$. This partial is unusual in that it has two terms. Most of the partials are either zero or consist of a single difference.

The first step is to conceptualize this as an unconstrained minimization problem by choosing a subset of the coordinate variables to be dependent variables whose values will be obtained by solving the constraints given the values for the independently specified coordinates. Since there are six constraints, there will be six dependent variables. This leaves six (12-6) independent variables. By coincidence, the number of independent variables is equal to the number of dependent variables in this problem. Using Gaussian elimination with double pivoting on the partial derivative matrix for the system resulted in x_1, x_2, x_3, z_3, x_4 and z_4 being used as the initial independent variables. So, given the values for these variables, the constraints were solved for the remaining dependent variables y_1, z_1, y_2, z_2, y_3 and y_4.

The initial derivatives of the objective function with respect to the independent variables are summarized in Table 4.5. At a minimum point, the values of all these derivatives will be as close to zero as the accuracy of the computations permits. Instead of constantly looking at this whole list of derivatives (which can be very long for a complex structure) to assess how close to a minimum the system is, two summary statistics can be examined, the geometric average of the absolute values of these derivatives, and the variance of the natural logarithm of (the absolute value of) these derivatives. The variance is an important statistic, since if the system starts going singular, one or more of the derivatives will start to diverge from the rest. This singularity is a signal that the partitioning of variables between independent and dependent variables needs to be redone.

The value of the objective function was initially 1.86923. The system was solved using the parallel tangent technique which resulted in an objective function value of 1.65453. Table 4.6 summarizes the corresponding point values, and Table 4.7 summarizes the lengths of the members in the objective function thus obtained.

This would be the end of the calculations, except that when the endogenous member forces

Point	Coordinates		
	x	y	z
P_1	0.887555	-0.438450	0.455646
P_2	0.677306	-0.505030	0.989215
P_3	0.614181	-0.076748	0.705421
P_4	0.710900	-0.048791	0.590190

Table 4.6: 4ν Diamond T-Tetrahedron: Preliminary Coordinate Values

Member ID	Length
t_{ab1}	0.940409
t_{ab2}	0.448489
t_{bb1}	0.455651
t_{bb2}	0.601166

Table 4.7: 4ν Diamond T-Tetrahedron: Preliminary Objective Member Lengths

are calculated, they indicate that "tendon" t_{12} is marginally in compression (see Table 7.1). This problem stems from the substitution of equalities for inequalities in the constraints. If inequalities had been used, this particular constraint would be found to be not effective. At this point the problem was dealt with by eliminating the member from the constraints (which means the tendon won't appear in the final structure).[4] Eliminating this constraint also means a new selection of independent variables needs to be made since seven are now needed. Repartitioning resulted in z_1 being added to the independent variables. Using the parallel tangent technique on this problem resulted in a final objective function value of 1.65174. Table 4.8 summarizes the corresponding point values; Table 4.9 summarizes the objective function member lengths, and Figure 4.8 shows the final design where the location of the omitted tendon is indicated by a dashed line.

[4]Alternatively, its length could have been shortened until it was effective.

Point	Coordinates		
	x	y	z
P_1	0.874928	-0.442843	0.484207
P_2	0.675644	-0.506061	0.981906
P_3	0.602311	-0.068420	0.715369
P_4	0.699892	-0.049794	0.605188

Table 4.8: 4ν Diamond T-Tetrahedron: Final Coordinate Values

Member ID	Length
t_{ab1}	0.937671
t_{ab2}	0.446946
t_{bb1}	0.473042
t_{bb2}	0.590748

Table 4.9: 4ν Diamond T-Tetrahedron: Final Objective Member Lengths

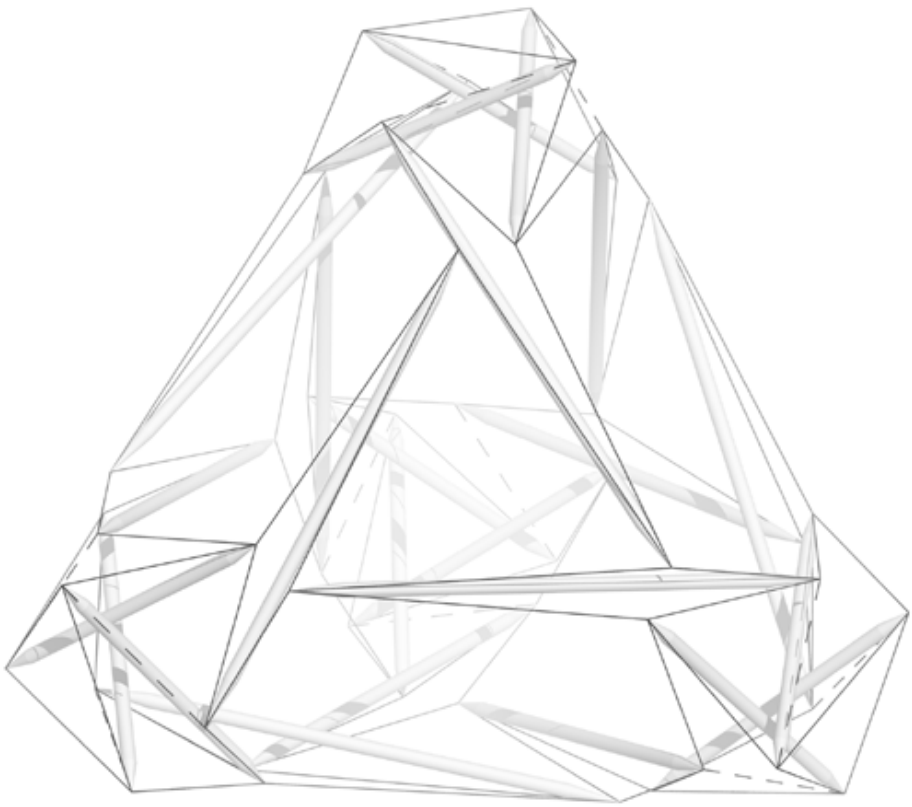

Figure 4.8: 4ν Diamond T-Tetrahedron: Final Design

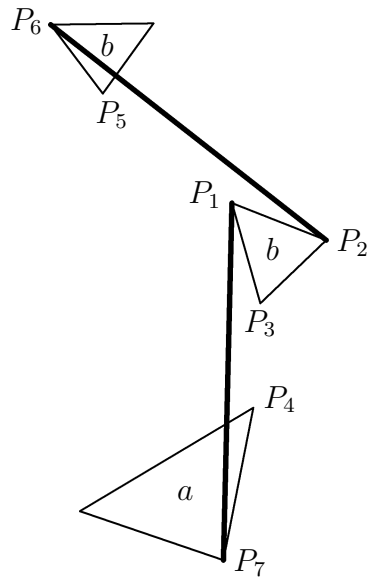

Figure 4.9: 4ν Zig-Zag T-Tetrahedron: Representative Struts

4.3 Zig-Zag Structures

4.3.1 Zig-Zag Structures: Descriptive Geometry

A zig-zag structure retains the struts and tendon triangles of the corresponding diamond structure; however, now adjacent tendon triangles are interconnected with only one tendon instead of two. This single tendon connects the "noses" of the two tendon triangles. Examination of the structure from the struts' point of view shows each strut is traversed by a "zig-zag" of three tendons. The simplest zig-zag tensegrity is the t-tetrahedron examined in Section 2.4 (Figure 2.8). Again, since more complex zig-zag structures are not amenable to the treatment used in that simple structure, the general procedure will be illustrated using the zig-zag version of the 4ν t-tetrahedron examined in Section 4.2.

Figures 4.9 and 4.10 respectively show representative examples of the interconnecting struts and tendons. In these figures, the model has been expanded so that the struts are longer than in the initial geodesic calculation, while the tendon triangles remain the same size. This is done since, in the initial configuration, the noses of the tendon triangles touch each other and so the interconnecting zig-zag tendons have zero length. Expanding the structure without increasing the sizes of the tendon triangles gives the interconnecting tendons a non-zero length. The lengths of these tendons can be minimized to get a valid tensegrity. In the initial configuration, these tendons are certainly of minimum length, and

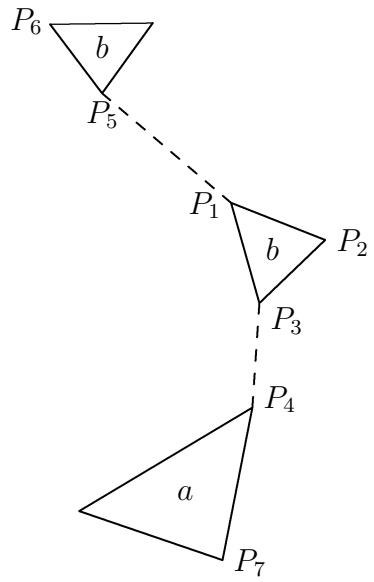

Figure 4.10: 4ν Zig-Zag T-Tetrahedron: Representative Tendons

Member #	ID	End Points		Comments
7	t_{ab}	P_3	P_4	To be minimized
8	t_{bb}	P_1	P_5	To be minimized

Table 4.10: 4ν Zig-Zag T-Tetrahedron: Zig-Zag Tendon End Points

the structure is theoretically a tensegrity in that configuration, but practically it isn't an interesting solution since the s_{bb} strut and its transformations intersect each other.

4.3.2 Zig-Zag Structures: Mathematical Model

The list of points is the same as that in Section 4.2.2, as is the list of constrained members. To avoid the problem of ending up with a solution in which the minimum of the objective is zero, the struts s_{ab} and s_{bb} are lengthened from $\sqrt{2}$ and 0.919401 to 2 and $\sqrt{3}$ respectively. In the objective function the diamond tendons of Section 4.2.2, t_{ab1}, t_{ab2}, t_{bb1} and t_{bb2}, are replaced by the zig-zag tendons t_{ab} and t_{bb}. As mentioned, their initial lengths are zero. Table 4.10 enumerates the end points of these additional members.

The relevant mathematical programming problem becomes:

$$\begin{array}{lll} \underset{P_1,P_2,P_3,P_4}{\text{minimize}} & \text{o} & \equiv \quad |P_3 - P_4|^2 + |P_1 - P_5|^2 \end{array}$$

subject to Tendon constraints:

$$\begin{array}{ccc} \frac{1}{3} & \geq & |P_1 - P_2|^2 \\ \tan\left(\frac{\pi}{12}\right) & \geq & |P_1 - P_3|^2 \\ \tan\left(\frac{\pi}{12}\right) & \geq & |P_2 - P_3|^2 \\ 1 & \geq & |P_4 - P_7|^2 \end{array}$$

Strut constraints:

$$\begin{array}{ccc} -4 & \geq & -|P_1 - P_7|^2 \\ -3 & \geq & -|P_2 - P_6|^2 \end{array}$$

As before, only the coordinates of P_1, P_2, P_3 and P_4 are variables in the minimization process since the coordinates of P_5, P_6 and P_7 are specified to be symmetry transforms of the coordinates of these points. Also, all inequality constraints are assumed to be met with equality.

4.3.3 Zig-Zag Structures: Solution

With the increased lengths of the struts, the initial values used for the problem no longer satisfy the constraints. With the best partitioning of the system (that used in Section 4.2.3), Newton's method diverges when it is applied to the system to solve the constraint equations. So, in this case, the penalty formulation was used with a penalty value of $\overline{\mu} = 10^5$. The problem thus becomes:

$$\begin{array}{ll} \underset{P_1,P_2,P_3,P_4}{\text{minimize}} & |P_3 - P_4|^2 + |P_1 - P_5|^2 + \overline{\mu}[\tfrac{1}{3} - |P_1 - P_2|^2]^2 + \\ & \overline{\mu}[\tan\left(\frac{\pi}{12}\right) - |P_1 - P_3|^2]^2 + \overline{\mu}[\tan\left(\frac{\pi}{12}\right) - |P_2 - P_3|^2]^2 + \\ & \overline{\mu}[1 - |P_4 - P_7|^2]^2 + \overline{\mu}[4 - |P_1 - P_7|^2]^2 + \overline{\mu}[3 - |P_2 - P_6|^2]^2 \end{array}$$

Ten iterations of the method of Fletcher-Reeves were applied to the modified objective function. These iterations brought the constraints close enough to a solution that the penalty formulation could be discarded for the exact formulation. Another ten iterations of Fletcher-Reeves brought the system to a solution.

The final values for the lengths of members in the objective function are summarized in Table 4.11. The corresponding point values are summarized in Table 4.12.

The value of the objective function was 1.03848. In this structure, there was no problem with non-effective constraints as there was in the previous structure. Figure 4.11 shows the final design.

Member ID	Length
t_{ab}	0.579238
t_{bb}	0.838431

Table 4.11: 4ν Zig-Zag T-Tetrahedron: Final Objective Member Lengths

Point	Coordinates		
	x	y	z
P_1	1.374465	-0.537613	1.081334
P_2	1.008191	-0.399971	1.505871
P_3	1.314861	-0.058122	1.267036
P_4	1.067078	0.464915	1.243542

Table 4.12: 4ν Zig-Zag T-Tetrahedron: Final Coordinate Values

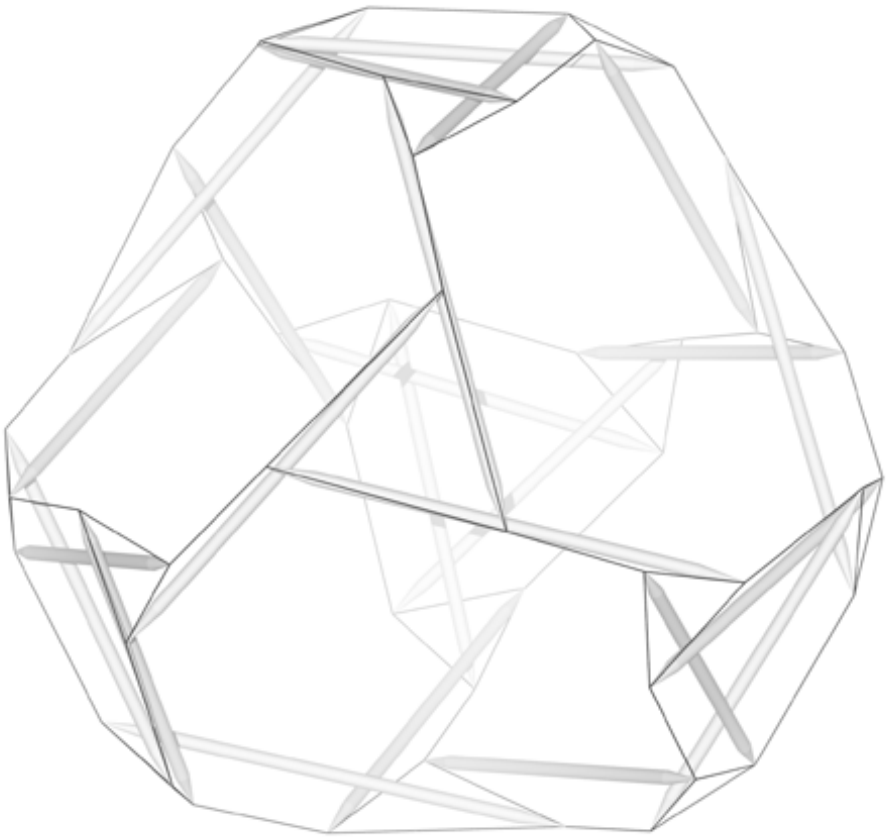

Figure 4.11: 4ν Zig-Zag T-Tetrahedron: Final Design

Chapter 5

Double-Layer Tensegrities

5.1 Double-Layer Tensegrities: Introduction

For most of the tensegrities discussed so far, the tensile members compose a single continuous spherical layer.[1] Such structures are resilient, but are not very rigid and tend to vibrate too much for many practical applications. Also, it seems likely that large-frequency realizations of these structures, as can happen with geodesic domes, will have little resistance to concentrated loads, so that it would be difficult to suspend substructures from the their roofs, and they might cave in excessively under an uneven load like snow.

These considerations are a strong motivation for the development of a space truss configuration for tensegrity structures. Such a configuration would be analogous to the space truss arrangements developed for the geodesic dome, like the Kaiser domes of Don Richter,[2] or Fuller and Sadao's Expo '67 Dome[3] and serve the same purpose. Tensegrity space trusses are characterized by an outer **and** inner shell of tendons interconnected by a collection of struts and tendons. The result is a more rigid structure which is more resistant to concentrated loads.

Designs for tensegrity trusses have been developed in a planar context by several authors. The trusses described in this book, especially the geodesic one described in Section 5.3, are akin to those experimented with by Kenneth Snelson in the 1950's.[4] Appendix A compares the truss of Section 5.3 with an example of another similar approach to tensegrity trusses by different authors.

In Section 5.2, a general approach to the design of tensegrity trusses is outlined. Then, in Sections 5.3 and 5.4, two examples are given of geometries which implement this approach. The second example demonstrates incidentally how icosahedral symmetries can be handled

[1] The only exception is the t-prism of Section 2.2 which has a more cylindrical shape.
[2] *Fuller73,* pp. 62-63, 224-227.
[3] *Kenner76,* p. 115.
[4] See photos in *Lalvani96,* p. 48.

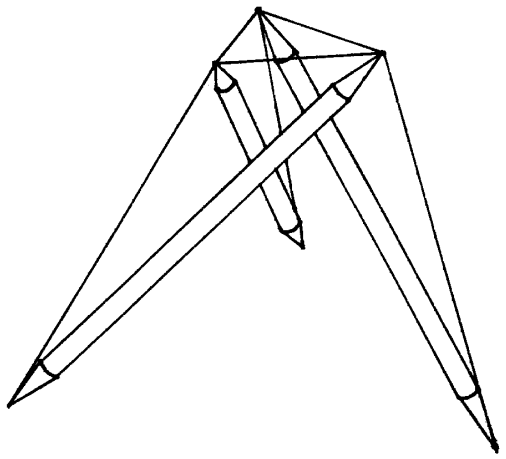

Figure 5.1: Tensegrity Tripod

within the Cartesian framework.

5.2 Double-Layer Tensegrities: Trusses

Take the finished t-prism introduced in Section 2.2 and remove the triangle of tendons corresponding to one of the ends. When pressed towards each other, the three free strut ends will strongly resist the effort and stay apart. This composite compression member, a tensegrity tripod or t-tripod, can thus be attached to three hubs of a tensegrity structure and keep them apart. It is illustrated in Figure 5.1. When used to support a single-layer tendon network, the t-tripods' struts will be outside the layer containing the three hubs, thus eliminating the intractable interference problems that can result in larger structures when simple two-hubbed struts lie in the same layer which they support.

Let the single-layer network supported by the t-tripods be spherical and composed of vertex-connected polylaterals.[5] No more than one vertex is shared between adjacent polylaterals, and every vertex is shared by exactly two polylaterals. The apexes of the t-tripods could point out or in, but assume they point out. In addition to the continuous single-layer spherical network, there will be a discontinuous outer network formed by the

[5]The term "polylateral" is used rather than polygon since a polygon is planar and the figure referenced here may not be. The polylateral concept envisions a ring of vertexes, each vertex corresponding to a hub in a tensegrity. The vertexes in the ring are continuously connected pair-wise by edges, each edge corresponding to a tendon in a tensegrity. Each edge connects two vertexes, and each vertex is connected to two edges. Flattening a polylateral would yield the boundary of a polygon, and a triangular polylateral is distinguished by the fact that it can always be considered the boundary of a polygon, the triangle. Fuller uses the term "polyvertexion" as an operational substitute for polyhedron with qualifications that seem applicable here as well. See *Fuller92,* pp. 130-131, Fig. 6.6 (p. 132) and p. 233.

tendon triangles of the apexes of the t-tripods being used as compression members. Call these apex tendons the **outer convergence** tendons, and call the t-tripod tendons connecting these triangles with the opposite ends of the t-tripod's struts the **primary interlayer** tendons.

To lend more stability to the structure, the outer network is completed by binding together the t-tripod apexes using another set of tendons called the **outer binding** tendons. Let the outer network have exactly the same topology as the inner network though of course the lengths of the outer network's tendons will be different. Untwisting a t-tripod removes the three free ends of the t-tripod even further from each other. Thus, if possible, the outer convergences should be bound together in such a way that tensioning the outer binding tendons untwists the t-tripods. In this way, while the outer network of tendons presses in, the inner network will press out under the impetus of its expanding compression members, the untwisting t-tripods.

When the struts meet on the inner network, they form convergences where struts from several different t-tripods are connected together with tendons that form a polylateral. These tendons are the **inner convergence** tendons and topologically they are equivalent to the outer binding tendons. The remaining tendons of the inner network are the **inner binding** tendons whose polygons alternate with those of the inner convergence tendons. They are topologically equivalent to the outer convergence tendons, which means they are triangles in this example.

A t-prism doesn't need to be based on a triangle; any polygon will do, and eliminating the tendons on one end will generate a "t-polypod" which can be used just like the t-tripod as a complex compression member to support a tendon network. Close examination of the tendons of an inner convergence will show that, in conjunction with the converging struts, they form an inward-pointing t-polypod when the appropriate tendons are added connecting the convergence polygon to the opposite ends of the struts. These connecting tendons are the **secondary interlayer** tendons and complete the truss network.

With this method of generating a tensegrity truss, the topology of the inner and outer layers will not only need to be identical, the tendon triangles and polygons which make up each layer will need to be divisible into two groups which alternate. A triangle or polygon from one group will need to be completely surrounded by polygons from the other group. An identical truss could have been generated by starting with the inward-pointing t-polypods supporting a complete outer network and then binding their apexes together and adding interlayer tendons to generate the outward-pointing t-tripods.

The end result is a rigid tensegrity space frame aimed at extremely large-scale applications like the covering of entire settlements or the superstructure of a space station. Though it is possible to have polylaterals alternating with polylaterals in the spherical network instead of one of the sets of polylaterals being restricted to triangles, an emphasis on triangles may yield a more rigid structure. The complexity of this tensegrity will require that designs be checked carefully to make sure struts and tendons have sufficient clearance and that member forces are appropriate, i.e. tendons are in tension and struts are in compression.

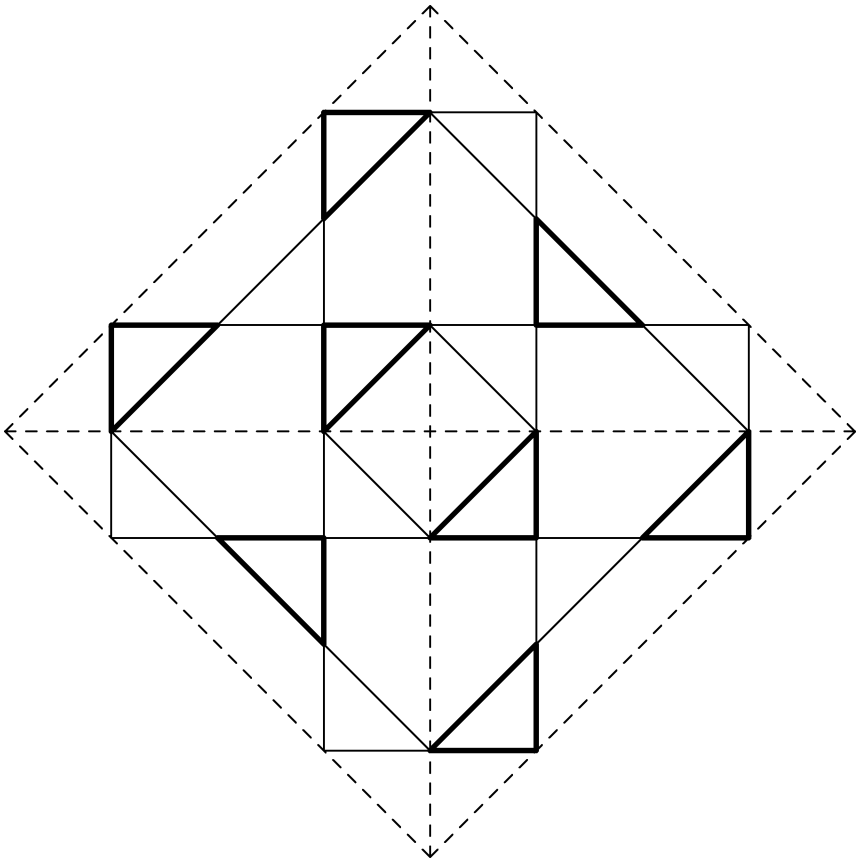

Figure 5.2: 4ν Octahedron: Alternating Triangles (Vertex View)

5.3 Double-Layer Tensegrities: Geodesic Networks

A network topology suitable for tensegrity designs can be obtained from an even-frequency Class I subdivision of the triangular faces of the tetrahedron, octahedron or icosahedron. Alternatively, Class II subdivisions of these same polyhedra can be used if the frequency is a multiple of four.[6] Network topologies generated this way are referred to as geodesic networks since they are based on subdivision systems used to design geodesic domes. A Class I subdivision was illustrated in Figure 4.2. Only Class I subdivisions are used in this book.

A 4ν breakdown of the octahedron serves for the example of this method of generating tensegrity trusses. The portion of this breakdown relevant to tensegrity structures is shown in Figure 5.2. The breakdown triangles are shown with solid lines, and the edges of the base octahedron are shown as dashed lines.

The first step in constructing the tensegrity is to divide the resulting network into two sets of alternating triangles. In Figure 5.2, one set is shown with light solid lines, and the other

[6]See *Kenner76,* Chapter 7, for a discussion of Class I and Class II subdivisions.

set is shown with heavy solid lines. A triangle of one set is adjacent only to triangles of the other set. This alternation requirement was mentioned in Section 5.2 and here means only geodesic subdivisions of the octahedron can be used. The tetrahedron and icosahedron are excluded since their odd three- and five-fold symmetries don't permit the required alternating classification of the triangles. The exclusive use of the octahedron makes the computational work simpler since, as mentioned in Section 2.3, the symmetries of the octahedron are very easily expressed in the Cartesian framework.

Here both the inwardly- and outwardly-pointing t-polypods mentioned in Section 5.2 are t-tripods. The placement of the struts is chosen to maximize the untwisting effect mentioned in Section 5.2. It differs from the usual way of threading struts between adjacent triangles in single layer tensegrities.

The truss is shown graphically in Figure 5.6. The fact that only t-tripods appear in the structure gives the struts more effectiveness. They overlap less than they would if there were t-polypods of greater frequency, so the set of struts covers more area. Since the struts will in general be the most expensive component, this is a desirable feature. Also, having t-tripods everywhere rather than higher-frequency t-polypods enhances the stiffness of the structure since triangles can't distort like other polylaterals.

Figure 5.3 is a schematic which shows the identity symmetry region corresponding to the structure along with portions of the other symmetry regions that surround it. Figure 5.4 shows how the symmetry regions appear when drawn on the base octahedron. The borders of the symmetry regions appear as dotted lines in Figure 5.3 and Figure 5.4. The points labeled A and B correspond to the centers of two adjacent octahedral triangles. Arrows are used to indicate the coordinate axes within the context of each of these triangles. In Figure 5.3, the numbers in circles indicate the correspondence of each region to a symmetry transformation in Table 5.5, and the position of each point is labeled with its number.

Due to the alternating triangles, the symmetry region for a double-layer tensegrity is twice the size of that for the corresponding single-layer tensegrity. The single-layer tensegrity's symmetry region is one third of an octahedral face, so the double-layer symmetry region is the union of one third of one octahedral face with one third of an adjacent face. The symmetry region for a geodesic is one sixth of an octahedral face since geodesics also exhibit reflective symmetry while single-layer tensegrities based on geodesic subdivisions don't.

Figure 5.3 also shows visually how the point correspondences of Table 5.6 are derived. For example, P_6 is at the same position[7] in symmetry region 2 as P_3 is in symmetry region 1. This means point 6 can be obtained by applying symmetry transformation 2 to point 3.

Figure 5.5 indicates the positions of the basic struts which compose the structure. An arrow in the center of each strut indicates the direction from the outer point to which the strut is connected to the inner point to which the strut is connected. These struts are clustered around two basic t-tripods whose centers are indicated with circles.

[7]In Figures 5.3 and 5.5, 6 rather than P_6 is used to mark the position of P_6 since it marks the position of both P_6 and P_6'.

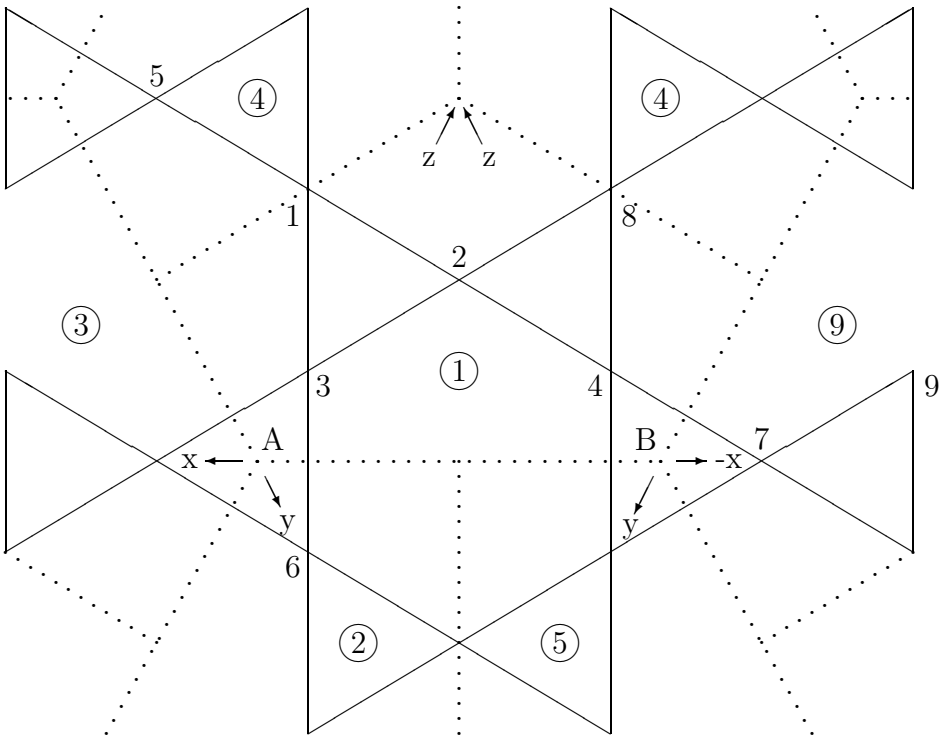

Figure 5.3: 4ν T-Octahedron Sphere: Symmetry Regions

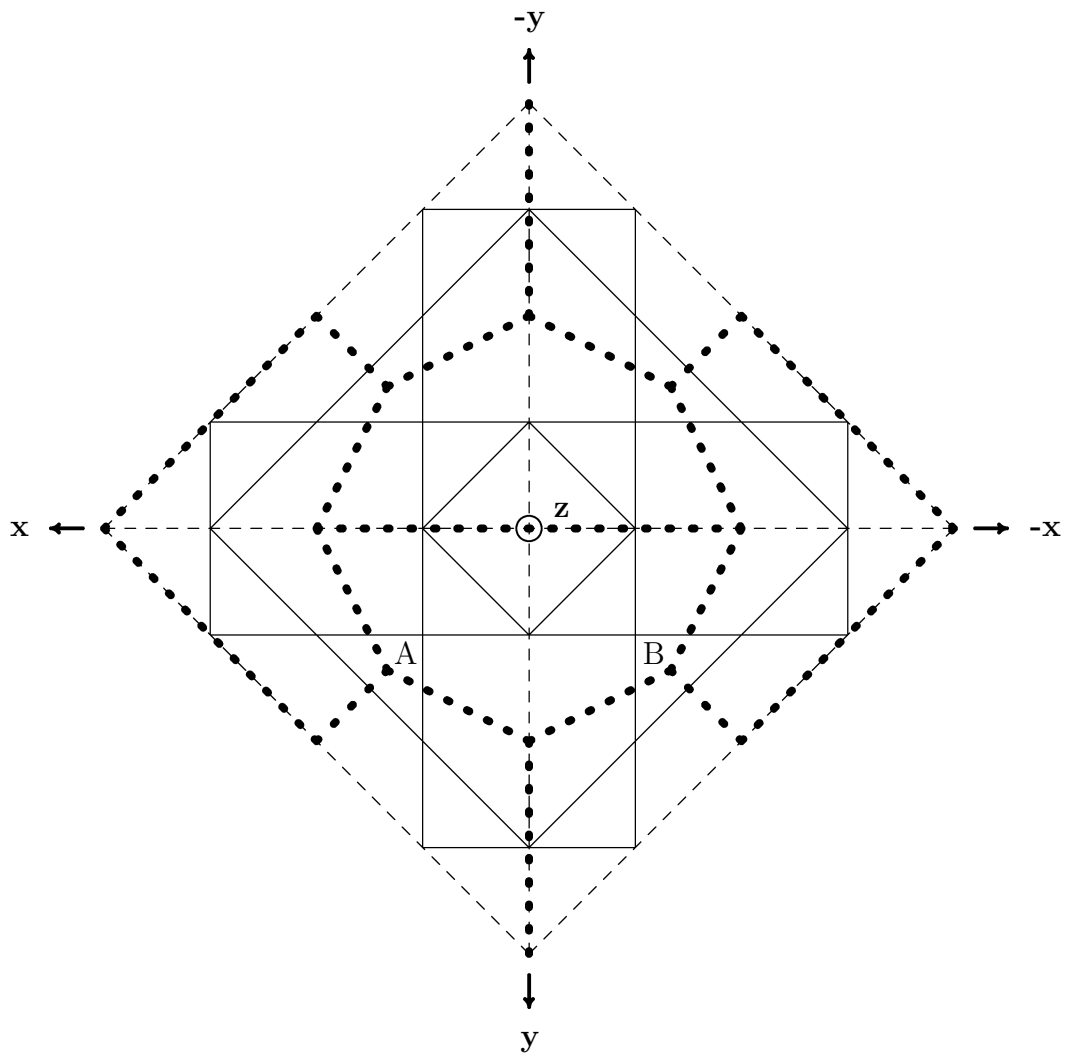

Figure 5.4: 4ν Octahedron: Double-Layer Symmetry Regions

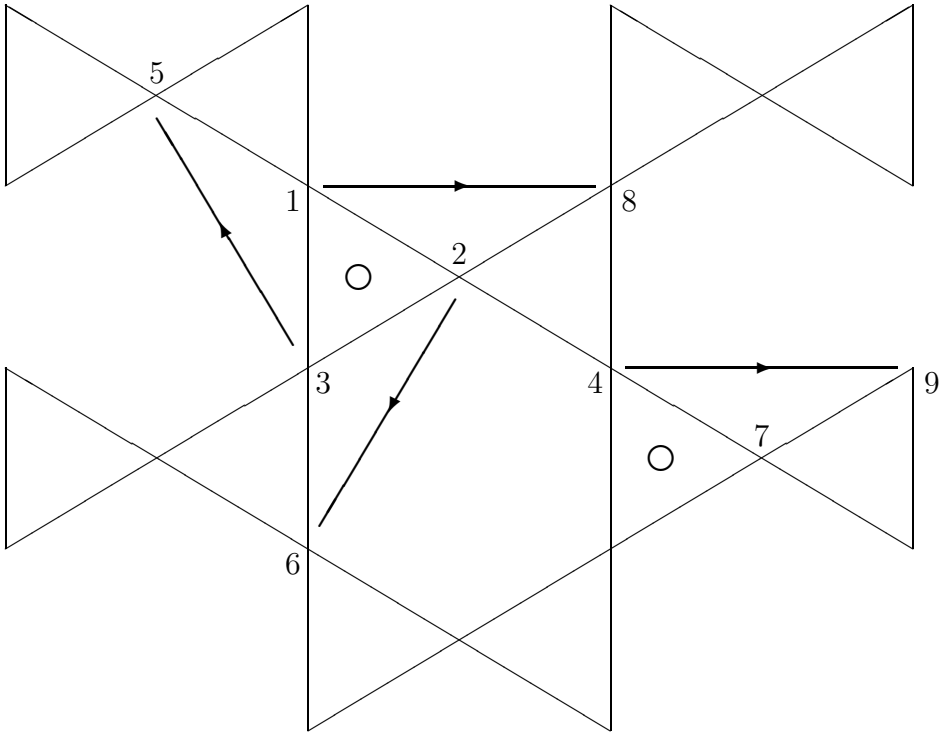

Figure 5.5: 4ν T-Octahedron Sphere: Truss Members

Table 5.1 enumerates the members of this structure. The end points of each member are shown along with its weight (if it will appear in the objective function) or its length (if it is a constraint). Outer points are indicated with the same labels as the corresponding inner points except that the labels of the outer points have a prime mark.

The inner and outer tendon networks are generated by projecting the alternating triangles of Figure 5.2 onto concentric spheres. This allows Kenner's tables[8] to be used to generate initial point coordinates. The radius of the inner network (2.0) was chosen so that the inner tendon lengths were all approximately 1.0, and the radius of the outer network (4.0) was chosen to yield strut lengths of approximately 3.0. Since this tensegrity doesn't share the mirror symmetry of geodesic structures, Kenner's table had to be expanded by rotating all the points about the z axis by 90°. This corresponds to increasing the value of what is there called ϕ (here it is called θ in accordance with the standard practice) by 90°.

Table 5.2 outlines the correspondence between the basic points and Kenner's coordinate system (rotated points are indicated with an asterisk). The resulting coordinate values for the inner and outer points are summarized in Table 5.3. The realized initial lengths are summarized in Table 5.4.

The symmetry transformations for any double-layer t-octahedron are enumerated in Table 5.5. It shows how the coordinates of a symmetry point are derived from those of a basic point under each possible transformation. The derivation of the symmetry points from the basic points is shown in Table 5.6. Outer points follow the same symmetries as inner points.

The strategy for computing the structure was to minimize a weighted[9] combination of the interlayer and binding tendons subject to constraints on the struts and convergence tendons. An initial iteration was done using the penalty formulation ($\overline{\mu} = 10^5$) in conjunction with PARTAN since an exact approach would have had difficulty given the divergence between the initial values and the constraints. After this four iterations were done with the exact formulation in conjunction with PARTAN to bring the values to convergence. The derivatives of the objective function with respect to the independent variables were all less than 10^{-6}. The coordinates selected to be independent variables were x_1, z_2, y_3, z_4, x'_1, z'_1, z'_2, x'_3, y'_3, z'_3, x'_4 and y'_4.

Table 5.7 shows the values for the final lengths and relative forces (see Chapter 7 for the method of computing relative forces); Table 5.8 shows the final values for the coordinates of the basic points, and Figure 5.6 shows the final design.

[8] *Kenner76,* "Octahedron Class I Coordinates: Frequencies 8, 4, 2", column 4ν, p. 128.
[9] The weights used are shown in Table 5.1.

Member #	End Points		Weight	Constrained Length	Comments
1	P'_1	P_8	N/A	3.0	Struts
2	P'_2	P_6	N/A	3.0	
3	P'_3	P_5	N/A	3.0	
4	P'_4	P_9	N/A	3.0	
5	P'_2	P_8	2.0	N/A	Primary Interlayer Tendons
6	P'_3	P_6	2.0	N/A	
7	P'_1	P_5	2.0	N/A	
8	P'_7	P_9	2.0	N/A	
9	P'_1	P_2	2.0	N/A	Secondary Interlayer Tendons
10	P'_2	P_3	2.0	N/A	
11	P'_3	P_1	2.0	N/A	
12	P'_4	P_7	2.0	N/A	
13	P'_1	P'_2	N/A	1.0	Outer Convergence Tendons
14	P'_2	P'_3	N/A	1.0	
15	P'_3	P'_1	N/A	1.0	
16	P'_4	P'_7	N/A	1.0	
17	P'_2	P'_8	0.4	N/A	Outer Binding Tendons
18	P'_3	P'_6	0.4	N/A	
19	P'_1	P'_5	0.4	N/A	
20	P'_7	P'_9	0.4	N/A	
21	P_1	P_2	1.0	N/A	Inner Binding Tendons
22	P_2	P_3	1.0	N/A	
23	P_3	P_1	1.0	N/A	
24	P_4	P_7	1.0	N/A	
25	P_2	P_8	N/A	1.0	Inner Convergence Tendons
26	P_3	P_6	N/A	1.0	
27	P_1	P_5	N/A	1.0	
28	P_7	P_9	N/A	1.0	

Table 5.1: 4ν T-Octahedron: Truss Members

Point	Kenner's Label	Coordinates θ	ϕ
P_1 (P'_1)	1,0	0.0	18.4349488
P_2 (P'_2)	1,1	90.0	18.4349488
P_3 (P'_3)	2,1	45.0	35.2643897
P_4 (P'_4)	2,1*	135.0	35.2643897

Table 5.2: 4ν T-Octahedron: Angular Point Coordinates

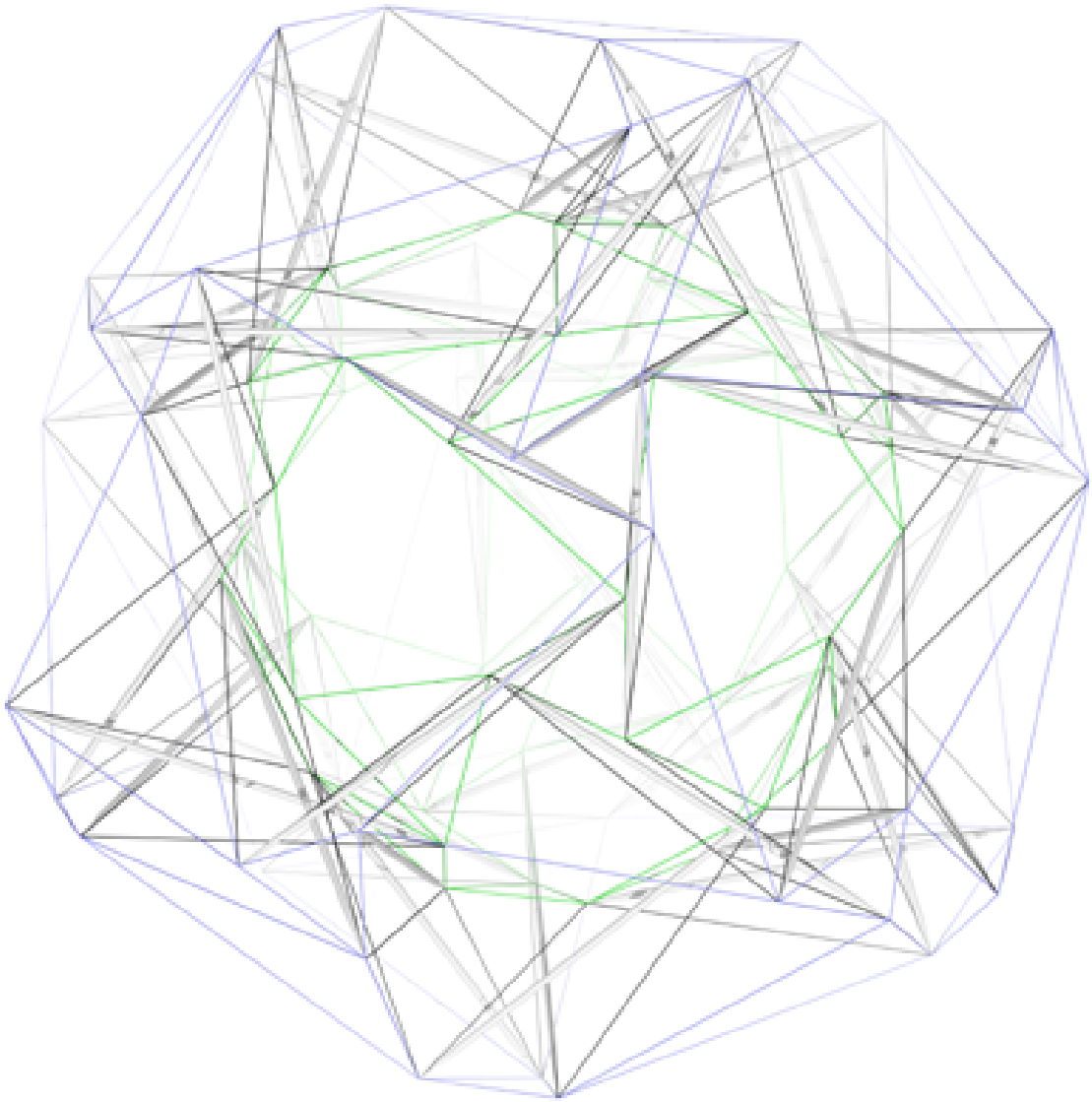

Figure 5.6: 4ν T-Octahedron: Final Design

Point	Coordinates x	y	z
P_1	0.632456	0.000000	1.897367
P_2	0.000000	0.632456	1.897367
P_3	0.816497	0.816497	1.632993
P_4	-0.816497	0.816497	1.632993
P'_1	1.264911	0.000000	3.794733
P'_2	0.000000	1.264911	3.794733
P'_3	1.632993	1.632993	3.265986
P'_4	-1.632993	1.632993	3.265986

Table 5.3: 4ν T-Octahedron: Initial Basic Point Coordinates

5.4 Double-Layer Tensegrities: Hexagon/Triangle Networks

A second approach to designing tensegrity trusses relies on networks which have triangles alternating with hexagons and pentagons, rather than triangles alternating with triangles as with the first approach. An advantage of this approach over the approach of Section 5.3 is that it works with all symmetries. Geodesic breakdowns of the tetrahedron, octahedron, icosahedron, cube, rhombic dodecahedron or triacontahedron can be used.

Geodesic networks are used here only as a first step in the derivation of a network. In the geodesic network's triangles, attention is now placed on the hexagons which fill up the gaps between the triangles. Thus, these triangles and the gaps between them form a system of alternating triangles and hexagons except at the vertices of the base polyhedron where a triangle, square or pentagon will be substituted for a hexagon.

For an example, see Figure 5.7 which illustrates a 2ν icosahedron. At this low frequency, the single triangles on each icosahedral face surround pentagonal gaps which correspond to the vertices of the base icosahedron. At higher frequencies, hexagonal gaps would appear on the edges (as in Figure 4.2) and/or the faces of the base polyhedron. At high frequencies, the hexagonal gaps dominate since the occasional pentagonal, square or triangular gaps only appear at the vertices of the base polyhedron. Hence, the final network is referred to as a "hexagon/triangle" network even though at the lowest 2ν frequency hexagons don't appear at all.

This recontextualized geodesic network is not suitable for a t-tripod-based tensegrity truss though since adjacent polylaterals share edges rather than just points. A suitable network can easily be constructed though by inscribing a smaller version of each polylateral within that polylateral by connecting the midpoints of its sides appropriately. This technique is illustrated for the 2ν icosahedron in Figure 5.8.

Member #	Length
1	2.683281
2	3.109991
3	3.055050
4	3.109990
5	2.366432
6	2.581988
7	2.353904
8	2.353903
9	2.366432
10	2.353904
11	2.353903
12	2.581988
13	1.788854
14	1.755484
15	1.755484
16	2.309401
17	1.788854
18	2.309401
19	1.755484
20	1.755484
21	0.894428
22	0.877743
23	0.877743
24	1.154700
25	0.894428
26	1.154700
27	0.877743
28	0.877743

Table 5.4: 4ν T-Octahedron: Initial Member Lengths

Transform Number	x	y	z
1	x	y	z
2	y	z	x
3	z	x	y
4	$-x$	$-y$	z
5	$-y$	z	$-x$
6	z	$-x$	$-y$
7	$-x$	y	$-z$
8	y	$-z$	$-x$
9	$-z$	$-x$	y
10	x	$-y$	$-z$
11	$-y$	$-z$	x
12	$-z$	x	$-y$

Table 5.5: T-Octahedron: Symmetry Transformations

	Coordinates			Basic	Transform
Point	x	y	z	Point	Number
P_5	$-x_4$	$-y_4$	z_4	P_4	4
P_6	y_3	z_3	x_3	P_3	2
P_7	$-z_4$	$-x_4$	y_4	P_4	9
P_8	$-x_1$	$-y_1$	z_1	P_1	4
P_9	$-z_2$	$-x_2$	y_2	P_2	9

Table 5.6: 4ν T-Octahedron: Symmetry Point Correspondences

Member #	Length	Relative Force
1	3.000000	-11.992
2	3.000000	-12.042
3	3.000000	-11.648
4	3.000000	-11.991
5	2.443023	4.886
6	2.436281	4.873
7	2.495792	4.992
8	2.422962	4.846
9	2.074289	4.149
10	2.068446	4.137
11	2.080869	4.162
12	2.046919	4.094
13	1.000000	3.443
14	1.000000	6.359
15	1.000000	3.112
16	1.000000	4.691
17	2.634124	1.054
18	2.651139	1.060
19	2.904639	1.162
20	2.885858	1.154
21	1.203002	1.203
22	1.252409	1.252
23	1.323913	1.324
24	1.292575	1.293
25	1.000000	4.981
26	1.000000	6.311
27	1.000000	4.638
28	1.000000	8.543

Table 5.7: 4ν T-Octahedron: Final Member Lengths and Forces

Point	Coordinates		
	x	y	z
P_1	1.010025	-0.112004	1.942398
P_2	-0.067774	0.387035	2.133503
P_3	0.769352	1.139748	1.584713
P_4	-0.712330	1.046316	1.746339
P'_1	1.569404	0.631114	3.383602
P'_2	0.616675	0.818931	3.622416
P'_3	1.177704	1.533667	3.204803
P'_4	-1.699080	2.137517	2.514813

Table 5.8: 4ν T-Octahedron: Final Basic Point Coordinates

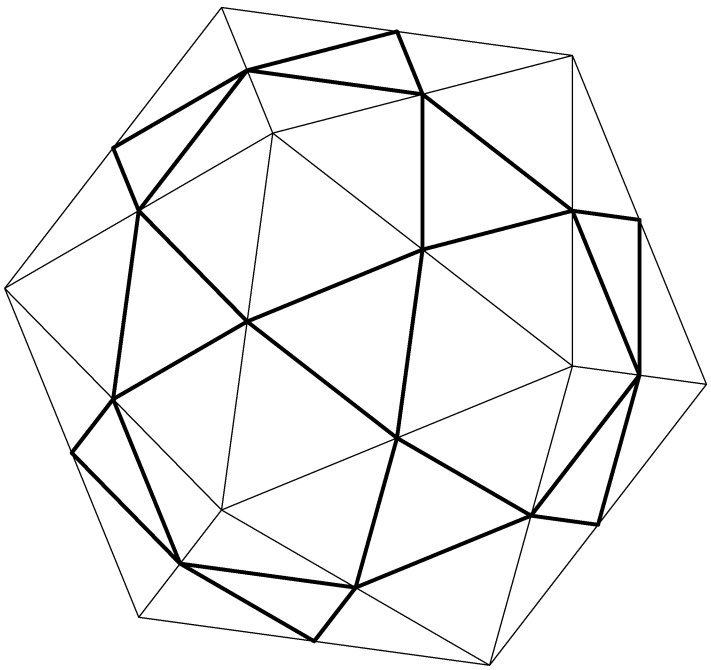

Figure 5.7: 2ν Icosahedron

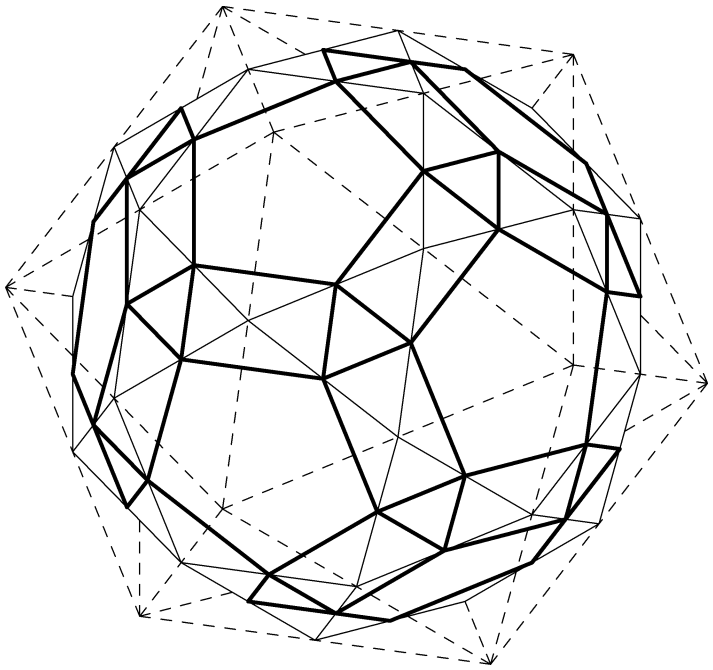

Figure 5.8: Hexagon/Triangle Tensegrity Network Inscribed in a 2ν Icosahedron

As in Section 5.3, this network is projected on a sphere and duplicated to form an inner and outer network. The triangles on the outer network form the apexes of outwardly-pointing t-tripods (the outer convergence triangles), while the hexagons on the outer network form the tendons which bind them together (the outer binding hexalaterals). On the inner sphere, the hexalaterals form the apexes of inwardly-pointing t-hexapods (the inner convergence hexalaterals), and the triangles form the tendons which bind them together (the inner binding triangles). The struts and their corresponding tendons (the primary and secondary interlayer tendons) connect the triangles on the outer network with the hexalaterals on the inner network. As before, struts are placed so that the untwisting effect of the binding tendons is enhanced.

Figure 5.9 illustrates this network as represented in Cartesian coordinates. This representation is meant to exploit the octahedral symmetries of the icosahedron as much as possible. Thus many of the symmetry points can be expressed as simple permutations of the basic points. To capture the icosahedral symmetries however, a general transformation matrix must be introduced.

In Figure 5.9, the axis labeled P represents the five-fold symmetry axis about which the structure is transformed.[10] This axis goes through a vertex of the reference, unit-side-length icosahedron. The coordinates of this vertex are $(\frac{1}{2}, 0, \frac{\tau}{2})$ where $\tau \equiv \frac{1+\sqrt{5}}{2} \approx 1.618034$ is the ratio constant of the golden section. This transformation is needed to express P_2 in terms of the basic point P_1. (Cartesian coordinates allow P_3 to be expressed more simply as just a permutation of P_1 ($P_3 = (z_1, x_1, y_1)$).) P_2 is generated from P_1 by a $-72°$ rotation of the

[10] P stands for **p**entagon.

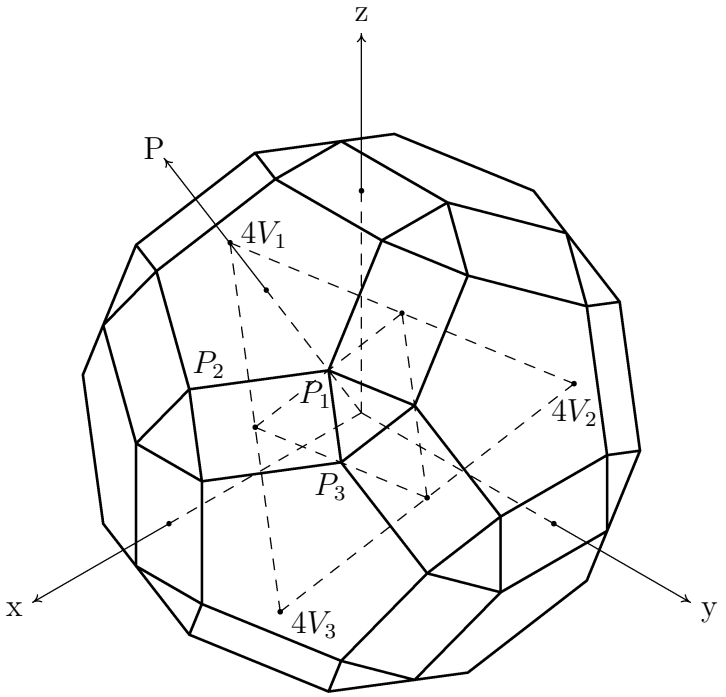

Figure 5.9: 2ν Hexagon/Triangle T-Icosahedron: Coordinate System

structure about the axis P. The matrix which achieves this transformation is:[11]

$$\mathbf{T} \equiv \begin{bmatrix} \frac{1}{2} & \frac{\tau}{2} & \frac{1}{2\tau} \\ \frac{-\tau}{2} & \frac{1}{2\tau} & \frac{1}{2} \\ \frac{1}{2\tau} & -\frac{1}{2} & \frac{\tau}{2} \end{bmatrix}$$

Thus each coordinate of P_2 is represented as a linear combination of the coordinates of P_1. In the model, this substitution could be made in all the formulas. However, it is simpler just to consider P_2 as a basic point and introduce the transformation matrix as three constraints expressing the coordinates of P_2 as linear combinations of the coordinates of P_1.

Figure 5.10 illustrates the basic members of the structure as well as an outline of some of the symmetry members embedded in the coordinate system which is used to analyze the structure. The low frequency of the structure means there are very few basic members to keep track of. On the other hand, the high order of symmetry of the icosahedron means that the structure as a whole will encompass about as much space as a structure based on a more complicated 4ν breakdown of the octahedron. This symmetry-induced simplicity is an important consideration in favor of icosahedral structures. Table 5.9 summarizes the member breakdown including weights for members included in the objective function and length constraints for the others.

[11] Derived using formulas provided in *Rogers76,* Chapter 3.

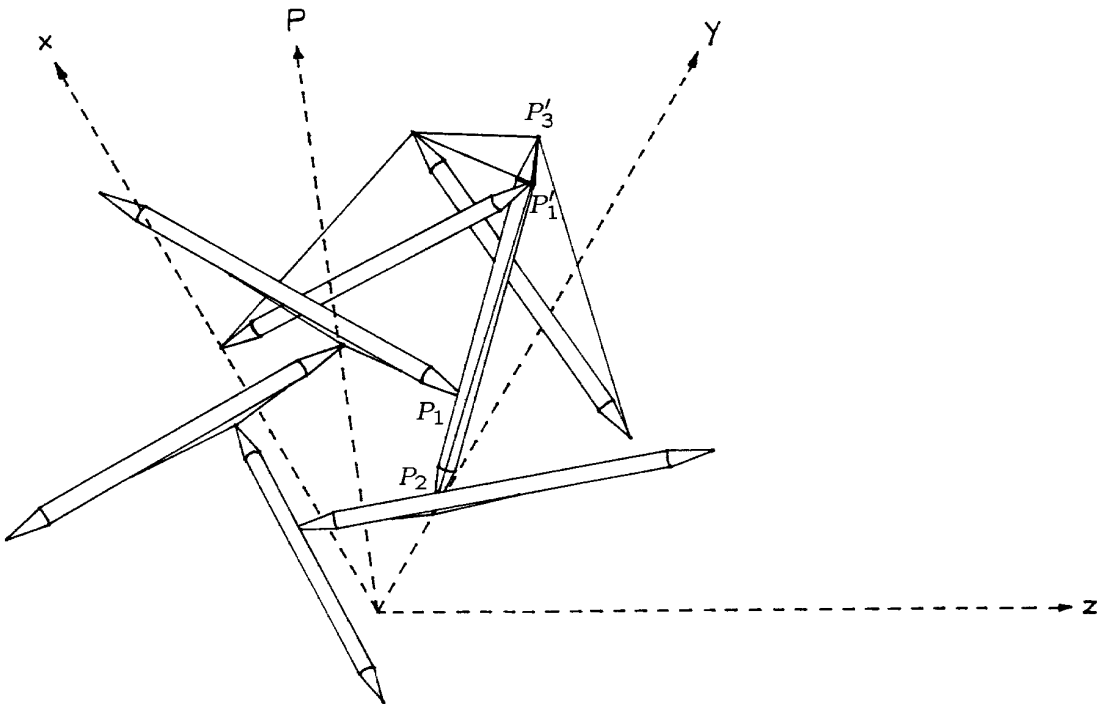

Figure 5.10: 2ν Hexagon/Triangle T-Icosahedron: Truss Members

Member #	End Points		Weight	Constrained Length	Comments
1	P_3'	P_2	N/A	3.0	Strut
2	P_1'	P_2	2.00	N/A	Primary Interlayer Tendon
3	P_3'	P_1	2.00	N/A	Secondary Interlayer Tendon
4	P_1'	P_3'	N/A	1.0	Outer Convergence Tendon
5	P_1'	P_2'	0.45	N/A	Outer Binding Tendon
6	P_1	P_3	1.00	N/A	Inner Binding Tendon
7	P_1	P_2	N/A	1.0	Inner Convergence Tendon

Table 5.9: 2ν Hexagon/Triangle T-Icosahedron: Truss Members

Vertex	Coordinates x	y	z
V_1	$\frac{1}{2}$	0	$\frac{\tau}{2}$
V_2	0	$\frac{\tau}{2}$	$\frac{1}{2}$
V_3	$\frac{\tau}{2}$	$\frac{1}{2}$	0

Table 5.10: Unit Icosahedron: Selected Vertex Coordinates

The mathematical programming problem reduces to:

$$\begin{array}{lcll} \underset{P_1, P_1', P_2, P_2'}{\text{minimize}} & \text{o} & \equiv & 2(|P_1' - P_2|^2 + |P_3' - P_1|^2) + \frac{2}{5}|P_1' - P_2'|^2 + |P_1 - P_3|^2 \\ \text{subject to} & \text{Tendon constraints:} & & \\ & 1 & \geq & |P_1' - P_3'|^2 \\ & 1 & \geq & |P_1 - P_2|^2 \\ & \text{Strut constraint:} & & \\ & -9 & \geq & -|P_3' - P_2|^2 \\ & \text{Symmetry constraints:} & & \\ & P_2 & = & \mathbf{T}P_1 \\ & P_2' & = & \mathbf{T}P_1' \end{array}$$

The latter "two" constraints actually represent six linear constraints in all and are the icosahedral symmetry transformations.

The next thing needed is initial coordinate values for the computation. These can be derived from the coordinates the unit icosahedron vertices, in particular, the coordinates of the icosahedral triangle generated by axes permutations located in the positive octant. Table 5.10 summarizes these coordinate values. The locations of $4V_1$, $4V_2$ and $4V_3$ are shown in Figure 5.9.

Taking the midpoints of the sides of the triangle represented by these three points yields the vertices of a triangle of a half-scale version of the unit icosadodecahedron. Taking the midpoints of this second triangle and multiplying by four yields the vertices of a triangle of a unit-scale version of the the reference network for the tensegrity being analyzed here. The coordinates of the point needed are:

Point	Coordinates x	y	z
P_1	1.809017	1.309017	2.118034
P_1'	2.713525	1.963525	3.177051

Table 5.11: 2ν Hexagon/Triangle T-Icosahedron: Initial Basic Point Coordinates

Member #	Length	Relative Force
1	3.000000	-11.325
2	2.395526	4.791
3	2.017577	4.035
4	1.000000	4.032
5	2.241086	1.008
6	1.471948	1.472
7	1.000000	5.899

Table 5.12: 2ν Hexagon/Triangle T-Icosahedron: Final Member Lengths and Forces

$$(\frac{2+\tau}{2}, \frac{1+\tau}{2}, \frac{1+2\tau}{2})$$

This serves as the initial value for P_1. The initial value for P_1' can be computed by scaling up P_1 until the strut length constraint is approximately satisfied. A value of 1.5 for the scale factor worked satisfactorily here. These initial coordinate values are summarized in Table 5.11.

Since P_2 and P_2' are being treated as control variables as well, initial values must be supplied for them. These initial values are computed by multiplying P_1 and P_1' by $\mathbf{T}$. The coordinates of P_3 expressed in terms of P_1 are (z_1, x_1, y_1). P_3' has the same relationship with P_1'. These last relationships fully determine the model.

The model was solved using a similar approach to that used for the 4ν t-octahedron in Section 5.3. An initial iteration was done using the penalty formulation ($\overline{\mu} = 10^5$) in conjunction with Fletcher-Reeves. After this 10 iterations were done with the exact formulation in conjunction with Fletcher-Reeves to bring the values to convergence. The derivatives of the objective function with respect to the independent variables were all less than 10^{-6}. Member clearances were all greater than 0.15 model units.

Table 5.12 shows the values for the final lengths and relative forces (see Chapter 7 for the method of computing relative forces); Table 5.13 shows the final values for the coordinates of the basic points, and Figure 5.11 shows the final design.

Point	Coordinates		
	x	y	z
P_1	1.635712	0.467068	1.294325
P_1'	2.427554	1.611718	1.991202

Table 5.13: 2ν Hexagon/Triangle T-Icosahedron: Final Coordinate Values

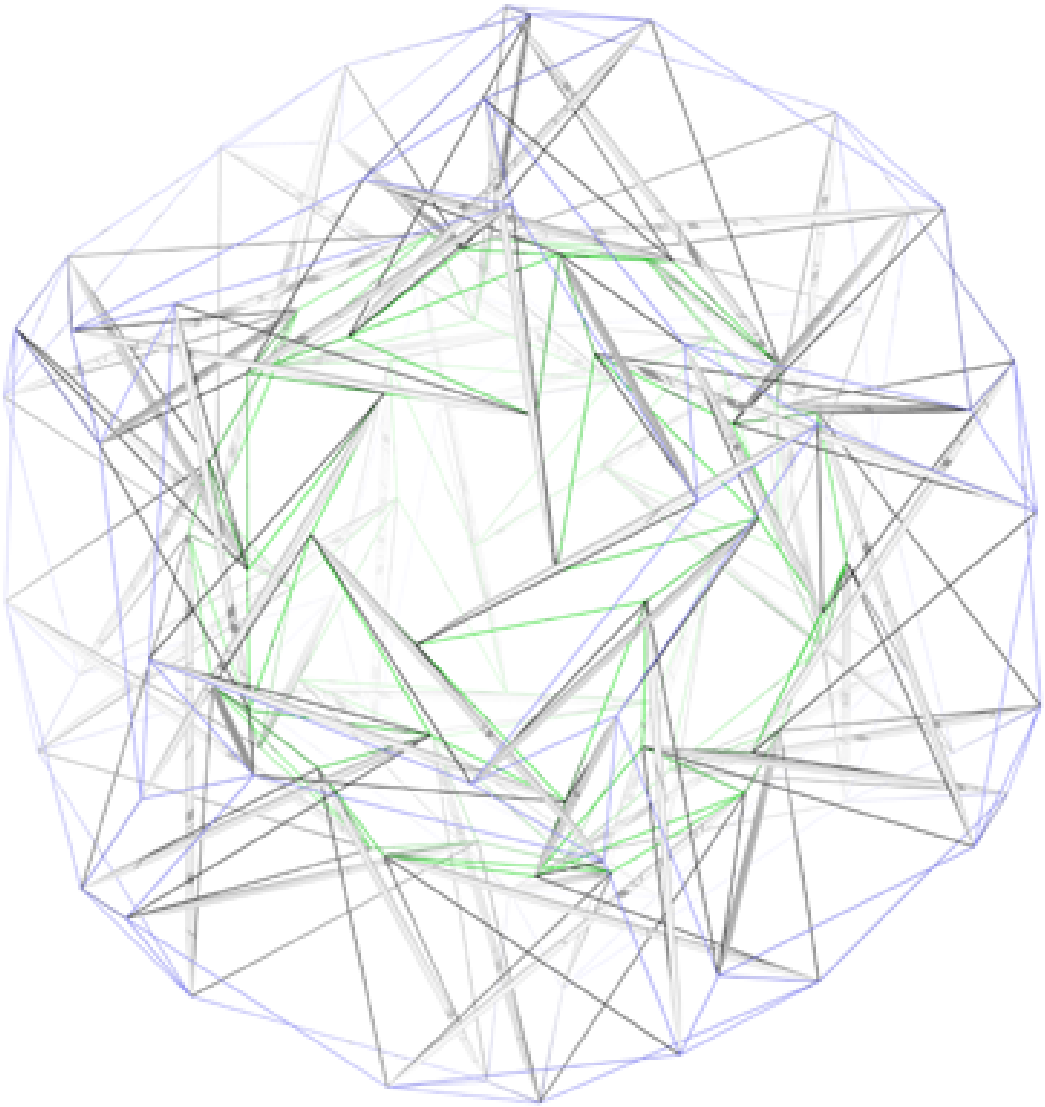

Figure 5.11: 2ν Hexagon/Triangle T-Icosahedron: Final Design

Chapter 6

Double-Layer Tensegrity Domes

6.1 Double-Layer Tensegrity Domes: Introduction

Tensegrity spheres seem appropriate for environments where external loads are evenly distributed about the surfaces of structures. Examples of this type of environment are underground, underwater, the atmosphere and outer space. For the surface of the earth, truncated structures, domes, are more likely to find favor as the base of such structures provides an effective way of dissipating the concentrated load of gravity as well as a needed source of floor space within the structure. With this consideration in mind, a method of truncating double-layer spherical tensegrity structures is presented in this chapter.

Truncating a single-layer tensegrity sphere amounts to removing a vertex-tangent group of triangles or other low-frequency polylaterals and replacing them with a single polylateral of high frequency. This high-frequency polylateral (the base mentioned above) will be tangent with the remaining polylaterals at the vertexes which were touched by the removed polylaterals.

To have a workable tensegrity, the truncation must be done so that each vertex of the new polylateral is tangent with exactly one vertex of one of the remaining original polylaterals. Situations where the new polylateral is tangent at more than one point with one of the original polylaterals are not admissible. This represents a restriction on the groups of polylaterals which can be removed. Figures 6.1 and 6.2 illustrate groups which meet and do not meet this restriction. Even with this restriction, single-layer truncated tensegrities don't seem practical since the re-routing of the struts in the neighborhood of the truncation invariably results in intractable interference problems.

For double-layer tensegrities where the tendon network is conceived of as an alternating set of polylaterals as was described in Section 5.2, an additional restriction is necessary: the remaining polylaterals tangent to the new polylateral must all belong to the same alternation group. This ensures the new polylateral is a well-defined member of the alternation group alternate to that of the remaining polylaterals tangent to it. In addition,

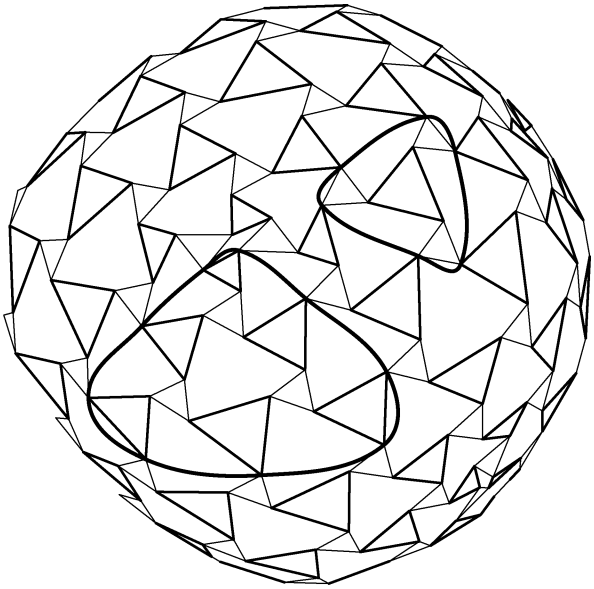

Figure 6.1: Valid Tensegrity Truncation Groups

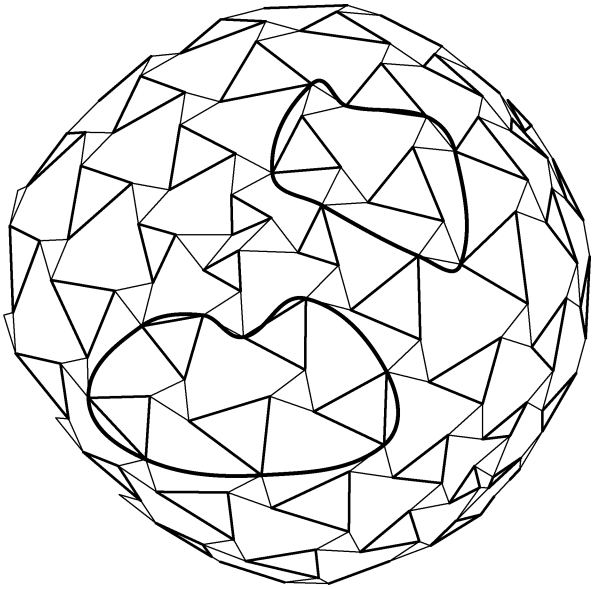

Figure 6.2: Invalid Tensegrity Truncation Groups

the problem with re-routing struts which plagues single-layer structures can be avoided in double-layer structures if the truncation polylateral is chosen so that it approximates a great circle; that is, the polylateral has no sharp turns.

A significant problem posed by a truncation is a loss of symmetry. This has the undesirable effect of greatly increasing the size of the programming problem whose solution is required to generate a structure at a given frequency. There is not much way around this unfortunately.

The large truncation needed to provide a base for a dome can also cause a structure to deviate to a great extent from its original configuration. These deviations are usually in a way which cause the base area to contract relative to the original cross-section it had in the sphere. These deviations can also introduce new, intractable interference problems. So, for this type of truncation, it is often desirable to fix all the points of the new polylateral and perhaps further adjust them to lie in a plane and observe other convenient regularities. Such constraints can also be desirable just from the point of view of easing the processes of designing and building a foundation for a tensegrity dome.

Attaching the dome to its base means introducing the material on which the dome is situated as a structural member which constrains the base points to stay at specified fixed positions. Such a structure is no longer a tensegrity according to some definitions since it now depends on the base material to help shape it. It is no longer self-supporting.

6.2 A Procedure for Designing Double-Layer Tensegrity Domes

The following steps implement the design of a truncated, double-layer structure along the lines discussed in Section 6.1 are as follows:

Step 1 Solve the tensegrity programming problem for the spherical version of the structure.

Step 2 Implement the topological changes required by the truncation.

Step 3 Adjust the base points (the points of the truncation polylateral as they manifest themselves on the inner tendon network) so they lie evenly-spaced on a circle which approximates as closely as possible their unadjusted positions in the original sphere.

Step 4 Add guys.

Step 5 Using the coordinate values from the sphere as initial values, solve the tensegrity programming problem for the truncated sphere.

Step 6 Make necessary adjustments to fix member force and interference problems.

To illustrate a method for truncating double-layer spheres, the tensegrity based on the 6ν octahedron is useful. It has a low-enough frequency to be pedagogically tractable and a high-enough frequency that the appearance of higher-frequency structures can be anticipated in studying it.

6.2.1 Dome Step 1: Compute the sphere

Figures 6.3 and 6.4 diagram the basic triangle network for the 6ν double-layer tensegrity octahedron sphere and a coordinate system for its analysis in the same manner as Figures 5.3 and 5.5 did for the 4ν version in Section 5.3. The main difference is that, with the higher frequency, there is more of everything. For example, now the struts in Figure 6.4 are clustered about three basic t-tripods instead of two as in Figure 5.5.

Table 6.1 enumerates the members of this 6ν version of the double-layer sphere. The anomalous value of 1.5 for the length of Member #33 in Table 6.1 was chosen in light of the experience with the 4ν structure.

The weights for the inner and outer binding tendons in the objective function are derived using the formula $k(\frac{b_1+b_2}{2b_1b_2})^2$ where the values used for k are 0.5 and 1.2 respectively for the outer and inner binding tendons. b_1 and b_2 represent the spherical excess corresponding to the initial values of the two endpoints of the tendon.[1] The spherical excess is the amount the sphere radius exceeds the distance of the unprojected endpoint from the center of the octahedron. This number is calculated as a ratio and is always greater than or equal to 1.0. It is equal to 1.0 at the vertexes of the octahedron. Giving a smaller weight to the tendons distant from the vertexes of the basis octahedron allows them to be longer than they would otherwise be. This allows the octahedral faces to bulge out more than they would otherwise and gives the structure a more-spherical, less-faceted, look. The objective-function weights for the primary and secondary interlayer tendons are 2.0 and 1.4 respectively independent of any spherical excess values.

As with the 4ν version of this sphere, the derivation of the initial point values is facilitated by the use of the geodesic breakdown. Kenner's tables[2] were used to generate initial point coordinates. Again, Kenner's table has to be expanded by rotating all the points about the z axis by 90°. Table 6.2 outlines the correspondence between the basic points and his coordinate system (rotated points are indicated with an asterisk).

The initial coordinate values for inner and outer realizations of these points are summarized in Table 6.3. These are derived from the angular values in Table 6.2 with inner and outer radiuses applied. The inner radius (3.15) was chosen so the triangle tendon

[1] b stands for **b**ulge.

[2] *Kenner76,* "Octahedron Class I Coordinates: Frequencies 12, 6, 3", column 6ν, p. 126.

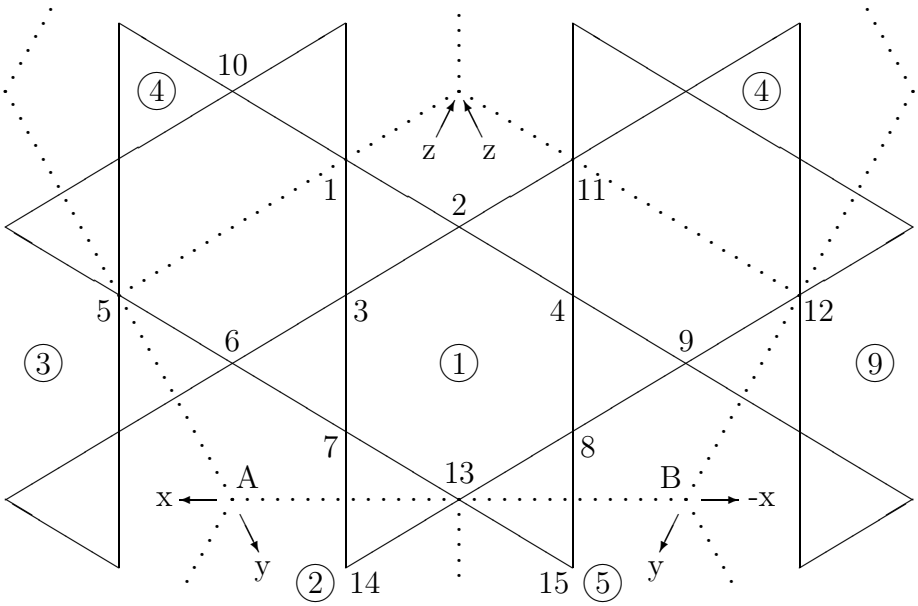

Figure 6.3: 6ν T-Octahedron Sphere: Symmetry Regions

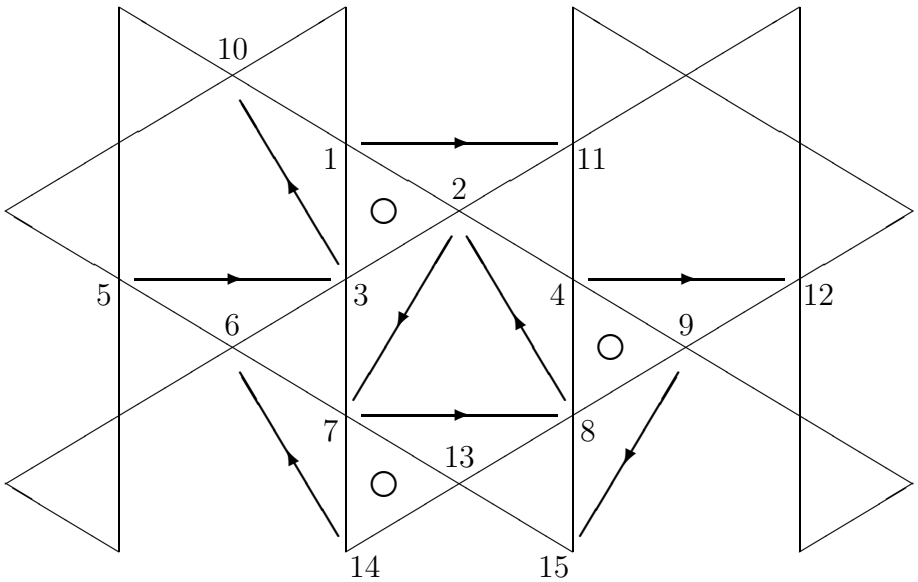

Figure 6.4: 6ν T-Octahedron Sphere: Truss Members

Member #	End Points		Weight	Constrained Length	Comments
1	P'_1	P_{11}	N/A	3.0	
2	P'_2	P_7	N/A	3.0	
3	P'_3	P_{10}	N/A	3.0	
4	P'_4	P_{12}	N/A	3.0	
5	P'_9	P_{15}	N/A	3.0	Struts
6	P'_8	P_2	N/A	3.0	
7	P'_7	P_8	N/A	3.0	
8	P'_5	P_3	N/A	3.0	
9	P'_{14}	P_6	N/A	3.0	
10	P'_2	P_{11}	2.0	N/A	
11	P'_3	P_7	2.0	N/A	
12	P'_1	P_{10}	2.0	N/A	
13	P'_9	P_{12}	2.0	N/A	
14	P'_8	P_{15}	2.0	N/A	Primary Interlayer Tendons
15	P'_4	P_2	2.0	N/A	
16	P'_{13}	P_8	2.0	N/A	
17	P'_6	P_3	2.0	N/A	
18	P'_7	P_6	2.0	N/A	
19	P'_1	P_2	1.4	N/A	
20	P'_2	P_3	1.4	N/A	
21	P'_3	P_1	1.4	N/A	
22	P'_4	P_9	1.4	N/A	
23	P'_9	P_8	1.4	N/A	Secondary Interlayer Tendons
24	P'_8	P_4	1.4	N/A	
25	P'_7	P_{13}	1.4	N/A	
26	P'_5	P_6	1.4	N/A	
27	P'_{14}	P_7	1.4	N/A	

Member #	End Points		Weight	Constrained Length	Comments
28	P_2	P_{11}	N/A	1.0	
29	P_3	P_7	N/A	1.0	
30	P_1	P_{10}	N/A	1.0	
31	P_9	P_{12}	N/A	1.0	
32	P_8	P_{15}	N/A	1.0	Inner Convergence Tendons
33	P_4	P_2	N/A	1.5	
34	P_{13}	P_8	N/A	1.0	
35	P_6	P_3	N/A	1.0	
36	P_7	P_6	N/A	1.0	
37	P'_1	P'_2	N/A	1.0	
38	P'_2	P'_3	N/A	1.0	
39	P'_3	P'_1	N/A	1.0	
40	P'_4	P'_9	N/A	1.0	
41	P'_9	P'_8	N/A	1.0	Outer Convergence Tendons
42	P'_8	P'_4	N/A	1.0	
43	P'_7	P'_{13}	N/A	1.0	
44	P'_5	P'_6	N/A	1.0	
45	P'_{14}	P'_7	N/A	1.0	
46	P'_2	P'_{11}	0.5000	N/A	
47	P'_3	P'_7	0.3065	N/A	
48	P'_1	P'_{10}	0.4196	N/A	
49	P'_9	P'_{12}	0.3065	N/A	
50	P'_8	P'_{15}	0.2692	N/A	Outer Binding Tendons
51	P'_4	P'_2	0.4196	N/A	
52	P'_{13}	P'_8	0.3065	N/A	
53	P'_6	P'_3	0.3065	N/A	
54	P'_7	P'_6	0.2692	N/A	

Member #	End Points		Weight	Constrained Length	Comments
55	P_1	P_2	1.2000	N/A	
56	P_2	P_3	1.0069	N/A	
57	P_3	P_1	1.0069	N/A	
58	P_4	P_9	0.7356	N/A	
59	P_9	P_8	0.6462	N/A	Inner Binding Tendons
60	P_8	P_4	0.7356	N/A	
61	P_7	P_{13}	0.7356	N/A	
62	P_5	P_6	0.7356	N/A	
63	P_{14}	P_7	0.6462	N/A	

Table 6.1: 6ν T-Octahedron Sphere: Truss Members

Point	Kenner's Label	Coordinates θ	ϕ
P_1 (P'_1)	1,0	0.0	11.3099
P_2 (P'_2)	1,1	90.0	11.3099
P_3 (P'_3)	2,1	45.0	19.4712
P_4 (P'_4)	2,1*	135.0	19.4712
P_5 (P'_5)	3,0	0.0	45.0
P_6 (P'_6)	3,1	26.5651	36.6992
P_7 (P'_7)	3,2	63.4349	36.6992
P_8 (P'_8)	3,1*	116.5651	36.6992
P_9 (P'_9)	3,2*	153.4349	36.6992

Table 6.2: 6ν T-Octahedron: Angular Point Coordinates

Point	Coordinates		
	x	y	z
P_1	0.6178	0.0000	3.0888
P_2	0.0000	0.6178	3.0888
P_3	0.7425	0.7425	2.9698
P_4	-0.7425	0.7425	2.9698
P_5	2.2274	0.0000	2.2274
P_6	1.6837	0.8419	2.5256
P_7	0.8419	1.6837	2.5256
P_8	-0.8419	1.6837	2.5256
P_9	-1.6837	0.8419	2.5256
P'_1	1.0100	0.0000	5.0500
P'_2	0.0000	1.0100	5.0500
P'_3	1.2139	1.2139	4.8555
P'_4	-1.2139	1.2139	4.8555
P'_5	3.6416	0.0000	3.6416
P'_6	2.7528	1.3764	4.1292
P'_7	1.3764	2.7528	4.1292
P'_8	-1.3764	2.7528	4.1292
P'_9	-2.7528	1.3764	4.1292

Table 6.3: 6ν T-Octahedron: Initial Basic Point Coordinates

lengths average approximately 1 (0.995729). The outer radius (5.15) was chosen so strut lengths in the double-layer versions of the structure would initially average approximately 3. The implied initial lengths are summarized in Table 6.4.

The derivation of the symmetry points from the basic points is shown in Table 6.5. The symmetry transforms on which this table is based are enumerated in Table 5.5. Outer points follow the same symmetries as inner points.

The structure was computed by minimizing a weighted combination of the interlayer and binding tendons subject to constraints on the struts and convergence tendons. Two initial iterations were done using the penalty formulation ($\overline{\mu} = 10^5$) in conjunction with Fletcher-Reeves to bring the initial points into approximate conformance with the constraints. After this five iterations were done with the exact formulation in conjunction with Fletcher-Reeves to bring the values to convergence. The derivatives of the objective function with respect to the independent variables were all less than 10^{-6}.

Table 6.6 shows the values for the final lengths and relative forces (see Chapter 7 for the method of computing relative force). Table 6.7 shows the final values for the coordinates of the basic points. Figure 6.5 shows how the final version of the spherical structure appears as viewed from outside one of the octahedral vertices. For clarity, interlayer tendons have been excluded and members in the background have been eliminated by truncation. For

Member #	Length	Member #	Length	Member #	Length
1	2.5487	2	2.7450	3	2.7577
4	3.0672	5	3.3095	6	2.7450
7	2.9385	8	3.0672	9	3.3095
10	2.2908	11	2.4057	12	2.2248
13	2.4057	14	2.5135	15	2.2248
16	2.4057	17	2.4057	18	2.5135
19	2.2908	20	2.2248	21	2.2248
22	2.4057	23	2.5135	24	2.4057
25	2.4057	26	2.4057	27	2.5135
28	0.8737	29	1.0456	30	0.7622
31	1.0456	32	1.1906	33	0.7622
34	1.0456	35	1.0456	36	1.1906
37	1.4284	38	1.2461	39	1.2461
40	1.7094	41	1.9465	42	1.7094
43	1.7094	44	1.7094	45	1.9465
46	1.4284	47	1.7094	48	1.2461
49	1.7094	50	1.9465	51	1.2461
52	1.7094	53	1.7094	54	1.9465
55	0.8737	56	0.7622	57	0.7622
58	1.0456	59	1.1906	60	1.0456
61	1.0456	62	1.0456	63	1.1906

Table 6.4: 6ν T-Octahedron: Initial Member Lengths

Point	Coordinates x	y	z	Basic Point	Transform Number
P_{10}	$-x_4$	$-y_4$	z_4	P_4	4
P_{11}	$-x_1$	$-y_1$	z_1	P_1	4
P_{12}	$-x_5$	$-y_5$	z_5	P_5	4
P_{13}	y_5	z_5	x_5	P_5	2
P_{14}	y_6	z_6	x_6	P_6	2
P_{15}	$-y_9$	z_9	$-x_9$	P_9	5

Table 6.5: 6ν T-Octahedron: Symmetry Point Correspondences

Member #	Length	Relative Force
1	3.0000	-11.294
2	3.0000	-9.788
3	3.0000	-10.052
4	3.0000	-10.125
5	3.0000	-10.019
6	3.0000	-9.925
7	3.0000	-10.052
8	3.0000	-10.064
9	3.0000	-9.870
10	2.3545	4.709
11	2.3871	4.774
12	2.4881	4.976
13	2.2793	4.559
14	2.2883	4.577
15	2.3153	4.631
16	2.2212	4.442
17	2.2209	4.442
18	2.2354	4.471
19	2.1286	2.980
20	2.0833	2.917
21	2.1669	3.033
22	2.0342	2.848
23	2.0334	2.847
24	1.6827	2.356
25	2.0342	2.848
26	2.0454	2.863
27	2.0516	2.872

reference, selected points are labeled.

6.2.2 Dome Step 2: Implement the truncation

Figure 6.6 diagrams the four "great" circle truncation possibilities for this structure as they fall on its reference octahedron. Figure 6.7 shows the same four truncation boundaries as they fall on the inner layer of the sphere. None of these boundaries corresponds to a true great circle. The true great circle lies at the center of their range and is not usable as a truncation at this frequency. In a higher-frequency structure there would be still more of these circles available. All of them are possibilities as truncation definitions, although the ones farther away from the true great circle would probably require greater adjustments to

Member #	Length	Relative Force
28	1.0000	4.945
29	1.0000	4.580
30	1.0000	3.811
31	1.0000	5.009
32	1.0000	5.092
33	1.0000	4.947
34	1.0000	4.958
35	1.0000	5.258
36	1.0000	5.163
37	1.0000	4.144
38	1.0000	4.887
39	1.0000	4.040
40	1.0000	4.865
41	1.0000	4.867
42	1.0000	5.214
43	1.0000	4.815
44	1.0000	5.083
45	1.0000	5.547
46	1.8502	0.925
47	2.4709	0.757
48	2.1613	0.907
49	2.6524	0.813
50	2.7414	0.738
51	2.4735	1.038
52	2.7549	0.844
53	2.6798	0.821
54	2.6482	0.713

Member #	Length	Relative Force
55	1.2081	1.450
56	1.2653	1.274
57	1.2626	1.271
58	1.3406	0.986
59	1.6730	1.081
60	1.2480	0.918
61	1.9008	1.398
62	1.8434	1.356
63	1.9693	1.273

Table 6.6: 6ν T-Octahedron Sphere: Final Member Lengths and Forces

	Coordinates		
Point	x	y	z
P_1	1.0378	-0.2360	3.5592
P_2	-0.0640	0.2053	3.7844
P_3	0.8711	1.0149	3.5173
P_4	-1.0998	1.2224	3.4065
P_5	2.9400	-0.4191	2.3400
P_6	1.7538	0.7511	3.1285
P_7	1.3434	1.6303	2.8864
P_8	-1.4134	2.2919	2.8451
P_9	-2.3233	0.8934	2.9682
P'_1	1.3525	0.2829	5.3714
P'_2	0.3628	0.4068	5.4440
P'_3	0.9467	1.1801	5.1968
P'_4	-1.5610	1.7442	4.6513
P'_5	3.7764	0.4745	3.0005
P'_6	3.0842	0.8558	3.6132
P'_7	1.4390	2.9290	3.5221
P'_8	-2.1735	2.3144	4.1038
P'_9	-2.4411	1.3815	4.3450

Table 6.7: 6ν T-Octahedron Sphere: Final Basic Point Coordinates

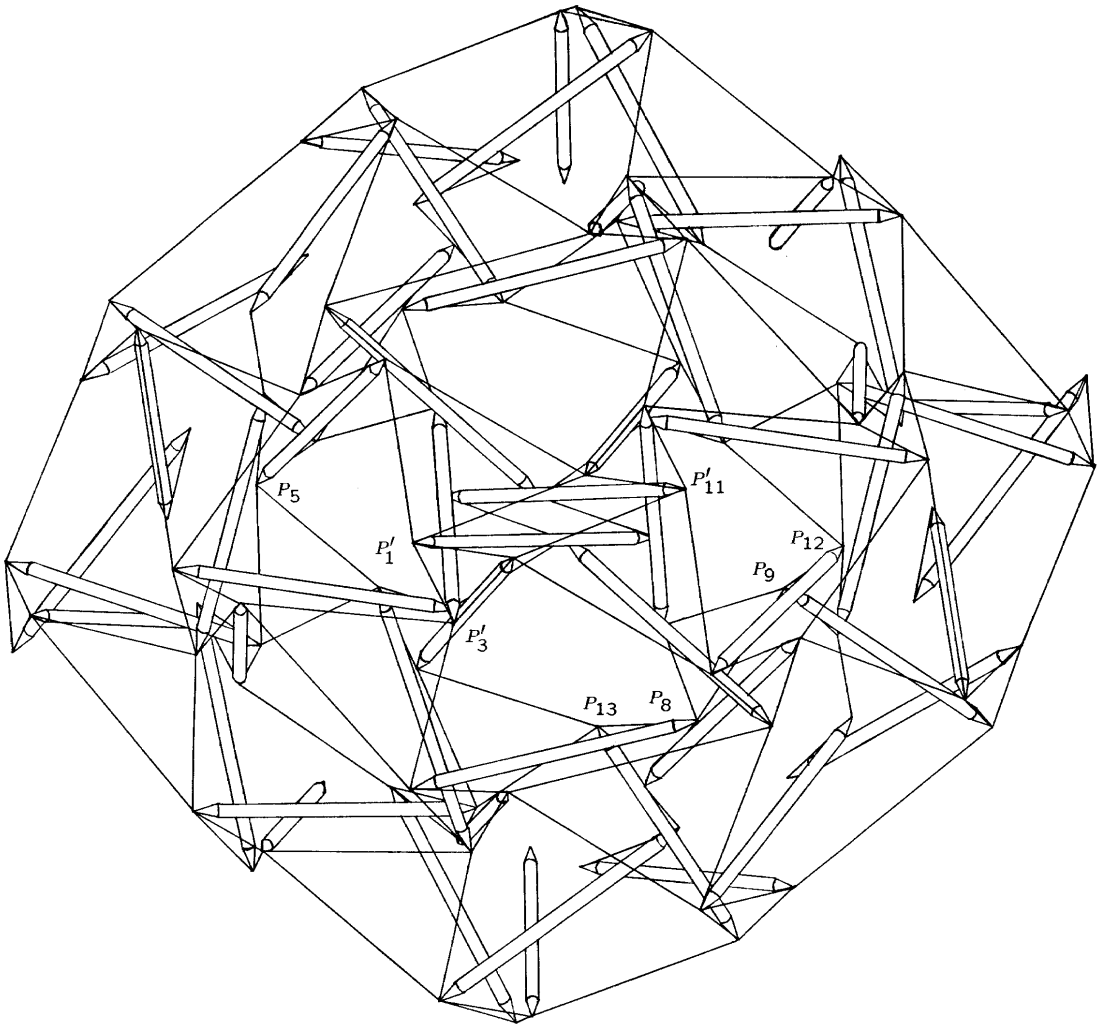

Figure 6.5: 6ν T-Octahedron Sphere: Vertex View

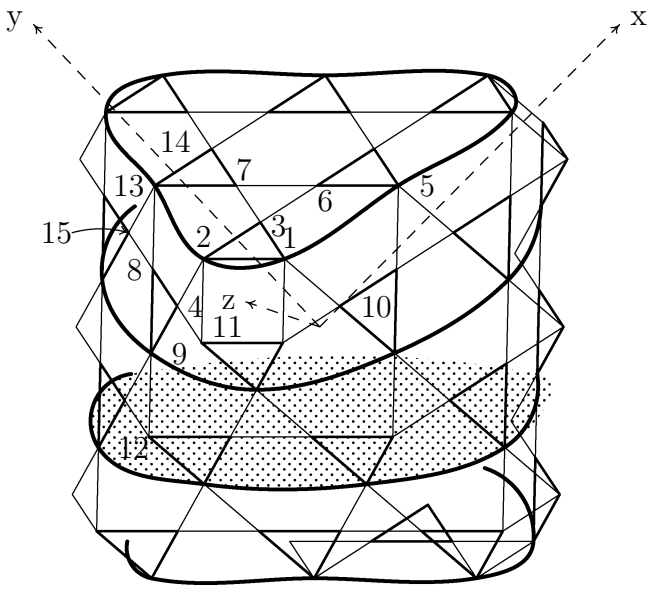

Figure 6.6: 6ν T-Octahedron: Truncation Boundaries (Octahedron)

work well. At this frequency, the two middle truncations are equally far from the true great circle, and so neither has an advantage as far as adjustments required. This being the case, the one that allows more volume was selected.

Figures 6.8 and 6.9 diagram the basic triangle network for the truncated structure and a coordinate system for its analysis. These figures are in roughly the same style as the corresponding figures for the 4ν and 6ν spheres. Figure 6.8 is more complex than for those earlier structures since it attempts to diagram the correspondence between the symmetry regions of the 6ν sphere and those of the dome.

The boundaries of the symmetry regions for the sphere are outlined with dotted lines as before and labeled with small numbers in circles. The numbers correspond to the symmetry transformations listed in Table 5.5. The boundaries for the dome are outlined by a hollow dotted line. The dome's symmetry regions are enumerated with larger numbers in circles. These numbers also correspond to the symmetry transformations listed in Table 5.5, although, due to the loss of symmetry, only the first three entries in the table are possibilities. A grasp of the correspondence between the two regions is useful for generating initial points for the dome calculations from the final values of the sphere calculations. These correspondences are used in Tables 6.16 and 6.17. As noted below, these correspondences are altered slightly for the inner points at the base of the dome.

Tables 6.8 through 6.15 enumerate the members of the truncated structure. The anomalous members which have a length of 1.5 correspond to Member #33 in Table 6.1 for the sphere. For the most part, the weights for this structure are mapped from the weights used for the corresponding members in the spherical version of the structure. The

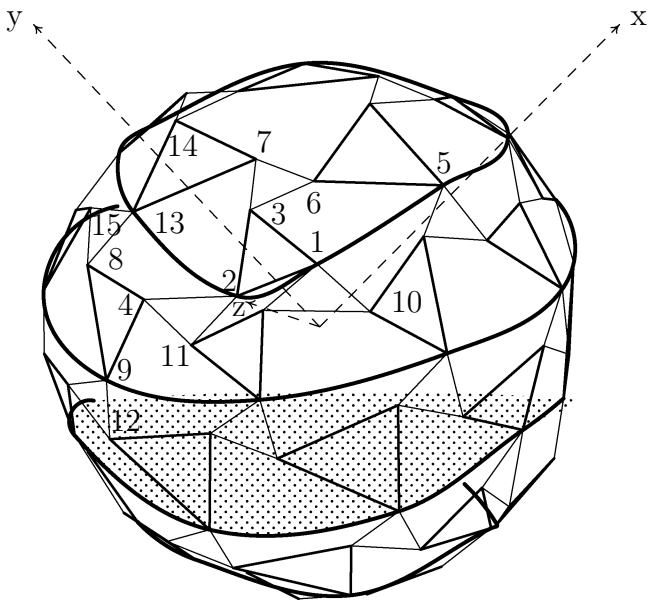

Figure 6.7: 6ν T-Octahedron: Truncation Boundaries (Sphere)

exceptions are the weights for members #160, #161, #163, #164, #166 and #167. The reasons for these exceptions are discussed below. In addition to the members enumerated in Tables 6.8 through 6.15, guys will be introduced in **Step 4**.

The tables for this structure are much larger, and the computations required are correspondingly more massive, due to the loss of symmetry induced by the truncation. The dome is composed of three symmetrical parts whereas the same area on the sphere was composed of about eight symmetrical parts. The net result is that the tables for the dome are over twice as large as those for the sphere.

Decisions must be made in the neighborhood of the truncation on how to reroute the struts whose inner terminal points lay on the set of triangles which were excluded. The best procedure seems to be to connect them to the inner binding triangle which underlies their tripod. To make this work, the weights are multiplied by $\frac{5}{12}$ for inner binding tendons which touch the base. These are the members mentioned above whose weights do not equal those of the corresponding members in the spherical structure (#160, #161, #163, #164, #166, #167). This reduction in the weights allows the final dome to achieve a height which approximates the height of its initial configuration. With unaltered weights, it would turn out more squat.

The secondary interlayer tendons at these positions, #64, #67 and #70, disappear since there are struts at those same positions in this configuration. Also, the tendons generated by the truncation are eliminated from the model. The inner truncation tendons are redundant since they connect the base points which are fixed. The outer truncation tendons are not necessary for structural integrity and detract from the appearance of the structure.

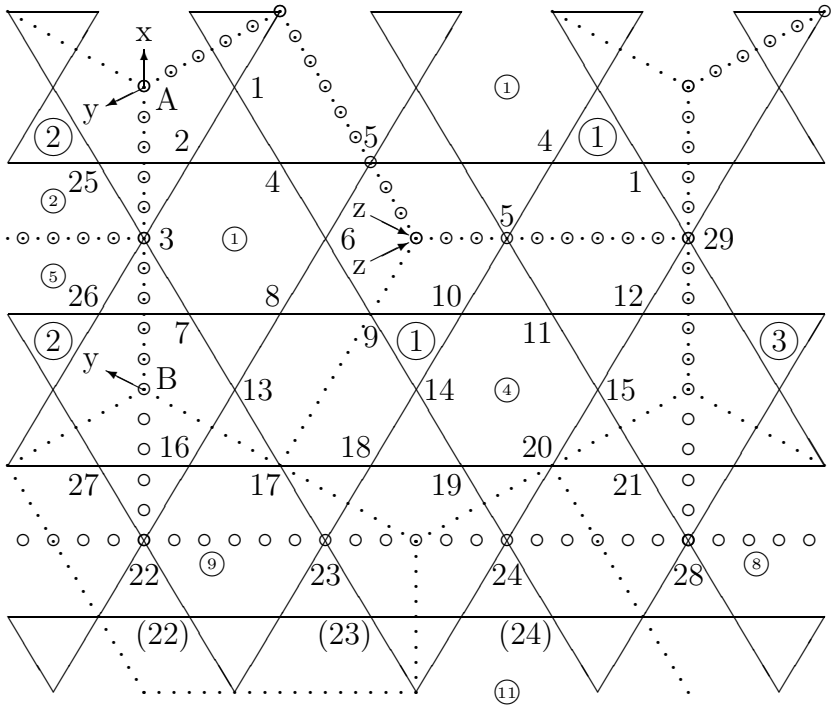

Figure 6.8: 6ν T-Octahedron Dome: Symmetry Regions

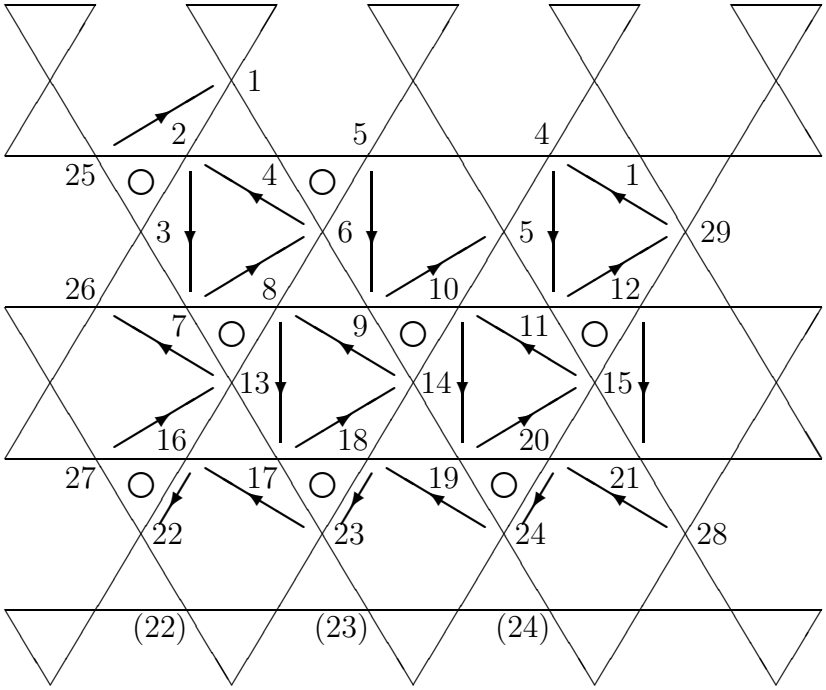

Figure 6.9: 6ν T-Octahedron Dome: Truss Members

Member #	End Points		Weight	Constrained Length	Sphere Member
1	P'_2	P_7	N/A	3.0	7
2	P'_{29}	P_4	N/A	3.0	8
3	P'_{25}	P_1	N/A	3.0	9
4	P'_5	P_9	N/A	3.0	1
5	P'_6	P_2	N/A	3.0	2
6	P'_4	P_{11}	N/A	3.0	3
7	P'_8	P_{17}	N/A	3.0	4
8	P'_{13}	P_{26}	N/A	3.0	5
9	P'_7	P_6	N/A	3.0	6
10	P'_{10}	P_{19}	N/A	3.0	2
11	P'_{14}	P_8	N/A	3.0	3
12	P'_9	P_5	N/A	3.0	1
13	P'_{12}	P_{21}	N/A	3.0	5
14	P'_{15}	P_{10}	N/A	3.0	6
15	P'_{11}	P_{29}	N/A	3.0	4
16†	P'_{16}	P_{22}	N/A	3.0	6
17	P'_{28}	P_{20}	N/A	3.0	4
18	P'_{27}	P_{13}	N/A	3.0	5
19†	P'_{18}	P_{23}	N/A	3.0	9
20	P'_{23}	P_{16}	N/A	3.0	7
21	P'_{17}	P_{14}	N/A	3.0	8
22†	P'_{20}	P_{24}	N/A	3.0	8
23	P'_{24}	P_{18}	N/A	3.0	9
24	P'_{19}	P_{15}	N/A	3.0	7

Table 6.8: 6ν T-Octahedron Dome: Struts

In Tables 6.8 through 6.15, members re-routed to a new inner point (as compared with the configuration of their corresponding member in the sphere) due to the truncation are marked with †. Members which were excluded (although for completeness they are included in the tables) are marked with ‡.

The basic points and their initial coordinate values (as derived from the final values for the corresponding points in the sphere) are summarized in Tables 6.16 and 6.17. The applicable transforms are listed in Table 5.5. The coordinates of P_{22}, P_{23} and P_{24} in Table 6.16 do not correspond exactly to the values of the corresponding points in the sphere. This is due to the **Step 3** adjustment.

P_{22}, P_{23} and P_{24} of the truncated sphere map from P_2, P_6 and P_3 respectively of the complete sphere, rather than P_4, P_7 and P_6 as would be expected from an unaltered symmetry mapping. This alteration was made so that, even with the change in topology,

Member #	End Points		Weight	Constrained Length	Sphere Member
25	P'_3	P_7	2.0	N/A	16
26	P'_1	P_4	2.0	N/A	17
27	P'_2	P_1	2.0	N/A	18
28	P'_6	P_9	2.0	N/A	10
29	P'_4	P_2	2.0	N/A	11
30	P'_5	P_{11}	2.0	N/A	12
31	P'_{13}	P_{17}	2.0	N/A	13
32	P'_7	P_{26}	2.0	N/A	14
33	P'_8	P_6	2.0	N/A	15
34	P'_{14}	P_{19}	2.0	N/A	11
35	P'_9	P_8	2.0	N/A	12
36	P'_{10}	P_5	2.0	N/A	10
37	P'_{15}	P_{21}	2.0	N/A	14
38	P'_{11}	P_{10}	2.0	N/A	15
39	P'_{12}	P_{29}	2.0	N/A	13
40†	P'_{22}	P_{22}	2.0	N/A	15
41	P'_{21}	P_{20}	2.0	N/A	13
42	P'_{16}	P_{13}	2.0	N/A	14
43†	P'_{23}	P_{23}	2.0	N/A	18
44	P'_{17}	P_{16}	2.0	N/A	16
45	P'_{18}	P_{14}	2.0	N/A	17
46†	P'_{24}	P_{24}	2.0	N/A	17
47	P'_{19}	P_{18}	2.0	N/A	18
48	P'_{20}	P_{15}	2.0	N/A	16

Table 6.9: 6ν T-Octahedron Dome: Primary Interlayer Tendons

Member #	End Points		Weight	Constrained Length	Sphere Member
49	P'_2	P_3	1.4	N/A	25
50	P'_{29}	P_1	1.4	N/A	26
51	P'_{25}	P_2	1.4	N/A	27
52	P'_5	P_6	1.4	N/A	19
53	P'_6	P_4	1.4	N/A	20
54	P'_4	P_5	1.4	N/A	21
55	P'_8	P_{13}	1.4	N/A	22
56	P'_{13}	P_7	1.4	N/A	23
57	P'_7	P_8	1.4	N/A	24
58	P'_{10}	P_{14}	1.4	N/A	20
59	P'_{14}	P_9	1.4	N/A	21
60	P'_9	P_{10}	1.4	N/A	19
61	P'_{12}	P_{15}	1.4	N/A	23
62	P'_{15}	P_{11}	1.4	N/A	24
63	P'_{11}	P_{12}	1.4	N/A	22
64‡	P'_{16}	P_{22}	N/A	N/A	24
65	P'_{28}	P_{21}	1.4	N/A	22
66	P'_{27}	P_{16}	1.4	N/A	23
67‡	P'_{18}	P_{23}	N/A	N/A	27
68	P'_{23}	P_{17}	1.4	N/A	25
69	P'_{17}	P_{18}	1.4	N/A	26
70‡	P'_{20}	P_{24}	N/A	N/A	26
71	P'_{24}	P_{19}	1.4	N/A	27
72	P'_{19}	P_{20}	1.4	N/A	25

Table 6.10: 6ν T-Octahedron Dome: Secondary Interlayer Tendons

Member #	End Points		Weight	Constrained Length	Sphere Member
73	P_3	P_7	N/A	1.0	34
74	P_1	P_4	N/A	1.0	35
75	P_2	P_1	N/A	1.0	36
76	P_6	P_9	N/A	1.0	28
77	P_4	P_2	N/A	1.0	29
78	P_5	P_{11}	N/A	1.0	30
79	P_{13}	P_{17}	N/A	1.0	31
80	P_7	P_{26}	N/A	1.0	32
81	P_8	P_6	N/A	1.5	33
82	P_{14}	P_{19}	N/A	1.0	29
83	P_9	P_8	N/A	1.0	30
84	P_{10}	P_5	N/A	1.0	28
85	P_{15}	P_{21}	N/A	1.0	32
86	P_{11}	P_{10}	N/A	1.5	33
87	P_{12}	P_{29}	N/A	1.0	31
88‡	P_{22}	P_{22}	N/A	N/A	33
89	P_{21}	P_{20}	N/A	1.0	31
90	P_{16}	P_{13}	N/A	1.0	32
91‡	P_{23}	P_{23}	N/A	N/A	36
92	P_{17}	P_{16}	N/A	1.0	34
93	P_{18}	P_{14}	N/A	1.0	35
94‡	P_{24}	P_{24}	N/A	N/A	35
95	P_{19}	P_{18}	N/A	1.0	36
96	P_{20}	P_{15}	N/A	1.0	34

Table 6.11: 6ν T-Octahedron Dome: Inner Convergence Tendons

Member #	End Points		Weight	Constrained Length	Sphere Member
97	P'_2	P'_3	N/A	1.0	43
98	P'_{29}	P'_1	N/A	1.0	44
99	P'_{25}	P'_2	N/A	1.0	45
100	P'_5	P'_6	N/A	1.0	37
101	P'_6	P'_4	N/A	1.0	38
102	P'_4	P'_5	N/A	1.0	39
103	P'_8	P'_{13}	N/A	1.0	40
104	P'_{13}	P'_7	N/A	1.0	41
105	P'_7	P'_8	N/A	1.0	42
106	P'_{10}	P'_{14}	N/A	1.0	38
107	P'_{14}	P'_9	N/A	1.0	39
108	P'_9	P'_{10}	N/A	1.0	37
109	P'_{12}	P'_{15}	N/A	1.0	41
110	P'_{15}	P'_{11}	N/A	1.0	42
111	P'_{11}	P'_{12}	N/A	1.0	40
112	P'_{16}	P'_{22}	N/A	1.0	42
113	P'_{28}	P'_{21}	N/A	1.0	40
114	P'_{27}	P'_{16}	N/A	1.0	41
115	P'_{18}	P'_{23}	N/A	1.0	45
116	P'_{23}	P'_{17}	N/A	1.0	43
117	P'_{17}	P'_{18}	N/A	1.0	44
118	P'_{20}	P'_{24}	N/A	1.0	44
119	P'_{24}	P'_{19}	N/A	1.0	45
120	P'_{19}	P'_{20}	N/A	1.0	43

Table 6.12: 6ν T-Octahedron Dome: Outer Convergence Tendons

Member #	End Points		Weight	Constrained Length	Sphere Member
121	P'_3	P'_7	0.3065	N/A	52
122	P'_1	P'_4	0.3065	N/A	53
123	P'_2	P'_1	0.2692	N/A	54
124	P'_6	P'_9	0.5000	N/A	46
125	P'_4	P'_2	0.3065	N/A	47
126	P'_5	P'_{11}	0.4196	N/A	48
127	P'_{13}	P'_{17}	0.3065	N/A	49
128	P'_7	P'_{26}	0.2692	N/A	50
129	P'_8	P'_6	0.4196	N/A	51
130	P'_{14}	P'_{19}	0.3065	N/A	47
131	P'_9	P'_8	0.4196	N/A	48
132	P'_{10}	P'_5	0.5000	N/A	46
133	P'_{15}	P'_{21}	0.2692	N/A	50
134	P'_{11}	P'_{10}	0.4196	N/A	51
135	P'_{12}	P'_{29}	0.3065	N/A	49
136‡	P'_{22}	P'_{22}	N/A	N/A	51
137	P'_{21}	P'_{20}	0.3065	N/A	49
138	P'_{16}	P'_{13}	0.2692	N/A	50
139‡	P'_{23}	P'_{23}	N/A	N/A	54
140	P'_{17}	P'_{16}	0.3065	N/A	52
141	P'_{18}	P'_{14}	0.3065	N/A	53
142‡	P'_{24}	P'_{24}	N/A	N/A	53
143	P'_{19}	P'_{18}	0.2692	N/A	54
144	P'_{20}	P'_{15}	0.3065	N/A	52

Table 6.13: 6ν T-Octahedron Dome: Outer Binding Tendons

Member #	End Points		Weight	Constrained Length	Sphere Member
145	P_2	P_3	0.7356	N/A	61
146	P_{29}	P_1	0.7356	N/A	62
147	P_{25}	P_2	0.6462	N/A	63
148	P_5	P_6	1.2000	N/A	55
149	P_6	P_4	1.0069	N/A	56
150	P_4	P_5	1.0069	N/A	57
151	P_8	P_{13}	0.7356	N/A	58
152	P_{13}	P_7	0.6462	N/A	59
153	P_7	P_8	0.7356	N/A	60
154	P_{10}	P_{14}	1.0069	N/A	56
155	P_{14}	P_9	1.0069	N/A	57
156	P_9	P_{10}	1.2000	N/A	55
157	P_{12}	P_{15}	0.6462	N/A	59
158	P_{15}	P_{11}	0.7356	N/A	60
159	P_{11}	P_{12}	0.7356	N/A	58
160	P_{16}	P_{22}	0.3758	N/A	60
161	P_{28}	P_{21}	0.3758	N/A	58
162	P_{27}	P_{16}	0.6462	N/A	59
163	P_{18}	P_{23}	0.2692	N/A	63
164	P_{23}	P_{17}	0.3065	N/A	61
165	P_{17}	P_{18}	0.7356	N/A	62
166	P_{20}	P_{24}	0.3462	N/A	62
167	P_{24}	P_{19}	0.3065	N/A	63
168	P_{19}	P_{20}	0.7356	N/A	61

Table 6.14: 6ν T-Octahedron Dome: Inner Binding Tendons

Member #	End Points	
169‡	P_{22}	P_{23}
170‡	P_{23}	P_{24}
171‡	P_{24}	P_{28}
172‡	P'_{22}	P'_{23}
173‡	P'_{23}	P'_{24}
174‡	P'_{24}	P'_{28}

Table 6.15: 6ν T-Octahedron Dome: Truncation Tendons

Point	Coordinates x	y	z	Sphere Point	Transform Number
P_1	1.7538	0.7511	3.1285	P_6	1
P_2	1.3434	1.6303	2.8864	P_7	1
P_3	-0.4191	2.3400	2.9400	P_5	2
P_4	0.8711	1.0149	3.5173	P_3	1
P_5	1.0378	-0.2360	3.5592	P_1	1
P_6	-0.0640	0.2053	3.7844	P_2	1
P_7	-1.4134	2.2919	2.8451	P_8	1
P_8	-1.0998	1.2224	3.4065	P_4	1
P_9	-1.0378	0.2360	3.5592	P_1	4
P_{10}	0.0640	-0.2053	3.7844	P_2	4
P_{11}	1.0998	-1.2224	3.4065	P_4	4
P_{12}	2.3233	-0.8934	2.9682	P_9	4
P_{13}	-2.3233	0.8934	2.9682	P_9	1
P_{14}	-0.8711	-1.0149	3.5173	P_3	4
P_{15}	1.4134	-2.2919	2.8451	P_8	4
P_{16}	-2.8451	1.4134	2.2919	P_8	9
P_{17}	-2.9400	0.4191	2.3400	P_5	4
P_{18}	-1.7538	-0.7511	3.1285	P_6	4
P_{19}	-1.3434	-1.6303	2.8864	P_7	4
P_{20}	0.4191	-2.3400	2.9400	P_5	11
P_{21}	0.8934	-2.9682	2.3233	P_9	8
P_{22}	-3.7309	-0.0860	0.0478	P_2	9
P_{23}	-3.1023	-1.7622	1.0954	P_6	9
P_{24}	-1.6100	-3.2017	1.0425	P_3	11

Table 6.16: 6ν T-Octahedron Dome: Initial Inner Coordinate Values

the initial positions and lengths of the struts would correspond to their final positions in the sphere computations. Since the spherical excesses of P_2 and P_3 differ from P_4 and P_6, the initial weights for members #160, #161, #166 and #167 also differ from the values for the corresponding members of the spherical structure. Note that in addition, as mentioned above, the actual weights used for these members are $\frac{5}{12}$ the weights corresponding to the sphere.

The derivation of the symmetry points from the basic points is shown in Table 6.18. Outer points follow the same symmetries as inner points. As mentioned above, due to the loss of symmetry as a result of the truncation, only the first three entries of Table 5.5 are possibilities here.

Point	Coordinates x	y	z	Sphere Point	Transform Number
P'_1	3.0842	0.8558	3.6132	P'_6	1
P'_2	1.4390	2.9290	3.5221	P'_7	1
P'_3	0.4745	3.0005	3.7764	P'_5	2
P'_4	0.9467	1.1801	5.1968	P'_3	1
P'_5	1.3525	0.2829	5.3714	P'_1	1
P'_6	0.3628	0.4068	5.4440	P'_2	1
P'_7	-2.1735	2.3144	4.1038	P'_8	1
P'_8	-1.5610	1.7442	4.6513	P'_4	1
P'_9	-1.3525	-0.2829	5.3714	P'_1	4
P'_{10}	-0.3628	-0.4068	5.4440	P'_2	4
P'_{11}	1.5610	-1.7442	4.6513	P'_4	4
P'_{12}	2.4411	-1.3815	4.3450	P'_9	4
P'_{13}	-2.4411	1.3815	4.3450	P'_9	1
P'_{14}	-0.9467	-1.1801	5.1968	P'_3	4
P'_{15}	2.1735	-2.3144	4.1038	P'_8	4
P'_{16}	-4.1038	2.1735	2.3144	P'_8	9
P'_{17}	-3.7764	-0.4745	3.0005	P'_5	4
P'_{18}	-3.0842	-0.8558	3.6132	P'_6	4
P'_{19}	-1.4390	-2.9290	3.5221	P'_7	4
P'_{20}	-0.4745	-3.0005	3.7764	P'_5	11
P'_{21}	1.3815	-4.3450	2.4411	P'_9	8
P'_{22}	-4.6513	1.5610	1.7442	P'_4	9
P'_{23}	-3.5221	-1.4390	2.9290	P'_7	9
P'_{24}	-0.8558	-3.6132	3.0842	P'_6	11

Table 6.17: 6ν T-Octahedron Dome: Initial Outer Coordinate Values

Point	Coordinates x	y	z	Basic Point	Transform Number
P_{25}	y_1	z_1	x_1	P_1	2
P_{26}	y_{12}	z_{12}	x_{12}	P_{12}	2
P_{27}	y_{21}	z_{21}	x_{21}	P_{21}	2
P_{28}	z_{22}	x_{22}	y_{22}	P_{22}	3
P_{29}	z_3	x_3	y_3	P_3	3

Table 6.18: 6ν T-Octahedron Dome: Symmetry Point Correspondences

Point	Coordinates x	y	z	Sphere Point	Transform Number
P_{22}	-3.784385	0.063992	0.205336	P_2	9
P_{23}	-3.128494	-1.753833	0.751127	P_6	9
P_{24}	-1.014868	-3.517327	0.871082	P_3	11

Table 6.19: 6ν T-Octahedron Dome: Base Point Initial Raw Coordinate Values

6.2.3 Dome Step 3: Adjust the base points

Table 6.19 shows the unadjusted raw coordinate values for the base points. The mathematical programming problem for the dome treats these three points are fixed. Strictly speaking, once these points are treated as fixed, the structure is no longer a tensegrity since it is no longer self-supporting.[3]

Practically speaking, this seems a useful approach to developing a dome. So, the self-support requirement some definitions make for a true tensegrity will be ignored and the constraints to fix the base points will be included with the point constraints discussed in Chapter 3. Certainly it would be possible to develop a dome which met the self-support requirement. Another truncation technique would need to be developed, but the truncation would probably be a little more ragged looking and the structural support from the fixed base points would probably be missed. The resulting dome would be more mobile though.

To facilitate construction and perhaps make the structure more aesthetically pleasing, the base points for the not-quite-a-tensegrity dome being designed here are adjusted to lie evenly spaced on a circle about the symmetry axis of the dome. This section gives the details of how that adjustment is made.

The symmetry axis is the line through the origin and the point (1.0, 1.0, 1.0). It is convenient to normalize the corresponding vector so it has length 1.0, so the vector $(\frac{1}{\sqrt{3}}, \frac{1}{\sqrt{3}}, \frac{1}{\sqrt{3}})$ is used whenever the symmetry axis is needed for computations and is called

[3]See *Wang98.* Wang goes beyond the definition by Pugh quoted in Chapter 1 to identify the following characteristics of a tensegrity structure:

1. It is composed of compression and tension elements.
2. The struts (compression elements) are discontinuous while the cables (tension elements) are continuous.
3. The structure is rigidified by self-stressing.
4. The structure is self-supporting.

Sometimes the second item is modified to allow struts which are attached to each other by pin joints. None of the examples discussed in this book are of that sort. Certainly all the techniques described here would apply to such tensegrities, but simpler procedures might apply in these cases and thus obviate the need for solving a mathematical programming problem. *Kenner76,* p. 6, uses the term "self-sufficient" to describe the quality of tensegrity structures characterized by the fourth item.

	$P^{\perp}$ Coordinates				
Point	x	y	z	r	h
P_{22}	-2.612699	1.235678	1.377022	3.201451	-2.029419
P_{23}	-1.751428	-0.376766	2.128194	2.781844	-2.385149
P_{24}	0.205503	-2.296956	2.091453	3.113264	-2.113745
Average	N/A	N/A	N/A	3.032187	-2.176104

Table 6.20: 6ν T-Octahedron Dome: Raw Base Point Characteristics

A.

The transformed points lie on a circle chosen so that the points are moved as little as possible because of the transformation. The radius of the circle is the average distance of the raw points from the symmetry axis (see Chapter 8 for the formula for calculating the distance of a point from a line). This value is called r_{avg}. In addition, the transformed points are selected so that they all have the same value when projected onto the symmetry axis, and it will be the average of the values for the three raw points. This common value is called as h_{avg}. The projection is computed by taking the dot product of the point with A. The component of the point orthogonal to the axis is called $P_i^{\perp}$ and is computed using the formula $P_i^{\perp} = P_i - (P_i \cdot A)A$. This data is summarized in Table 6.20.

The transformed value of P_{22}, call it P_{22}^*, is generated using the formula $P_{22}^* = h_{avg}A + \frac{r_{avg}}{|P_{22}^{\perp}|}P_{22}^{\perp}$. The transformed values for the other two points are generated by by rotating P_{22}^* about the symmetry axis by $\frac{2\pi}{9}$ and $\frac{4\pi}{9}$. Nine was chosen as the divisor for the two rotation angles since there are nine base points when all symmetry transformations are taken into account. The general matrix for rotating a point about a normalized (so it has length one) vector $(x,\ y,\ z)$ by an angle θ is:[4]

$$\begin{bmatrix} x^2 + (1-x^2)\cos\theta & xy(1-\cos\theta) - z\sin\theta & xz(1-\cos\theta) + y\sin\theta \\ xy(1-\cos\theta) + z\sin\theta & y^2 + (1-y^2)\cos\theta & yz(1-\cos\theta) - x\sin\theta \\ xz(1-\cos\theta) - y\sin\theta & yz(1-\cos\theta) + x\sin\theta & z^2 + (1-z^2)\cos\theta \end{bmatrix}$$

In the present situation, the normalized vector in question is just A and the value of θ is $\frac{2\pi}{9}$. Substituting these values yields the matrix:

$$\begin{bmatrix} \frac{1}{3} + \frac{2}{3}\cos\left(\frac{2\pi}{9}\right) & \frac{(1-\cos\left(\frac{2\pi}{9}\right))}{3} - \frac{\sin\left(\frac{2\pi}{9}\right)}{\sqrt{3}} & \frac{(1-\cos\left(\frac{2\pi}{9}\right))}{3} + \frac{\sin\left(\frac{2\pi}{9}\right)}{\sqrt{3}} \\ \frac{(1-\cos\left(\frac{2\pi}{9}\right))}{3} + \frac{\sin\left(\frac{2\pi}{9}\right)}{\sqrt{3}} & \frac{1}{3} + \frac{2}{3}\cos\left(\frac{2\pi}{9}\right) & \frac{(1-\cos\left(\frac{2\pi}{9}\right))}{3} - \frac{\sin\left(\frac{2\pi}{9}\right)}{\sqrt{3}} \\ \frac{(1-\cos\left(\frac{2\pi}{9}\right))}{3} - \frac{\sin\left(\frac{2\pi}{9}\right)}{\sqrt{3}} & \frac{(1-\cos\left(\frac{2\pi}{9}\right))}{3} + \frac{\sin\left(\frac{2\pi}{9}\right)}{\sqrt{3}} & \frac{1}{3} + \frac{2}{3}\cos\left(\frac{2\pi}{9}\right) \end{bmatrix}$$

Applying this matrix once to P_{22}^* yields P_{23}^*. Applying this matrix twice to P_{22}^* yields P_{24}^*.

[4]From *Rogers76,* Chapter 3.

The transformed values are what appear in Table 6.16.

6.2.4 Dome Step 4: Add guys

With the truncation methodology discussed here, adding guys, and points on the ground to attach them to, is usually advisable. A valid tensegrity could be obtained without these guys, but it would be a very rickety one. Minor lateral forces applied to the structure would move it substantially. With the guys in place, the structure will resist lateral forces more robustly.

The guys are where the outer layer of tendons meets the ground. Their attachment points should be chosen so they mimic the effect of the outer-layer tendons which would have appeared in this vicinity but were discarded due to the truncation. The guy attachment points are in the same plane as the base points and will fall on a circle which is a dilatation of the base-point circle. More precisely, the attachment-point circle is chosen to be the intersection of a sphere approximating the outer layer of tendons with the ground. Call the radius of this circle r'_{avg}. r'_{avg} is calculated using the formula

$$r'_{avg} = \sqrt{(\frac{\sum_{i=1}^{\frac{n_h^s}{2}} |P'_i|}{\frac{n_h^s}{2}})^2 - h_{avg}^2}$$

where n_h^s is the number of basic points in the sphere, and P'_i is an outer-layer basic point of the sphere. For the 6ν sphere, the value of n_h^s is 18, and the value of r'_{avg} is $\sqrt{5.15085^2 - (-2.176104)^2} = 4.66860$.

Another question is how much to rotate the guy-attachment points relative to the base points. A sensible place to start would seem to be half the angle between the base points, $\frac{\pi}{9}$ in this case. These can be adjusted later if that can help ease distortions of the realization of the sphere's configurations in the dome. With this in mind, it seems reasonable to put the guys in the objective function to let the computations themselves give feedback on the necessary rotation factor.

The guy weights should be chosen also so as to aid the realization of the sphere's configurations in the dome as closely as possible.

Table 6.21 lists the coordinates which resulted from applying the above procedures to deriving the guy attachment points. Table 6.22 gives the data for the one guy attachment point which is generated using a symmetry transformation. Table 6.23 enumerates the data for the six guys which are added to the model in this step.

Point	Coordinates x	y	z
P'_{30}	-4.795937	-0.711963	1.738777
P'_{31}	-3.058334	-3.264453	2.553663
P'_{32}	-0.477574	-4.877340	1.585790

Table 6.21: 6ν T-Octahedron Dome: Guy Attachment Point Coordinates

Point	Coordinates x	y	z	Basic Point	Transform Number
P'_{33}	z'_{30}	x'_{30}	y'_{30}	P'_{30}	3

Table 6.22: 6ν T-Octahedron Dome: Guy-Attachment-Point Symmetry Correspondence

Member #	End Points		Weight	Constrained Length	Sphere Member
175	P'_{30}	P'_{23}	0.4000	N/A	N/A
176	P'_{23}	P'_{31}	0.4000	N/A	N/A
177	P'_{31}	P'_{24}	0.4000	N/A	N/A
178	P'_{24}	P'_{32}	0.4000	N/A	N/A
179	P'_{32}	P'_{28}	0.4000	N/A	N/A
180	P'_{28}	P'_{33}	0.4000	N/A	N/A

Table 6.23: 6ν T-Octahedron Dome: Guys

Member Pair	Preliminary Clearance	Final Clearance
7-20	0.1373	0.1994
13-17	0.1596	0.1855
13-24	0.1587	0.1811
17-24	0.1591	0.1894
18-20	0.1403	0.1927
21-23	0.1741	0.1901
18-44	0.1101	0.1519
20-31	0.1106	0.1616

Table 6.24: 6ν T-Octahedron Dome: Preliminary and Final Values for Problem Clearances

6.2.5 Dome Step 5: Compute the dome

As usual, the structure was computed by minimizing a weighted combination of the interlayer and binding tendons subject to constraints on the struts and convergence tendons. The big difference was the base points were kept fixed. In addition to providing the benefits mentioned previously, fixing these points also makes the structure mathematically determinate.

Two initial iterations were done using the penalty formulation ($\overline{\mu} = 10^5$) in conjunction with Fletcher-Reeves to bring the initial points into approximate conformance with the constraints. The source of the initial non-conformity with the constraints is the adjustment of the base points that was done in **Step 3**. After this three iterations were done with the exact formulation in conjunction with Fletcher-Reeves to bring the values to convergence. The derivatives of the objective function with respect to the independent variables were all less than 10^{-5}.

6.2.6 Dome Step 6: Make adjustments to fix problems

The same clearance goals that are used for the 4ν t-octahedron spherical truss in Section 8.2.3 seem appropriate for this structure. With these thresholds, eight member pairs were singled out as having poor clearances. The poor clearances were mostly between pairs of struts. Table 6.24 enumerates the member pairs involved and the corresponding clearances. In addition, the solution exhibited a substantial range in member forces in the tendons, from a minimum of 0.7076 (#143) to a maximum of 5.5859 (#99).

The interference problem is the most fundamental one. A range of tendon forces can be dealt with at construction time by using different materials depending on the relative force for the tendons, though in some situations it might be worthwhile to see what can be done

Strut #	Outer Binding Tendon #	Revised Weight
18	138	0.4038
20	140	0.4597
13	133	0.4038
24	144	0.3371
21	141	0.3678
17	137	0.3371

Table 6.25: 6ν T-Octahedron Dome: Member Weight Adjustments

to moderate the range of forces at design time. The forces are greatest in the convergence and interlayer tendons and smallest in the binding tendons and guys.

The interference problem can mostly be attributed to the low frequency of the model. At lower frequencies, the inward-pointing tripods whose peaks are the inner convergence tendon triangles tend to be shallow. This means the non-adjacent component members approach each other too closely in the vicinity of the convergence triangle.

The interference problem can be fixed by decreasing the lengths of the outer binding tendons which constrain the extent of the base of the tripod. Since the binding tendons are all weighted members of the objective function in this model, this means increasing the weight corresponding to the outer binding tendon in question. The outer binding tendon to select is the one which most parallels the strut with the clearance problem. Increasing the weight on this tendon gives the strut a steeper trajectory on its path from the outer to the inner layer and thus keeps it from approaching nearby tendons and struts at the convergence too closely. Table 6.25 lists the outer-binding tendon corresponding to each strut with an interference problem and the new value which was selected for the tendon's weight.

The revised model was brought to convergence using three iterations with the exact method in conjunction with Fletcher-Reeves. The derivatives of the objective function with respect to the independent variables were all less than 10^{-5} and all clearances were above their respective thresholds.

Tables 6.26 to 6.30 show the values for the final lengths and relative forces. As before, excluded members are marked with ‡. Tables 6.31 and 6.32 show the final values for the coordinates of the basic points. Figures 6.10 and 6.11 show how the final structure appears as viewed from the side and base of the structure respectively. For clarity, interlayer tendons have been excluded[5] and members in the background have been eliminated by truncation. For reference, selected points are labeled.

[5]In Figure 6.10 the interlayer tendons at the base are included. In Figure 6.11 guys are also excluded.

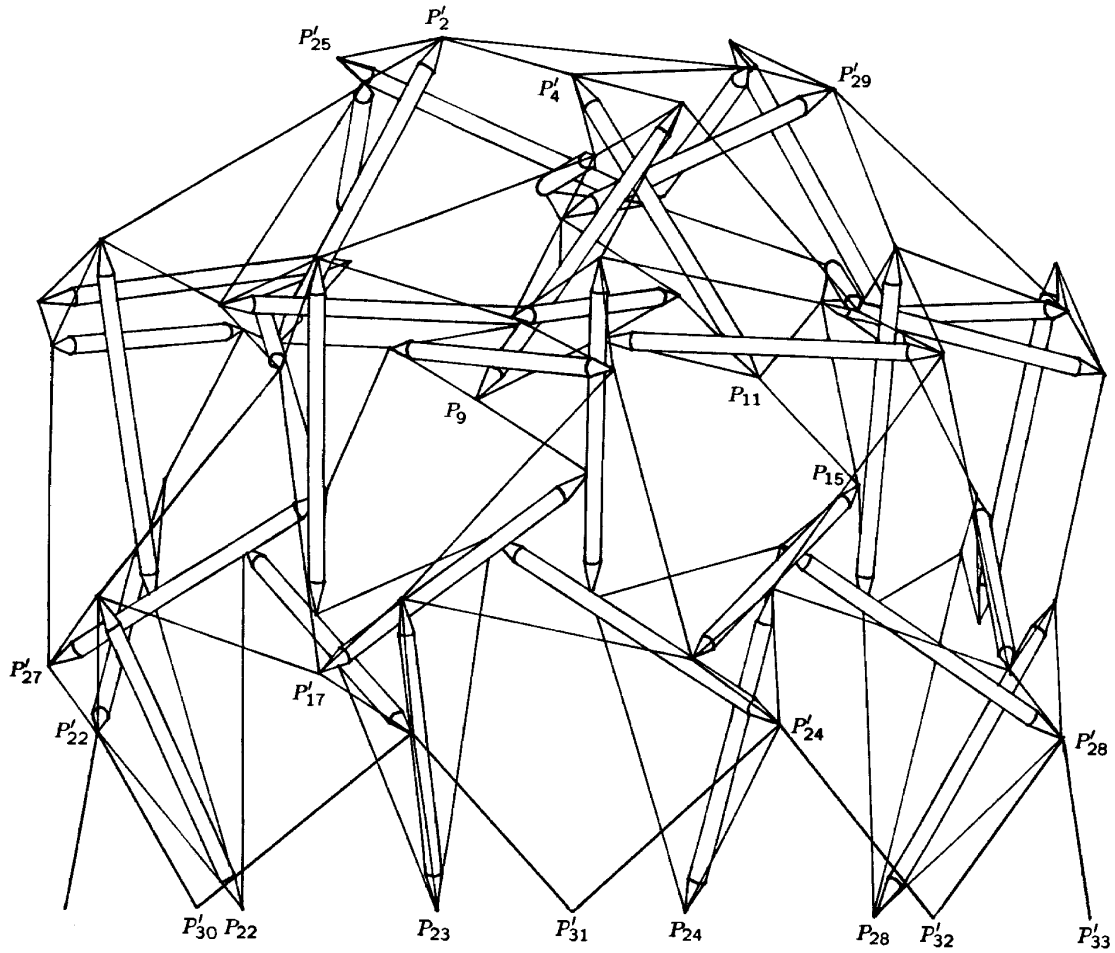

Figure 6.10: 6ν T-Octahedron Dome: Side View

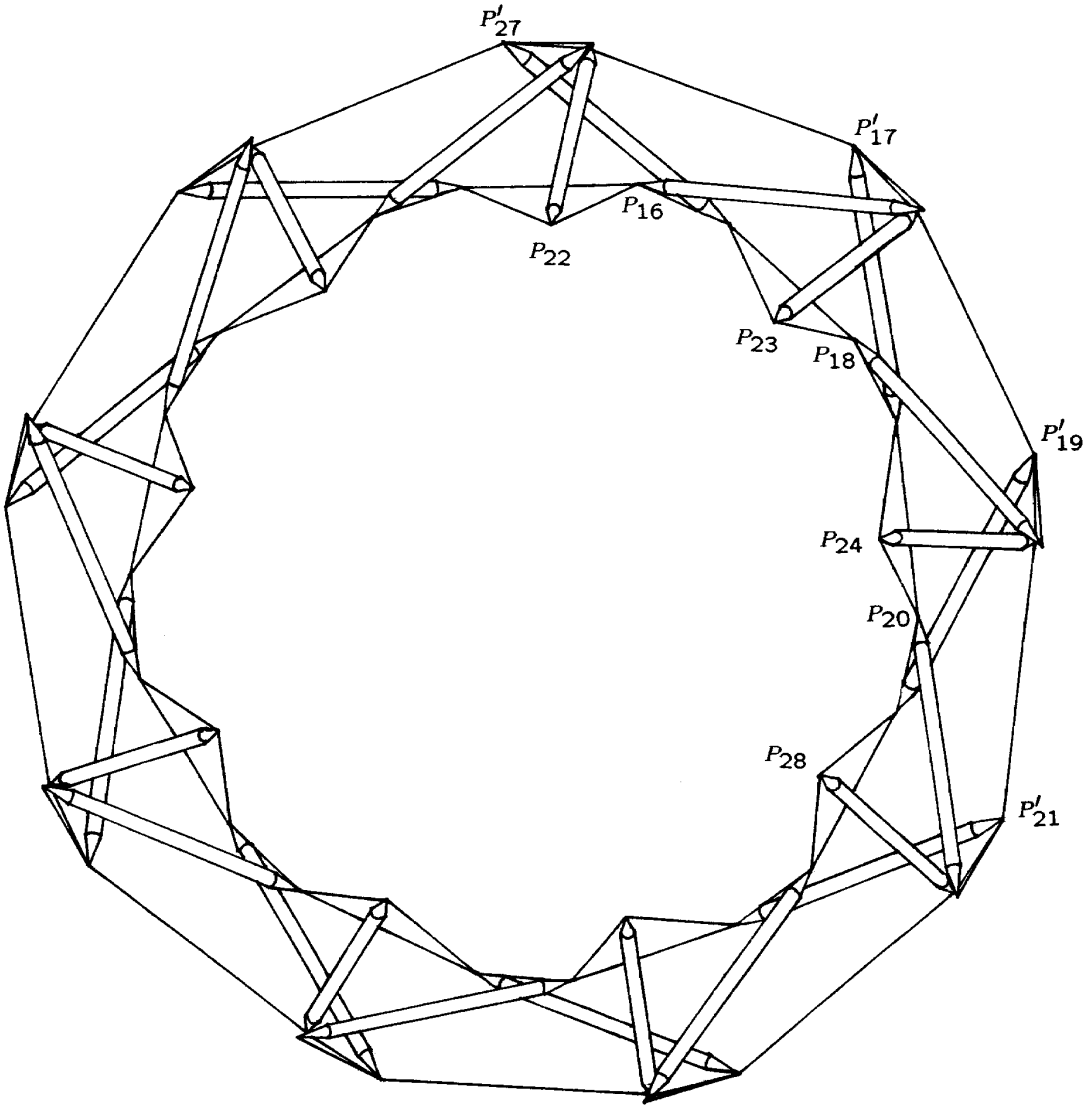

Figure 6.11: 6ν T-Octahedron Dome: Base View

Member #	Relative Force	Member #	Relative Force
1	-10.0652	13	-10.1760
2	-10.0700	14	-9.9202
3	-9.8692	15	-10.1476
4	-11.3735	16	-6.9104
5	-9.7762	17	-9.8347
6	-9.9708	18	-10.6229
7	-10.4024	19	-6.8948
8	-10.0965	20	-9.9960
9	-9.8578	21	-10.0265
10	-10.0713	22	-6.9341
11	-9.9785	23	-9.5009
12	-11.2464	24	-10.1033

Table 6.26: 6ν T-Octahedron Dome: Final Strut Forces

Member #	Length	Relative Force	Member #	Length	Relative Force
25	2.21528	4.43056	49	2.03547	2.84966
26	2.21563	4.43127	50	2.04556	2.86379
27	2.23160	4.46319	51	2.05261	2.87366
28	2.34655	4.69309	52	2.11527	2.96138
29	2.38618	4.77235	53	2.08314	2.91640
30	2.49013	4.98025	54	2.14563	3.00388
31	2.27745	4.55489	55	2.04900	2.86860
32	2.29331	4.58661	56	2.03644	2.85101
33	2.32354	4.64708	57	1.66652	2.33313
34	2.38195	4.76390	58	2.06601	2.89242
35	2.49956	4.99913	59	2.15096	3.01134
36	2.37208	4.74416	60	2.11199	2.95678
37	2.26419	4.52838	61	2.03412	2.84777
38	2.29568	4.59136	62	1.64781	2.30693
39	2.26971	4.53941	63	2.03600	2.85040
40	2.25878	4.51755	64‡	N/A	N/A
41	2.24921	4.49841	65	2.03254	2.84556
42	2.23545	4.47090	66	2.04716	2.86602
43	2.25887	4.51773	67‡	N/A	N/A
44	2.24099	4.48198	68	2.04286	2.86000
45	2.25145	4.50290	69	2.03439	2.84814
46	2.22034	4.44068	70‡	N/A	N/A
47	2.23455	4.46910	71	2.04209	2.85893
48	2.21944	4.43888	72	2.03221	2.84510

Table 6.27: 6ν T-Octahedron Dome: Final Primary and Secondary Interlayer Tendon Lengths and Forces

Member #	Relative Force	Member #	Relative Force
73	4.94358	97	4.80745
74	5.26772	98	5.13742
75	5.16773	99	5.60404
76	4.99886	100	4.16775
77	4.65185	101	4.90834
78	3.74185	102	4.01986
79	5.18694	103	5.00085
80	5.03322	104	4.84606
81	4.93701	105	5.26904
82	5.14960	106	4.86884
83	3.71641	107	3.88380
84	4.87812	108	4.23798
85	5.03940	109	5.26776
86	5.07807	110	5.32991
87	5.16635	111	4.92827
88‡	N/A	112	4.59887
89	5.01478	113	5.07911
90	5.46741	114	5.78452
91‡	N/A	115	5.09214
92	4.28841	116	4.80643
93	4.59298	117	5.27596
94‡	N/A	118	4.72593
95	4.69291	119	5.04795
96	4.92845	120	5.43235

Table 6.28: 6ν T-Octahedron Dome: Final Inner and Outer Convergence Tendon Forces

Member #	Length	Relative Force	Member #	Length	Relative Force
121	2.71468	0.83201	145	1.89573	1.39443
122	2.63323	0.80705	146	1.83588	1.35041
123	2.66060	0.71632	147	2.01047	1.29907
124	1.83931	0.91966	148	1.21969	1.46362
125	2.46934	0.75682	149	1.28634	1.29525
126	2.30250	0.96601	150	1.28603	1.29493
127	2.54956	0.78140	151	1.28778	0.94725
128	2.61512	0.70407	152	1.65590	1.06997
129	2.59438	1.08847	153	1.28393	0.94442
130	2.56952	0.78752	154	1.25425	1.26293
131	2.18508	0.91675	155	1.27167	1.28048
132	1.85150	0.92575	156	1.22455	1.46946
133	2.63419	1.06381	157	1.75026	1.13094
134	2.60938	1.09477	158	1.32695	0.97606
135	2.73434	0.83804	159	1.39698	1.02757
136‡	N/A	N/A	160	2.90432	1.09132
137	2.69610	0.90895	161	2.54133	0.95493
138	2.72853	1.10191	162	1.84911	1.19481
139‡	N/A	N/A	163	2.94704	0.79343
140	2.54147	1.16838	164	2.52654	0.77435
141	2.69328	0.99054	165	1.79527	1.32054
142‡	N/A	N/A	166	2.87212	0.99419
143	2.66242	0.71680	167	2.67465	0.81974
144	2.68231	0.90430	168	1.89872	1.39663

Table 6.29: 6ν T-Octahedron Dome: Final Outer and Inner Binding Tendon Lengths and Forces

Member #	Length	Relative Force
175	2.13957	0.85583
176	2.03774	0.81510
177	2.20311	0.88124
178	2.06426	0.82570
179	2.23546	0.89419
180	2.00217	0.80087

Table 6.30: 6ν T-Octahedron Dome: Final Guy Lengths and Forces

Point	Coordinates		
	x	y	z
P_1	1.80813	0.75948	3.17349
P_2	1.37576	1.63043	2.94000
P_3	-0.38534	2.33141	2.97035
P_4	0.93791	1.01456	3.59498
P_5	1.08789	-0.26100	3.66069
P_6	0.00032	0.20887	3.95059
P_7	-1.37989	2.26180	2.89276
P_8	-1.03831	1.21623	3.55502
P_9	-0.98267	0.24115	3.76980
P_{10}	0.13756	-0.21195	3.96804
P_{11}	1.10801	-1.24300	3.47290
P_{12}	2.34501	-0.88144	2.93375
P_{13}	-2.16855	0.81829	3.08325
P_{14}	-0.80566	-1.01805	3.78455
P_{15}	1.36294	-2.31666	2.73597
P_{16}	-2.65858	1.30563	2.36051
P_{17}	-2.80252	0.32432	2.48821
P_{18}	-1.69815	-0.70421	3.46056
P_{19}	-1.33769	-1.58608	3.15663
P_{20}	0.38282	-2.35663	2.93031
P_{21}	0.77488	-2.93589	2.21564
P_{22}	-3.73094	-0.08603	0.04784
P_{23}	-3.10232	-1.76219	1.09539
P_{24}	-1.60996	-3.20168	1.04252

Table 6.31: 6ν T-Octahedron Dome: Final Inner Coordinate Values

Point	Coordinates		
	x	y	z
P'_1	3.14866	0.86815	3.60831
P'_2	1.46480	2.92782	3.57404
P'_3	0.49843	2.97345	3.82708
P'_4	1.12403	1.16198	5.26616
P'_5	1.52593	0.25847	5.41497
P'_6	0.54407	0.39653	5.54496
P'_7	-2.11381	2.32487	4.18070
P'_8	-1.49949	1.78849	4.75941
P'_9	-1.19400	-0.20205	5.60735
P'_{10}	-0.20625	-0.35308	5.64651
P'_{11}	1.60916	-1.87445	4.55170
P'_{12}	2.49145	-1.52781	4.23324
P'_{13}	-2.36532	1.39524	4.45003
P'_{14}	-0.82018	-1.11302	5.43305
P'_{15}	2.16560	-2.42225	3.92697
P'_{16}	-3.97029	1.88345	2.29814
P'_{17}	-3.70848	-0.43912	3.29623
P'_{18}	-3.04238	-0.81407	3.94099
P'_{19}	-1.41738	-2.90865	3.69479
P'_{20}	-0.43534	-3.06546	3.79964
P'_{21}	1.37815	-4.22827	2.17849
P'_{22}	-4.47657	1.26415	1.69803
P'_{23}	-3.50421	-1.41803	3.29141
P'_{24}	-0.95692	-3.59216	3.12842
P'_{30}	-4.79594	-0.71196	1.73878
P'_{31}	-3.05833	-3.26445	2.55366
P'_{32}	-0.47757	-4.87734	1.58579

Table 6.32: 6ν T-Octahedron Dome: Final Outer Coordinate Values

Chapter 7

Tensegrity Member Force Analysis

7.1 Force Analysis: Introduction

A method for ascertaining the forces in the various members of a tensegrity structure is useful to the builder. It allows the builder to make a sensible choice of materials for the different members which will meet the requirements of the loads the members will have to bear. In early design stages, force analysis will point up any overloaded members in the structure as well as situations where a member is bearing no load or a load which is not appropriate to it (for instance when calculations show a tensile member is bearing a compressive load). Force analysis aids the formulation of an assembly strategy: it is easier to install the tighter members earlier when they bear less of their full load.

The gross analysis of forces in a tensegrity structure is comparatively simple due to the flexible interconnection of the members. Shear forces can be neglected, and only the axial tensile and compressive forces need to be taken into account.[1] However, a detailed analysis of a tensegrity, for example of the various parts of a hub, may require attention to shear forces.

In most non-tensegrity trusses, the forces in the members of the truss are only due to the propagation through the structure of external loads **exogenous** to the structure such as the force of gravity and the foundation of the structure pressing up against it. However, tensegrity structures are prestressed so that an additional portion (and, in some applications, the total portion) of the force in a member can be attributed to the structure itself. This is due to the fact that a tensegrity structure relies on the isometric straining of the inwardly pulling tensile members against the outwardly pushing compression members to create a stable structural system. The geometry of the structure determines the magnitude (up to a scale factor) of the member forces due to these **endogenous** factors.

[1] For example, see *Chajes83*, pp. 36-37. "Axial" means the direction of the force coincides with the direction of the member.

So, in analyzing the forces in a tensegrity structure, both **exogenous** and **endogenous** factors must be taken into account. The analysis of the endogenous forces is derived directly from the model used for computing tendon lengths and is discussed first. The analysis of exogenous forces is discussed second since it presumes the analysis of endogenous forces has already been done.

7.2 Endogenous Member Forces

7.2.1 Endogenous Force Analysis: Method

The analysis of endogenous forces falls in large measure out of the mathematical programming procedures which were used to design the structure. This is due to the fact that the distribution of forces in the structure can be viewed as the solution to an extremal problem very similar to the one which was solved to design the structure. In this new problem, potential energy is being minimized instead of tendon lengths. It will be shown that, for members appearing as constraints, the relative force the member is subject to is obtained merely by differentiating the objective function with respect to the constraint value and multiplying the result by minus the member length (the second root of the constraint value). For members appearing in the objective function, the relative force will be just the member length multiplied by its weight in the objective function. These results can be scaled up or down according to how hard the structure is to be tensioned.

The analysis of endogenous forces, also called prestress forces, assumes the structure is floating in space and not subject to external loads. The analysis comes back to Earth when the response of members to external loads is examined in Section 7.3.

7.2.2 Endogenous Force Analysis: A Justification for the Method

One justification for the method described above lies in the principle that any system in stable equilibrium is at a local minimum in its potential energy. Theodore Tauchert[2] gives the following formal statement of this Principle of Minimum Potential Energy:

> Of all displacement fields which satisfy the prescribed constraint conditions, the correct state is that which makes the total potential energy of the structure a minimum.

In a tensegrity system, the potential energy is the energy bound up in the tendons and struts. When a member changes length, its potential energy changes according to how much work is done on it. (The members are assumed to be linearly elastic.):

[2] *Tauchert74,* p. 74.

$$de_{i_m} = f_{i_m} dl_{i_m}$$

where de_{i_m} is the change in potential energy of the i_mth member, f_{i_m} is the stress on the member and dl_{i_m} is the change in length of the member. The usual convention that f_{i_m} is negative when the stress is compressive and positive when the stress is tensile applies here. If the system is in equilibrium, a small feasible[3] change in the lengths of all the members should result in a zero change in the aggregate potential energy of the system since that potential energy must be at a minimum. [4] The condition for zero aggregate energy change can be summarized as:

$$0 = de_1 + de_2 + \cdots + de_{n_m}$$

where, as in Chapter 3, n_m is the number of members.

Using the other formula, this can be rewritten as:

$$0 = f_1 dl_1 + f_2 dl_2 + \cdots + f_{n_m} dl_{n_m}$$

How does this relate to the mathematical programming problem of Chapter 3? Since members 1 through n_o appear in the objective function and members $n_o + 1$ through n_m appear as constraints, and using $\frac{\partial \mathrm{o}}{\partial(\bar{l}^2_{i_{\bar{o}}})}$ to denote the amount the objective function changes in response to a change in the **second power** of the length of the $i_{\bar{o}}$th constrained member, it must be that the response of the objective function to an arbitrary change in the lengths of the constrained members is:

$$\begin{aligned} d\mathrm{o} &= \frac{\partial \mathrm{o}}{\partial(\bar{l}^2_{n_o+1})} d(\bar{l}^2_{n_o+1}) + \cdots + \frac{\partial \mathrm{o}}{\partial(\bar{l}^2_{n_m})} d(\bar{l}^2_{n_m}) \\ &= 2\frac{\partial \mathrm{o}}{\partial(\bar{l}^2_{n_o+1})} \bar{l}_{n_o+1} d\bar{l}_{n_o+1} + \cdots + 2\frac{\partial \mathrm{o}}{\partial(\bar{l}^2_{n_m})} \bar{l}_{n_m} d\bar{l}_{n_m} \end{aligned}$$

The formula for o says, for the objective members, it is also true that:

$$d\mathrm{o} = \overline{w}_1 d(l^{*2}_1) + \overline{w}_2 d(l^{*2}_2) + \cdots + \overline{w}_{n_o} d(l^{*\ 2}_{n_o})$$

[3] Feasible here means that all constraint equations continue to be satisfied. In contrast to the situation in Chapter 3 however, all member lengths may change. This means $\bar{l}_{n_o+1}, \ldots, \bar{l}_{n_m}$ may change. In addition the constraints are met with equality

[4] A negative change would directly violate the assumption that the original configuration was a minimum. A positive change would indirectly violate the assumption since the point displacement which resulted in the change could be negated and this would result in a negative change from the original configuration.

which reduces to:

$$d\mathrm{o} = 2\overline{w}_1 l_1^* dl_1^* + 2\overline{w}_2 l_2^* dl_2^* + \cdots + 2\overline{w}_{n_o} l_{n_o}^* dl_{n_o}^*$$

where $l_{i_o}^*$ is the **minimizing** length of the i_oth unconstrained member.

If all the constraints are changed by an arbitrary amount, then it must be true that:

$$2\overline{w}_1 l_1^* dl_1^* + \cdots + 2\overline{w}_{n_o} l_{n_o}^* dl_{n_o}^* = 2\frac{\partial \mathrm{o}}{\partial(\bar{l}_{n_o+1}^2)}\bar{l}_{n_o+1} d\bar{l}_{n_o+1} + \cdots + 2\frac{\partial \mathrm{o}}{\partial(\bar{l}_{n_m}^2)}\bar{l}_{n_m} d\bar{l}_{n_m}$$

or (using the fact that the constraints are met with equality, canceling the common factor of two and collecting terms):

$$0 = \overline{w}_1 l_1^* dl_1^* + \cdots + \overline{w}_{n_o} l_{n_o}^* dl_{n_o}^* + -\frac{\partial \mathrm{o}}{\partial(\bar{l}_{n_o+1}^2)} l_{n_o+1} dl_{n_o+1} + \cdots + -\frac{\partial \mathrm{o}}{\partial(\bar{l}_{n_m}^2)} l_{n_m} dl_{n_m}$$

The similarity of this formula to the formula for potential energy minimization indicates a conclusion is almost at hand. The only complication is that in this latter formula, although the changes in the lengths of the constrained members may be considered arbitrary, the changes in the lengths of members included in the objective function must be regarded as changes in the minimizing tendon lengths and are not arbitrary feasible changes. This complication can be disposed of by noticing that it is assumed feasible displacements from a minimizing solution are being examined. Since the objective function is at a minimum, any feasible displacement of the objective variables away from their minimizing values will have no effect on the objective function value.

Thus, a feasible displacement of the member lengths is broken into two parts. First, the lengths of the constrained members are displaced. That displacement will result in a corresponding minimizing displacement of the unconstrained member lengths such that the equation just set forth is satisfied. Then an additional displacement is added to the lengths of the unconstrained members so that the total displacement is equal to the initial arbitrary feasible displacement. The additional effect of this displacement on the objective function value must be zero since it is a feasible displacement from a minimum with no change in the constraints. Therefore, the change in the objective function resulting from the arbitrary displacement is the same as the result obtained when the unconstrained members change in a minimizing manner.

So it is verified that for an arbitrary feasible deviation from a minimizing solution:

$$\overline{w}_1 l_1 dl_1 + \cdots + \overline{w}_{n_o} l_{n_o} dl_{n_o} = \overline{w}_1 l_1^* dl_1^* + \cdots + \overline{w}_{n_o} l_{n_o}^* dl_{n_o}^*$$

Thus:

$$0 = \overline{w}_1 l_1 dl_1 + \cdots + \overline{w}_{n_o} l_{n_o} dl_{n_o} + -\frac{\partial \mathrm{o}}{\partial(\bar{l}^2_{n_o+1})} l_{n_o+1} dl_{n_o+1} + \cdots + -\frac{\partial \mathrm{o}}{\partial(\bar{l}^2_{n_m})} l_{n_m} dl_{n_m}$$

So, if

$$\begin{aligned} f_1 &= \lambda \overline{w}_1 l_1 \\ &\cdots \\ f_{n_o} &= \lambda \overline{w}_{n_o} l_{n_o} \\ f_{n_o+1} &= -\lambda \frac{\partial \mathrm{o}}{\partial(\bar{l}^2_{n_o+1})} l_{n_o+1} \\ &\cdots \\ f_{n_m} &= -\lambda \frac{\partial \mathrm{o}}{\partial(\bar{l}^2_{n_m})} l_{n_m} \end{aligned}$$

where λ is some positive constant, the system will be in stable equilibrium. These are precisely the formulas described in Section 7.2.1. Notice that since for a strut $\frac{\partial \mathrm{o}}{\partial(\bar{l}^2_{i_{\tilde{o}}})}$ is positive, $f_{i_{\tilde{o}}}$ will be negative, a compressive force. And since $\frac{\partial \mathrm{o}}{\partial(\bar{l}^2_{i_{\tilde{o}}})}$ is negative for a tendon, $f_{i_{\tilde{o}}}$ is positive, a tensile force.

This manner of computing the member forces is very convenient since it derives from the method for computing member lengths. These force computations can be used to check proposed solutions of the mathematical programming problem which characterizes a given tensegrity. If tendons are not in tension, or struts are not in compression, the solution is not valid. (Perhaps some constraints which have been assumed to hold with equality are actually not effective.) In more complex structures, such a check is almost obligatory since some adjustments may need to be made for a valid solution to be attained. Thus, the processes of length computation and endogenous force computation are highly interdependent.

It is also interesting to use this result to examine a characteristic which has been attributed to Kenneth Snelson's structures. In his article "Kenneth Snelson", Grégoire Müller[5] states:

> ... in Snelson's pieces the degree of tension in the tension elements is directly proportional to the amount of space they occupy – a practical fact that he has encountered in the making of his sculptures, ...

Given the above-justified formulas for computing endogenous member forces, Müller's statement would seem to indicate that Snelson's design methodology is equivalent to

[5] *Müller71,* p. 26.

minimizing a simple unweighted sum of second powers of member lengths. It may be that the approach of minimizing an unweighted sum of second powers yields the most rigid and strongest designs and may be the appropriate choice in many situations, but it should be recalled how, in Section 6.2.1, the weighted approach helped to develop a spherical appearance when an unweighted sum of second powers would have yielded something very faceted looking.

7.2.3 Endogenous Force Analysis: Another Justification for the Method

Another justification for the method can be found by correlating the following two facts:

1. A solution to the member-force problem must necessarily exhibit an equilibrium of forces for any particular coordinate value.
2. The necessary first-order conditions for a solution to the tensegrity optimization problem require a set of terms to sum to zero.

Correlating these two facts will provide a solution to the member-force problem which also generalizes to non-member constraints like those pertaining to vectors.

The necessary equilibrium of forces in all coordinate directions for a solution to the member-force problem is an implication of Newton's second law of motion: if a body is to be at rest, the net sum of forces on that body must be zero. For a tensegrity, this means that, for a given hub to be at rest, the forces due to all the members and point constraints that impact that hub must sum to zero in all the three coordinate directions for the basic point corresponding to that hub.

The necessary first-order conditions for a solution to the tensegrity optimization problem can be obtained using the method of Lagrange which was used in Section 2.3. In contrast with that section, here the method of Lagrange is not useful for reaching a solution; but once a solution is obtained, it is useful in interpreting and applying it. For the general tensegrity programming problem, the adjoined objective function appears as:

$$\begin{gathered}
\overline{w}_1 l_1^2 + \cdots + \overline{w}_{n_o} l_{n_o}^2 + \\
\mu_{n_o+1}(\overline{l}_{n_o+1}^2 - l_{n_o+1}^2) + \cdots + \mu_{n_m}(\overline{l}_{n_m}^2 - l_{n_m}^2) + \\
\sigma_1(\overline{s}_1 - s_1(\cdots)) + \cdots + \sigma_{n_s}(\overline{s}_{n_s} - s_{n_s}(\cdots)) + \\
\delta_1(\overline{d}_1 - (\overline{W}_1 \cdot P_{d_1})) + \cdots + \delta_{n_d}(\overline{d}_{n_d} - (\overline{W}_{n_d} \cdot P_{d_{n_d}})) + \\
\gamma_1(\overline{c}_1 - c_1(\cdots)) + \cdots + \gamma_{n_c}(\overline{c}_{n_c} - c_{n_c}(\cdots))
\end{gathered}$$

where $\mu_{i_{\tilde{o}}}$, σ_{i_s}, δ_{i_d} and γ_{i_c} are the Lagrange multipliers for the member, symmetry, point and vector constraints respectively. Using a result from advanced calculus[6] which states that the value of the Lagrange multiplier at a solution point is just the derivative of the objective function value with respect to the constraint parameter, the adjoined objective function can be rewritten as:

$$\begin{gathered}
\overline{w_1} l_1^2 + \cdots + \overline{w}_{n_o} l_{n_o}^2 + \\
\frac{\partial \mathrm{o}}{\partial(\bar{l}_{n_o+1}^2)}(\bar{l}_{n_o+1}^2 - l_{n_o+1}^2) + \cdots + \frac{\partial \mathrm{o}}{\partial(\bar{l}_{n_m}^2)}(\bar{l}_{n_m}^2 - l_{n_m}^2) + \\
\frac{\partial \mathrm{o}}{\partial \overline{s}_1}(\overline{s}_1 - s_1(\cdots)) + \cdots + \frac{\partial \mathrm{o}}{\partial \overline{s}_{n_s}}(\overline{s}_{n_s} - s_{n_s}(\cdots)) + \\
\frac{\partial \mathrm{o}}{\partial \overline{d}_1}(\overline{d}_1 - (\overline{W}_1 \cdot P_{d_1})) + \cdots + \frac{\partial \mathrm{o}}{\partial \overline{d}_{n_d}}(\overline{d}_{n_d} - (\overline{W}_{n_d} \cdot P_{d_{n_d}})) + \\
\frac{\partial \mathrm{o}}{\partial \overline{c}_1}(\overline{c}_1 - c_1(\cdots)) + \cdots + \frac{\partial \mathrm{o}}{\partial \overline{c}_{n_c}}(\overline{c}_{n_c} - c_{n_c}(\cdots))
\end{gathered}$$

The necessary first-order conditions require that the derivative of this equation with respect to any coordinate value be zero. So, if $-\frac{\lambda}{2}$ times the derivative of a term in the adjoined objective function with respect to a coordinate value is used as the force corresponding to that coordinate direction for the object the term corresponds to, those force values for that particular coordinate value will sum to zero as required for the hub corresponding to that coordinate to be at rest according to Newton's second law of motion. The $-\frac{\lambda}{2}$ is introduced to cancel a ubiquitous two which would otherwise appear due to all the second powers and so the direction of the forces is correct. As in Section 7.2.2, λ is an arbitrary positive scaling value.

As an example, consider the member constraints. The force vectors corresponding to the two endpoints, call them P_a and P_b, of the constrained $i_{\tilde{o}}$th member will be

$$\lambda \frac{\partial \mathrm{O}}{\partial(\bar{l}_{i_{\tilde{o}}}^2)}(P_a - P_b) \quad \text{and} \quad \lambda \frac{\partial \mathrm{O}}{\partial(\bar{l}_{i_{\tilde{o}}}^2)}(P_b - P_a) \quad \text{respectively.}$$

Notice that since, for a strut, $\frac{\partial \mathrm{O}}{\partial(\bar{l}_{i_{\tilde{o}}}^2)}$ is positive, if this constrained member is a strut, the endpoint forces are in an outward direction which would be expected. The magnitude of this force is $\lambda \frac{\partial \mathrm{O}}{\partial(\bar{l}_{i_{\tilde{o}}}^2)} l_{i_{\tilde{o}}}$ which is the result which was obtained in Section 7.2.2. For the i_oth member in the objective function, the force vectors corresponding to the two endpoints will be

$$-\lambda \overline{w}_{i_o}(P_a - P_b) \quad \text{and} \quad -\lambda \overline{w}_{i_o}(P_b - P_a) \quad \text{respectively.}$$

[6] See the "Sensitivity Theorem" in *Luenberger73*, p. 231.

Since, for a strut, w_{i_o} is negative and therefore $-\lambda\overline{w}_{i_o}$ is positive, if this objective member is a strut, the endpoint forces are in an outward direction which would be expected. The magnitude of this force is $\lambda\overline{w}_{i_o}l_{i_o}$ which again is the result which was obtained in Section 7.2.2.

As another example, consider the case of the i_dth point constraint. In this case, differentiating the expression $\frac{\partial \mathrm{O}}{\partial \overline{d}_{i_d}}(\overline{d}_{i_d} - (\overline{W}_{i_d} \cdot P_{d_{i_d}}))$ with respect to the three coordinates of $P_{d_{i_d}}$ yields $\frac{\lambda}{2}\frac{\partial \mathrm{O}}{\partial \overline{d}_{i_d}}\overline{W}_{i_d}$ An increase in $\overline{d}_{i_d}$ implies the constraint plane is moving in the direction of $\overline{W}_{i_d}$. If $\frac{\partial \mathrm{O}}{\partial \overline{d}_{i_d}}$ is positive, this means an increase in $\overline{d}_{i_d}$ represents more constraint; hence, it makes sense that the reaction force from the constraint is pushing (or pulling) in the direction of $\overline{W}_{i_d}$.

Again it is seen that for tensegrities the solution of the optimization problem also provides useful information about the distribution of forces in the structure. The main advantage of this way of looking at the problem of computing forces in tensegrities is that it provides a way of computing the forces corresponding to non-member constraints which the previous approach had nothing to say about. The previous approach is valuable for the additional perspective it provides on the problem.

7.2.4 Endogenous Force Analysis: A Sample Calculation for the Exact Formulation

The analysis of the solution to the mathematical programming problem for the 4ν diamond tensegrity tetrahedron in Section 4.2.3 mentioned that the analysis of endogenous forces indicated that the initial solution which satisfied the first-order conditions was not valid since member force calculations indicated one of the tendons was acting as a strut. In this section, the details of those calculations are presented.

The formulas for the relative forces on the members included in the objective function pose no problem since they are just the lengths of the members. To calculate the relative force for the constrained $i_{\tilde{o}}$th member, the value of $\frac{\partial \mathrm{O}}{\partial(\bar{l}^2_{i_{\tilde{o}}})}$, the total derivative of the objective function with respect to the second power of the length of the $i_{\tilde{o}}$th member, is necessary. The method used to calculate $\frac{\partial \mathrm{O}}{\partial(\bar{l}^2_{i_{\tilde{o}}})}$ depends on whether the penalty or exact formulation (see Section 3.2) is being used.

For the 4ν diamond tensegrity tetrahedron, the final computations were made using the exact formulation. For this formulation, computing $\frac{\partial \mathrm{O}}{\partial(\bar{l}^2_{i_{\tilde{o}}})}$ is a straight forward exercise in linear algebra. By the envelope theorem of economics[7], the total derivative of the objective function with respect to a change in a constraint parameter (in this case the second power of the length of the $i_{\tilde{o}}$th member) is equal to the partial effect on the objective function due

[7] *Varian78,* p. 267.

to changes in the dependent variables (which must change since the equations determining them have changed). Due to the minimization, the effects on the objective function due to changes in the independent variables do not need to be taken into account. So, to find $\frac{\partial O}{\partial(\bar{l}^2_{i_{\bar{o}}})}$, the response of the dependent variables to a unit change in the length of the $i_{\bar{o}}$th member is computed; then, using the partial derivatives of the objective function with respect to the dependent variables, the corresponding response of the objective function is computed.

To calculate the response of the dependent variables, the following linear system is solved:

$$\mathbf{Jx} = \mathbf{b}$$

where $\mathbf{J}$ is an $n_{\bar{o}} + n_c + n_s + n_d$ by $n_{\bar{o}} + n_c + n_s + n_d$ matrix and $\mathbf{x}$ and $\mathbf{b}$ are $n_{\bar{o}} + n_c + n_s + n_d$ column vectors.

$\mathbf{J}$ is the submatrix of the matrix of member (and other equation) partials corresponding to the system of equations which determine the dependent variables as a function of the constraint parameters (mainly second powers of member lengths) and the independent variables.

$\mathbf{b}$ is a vector with zeros everywhere except for a 1 in the $i_{\bar{o}}$th position and represents a unit change in the second power of the length of the $i_{\bar{o}}$th member. $\mathbf{x}$ is the vector corresponding to the solution of the linear equation system. Its ith component is the response of the ith dependent variable to a unit change in the second power of the length of the $i_{\bar{o}}$th member.

Having obtained $\mathbf{x}$, its inner product (also called dot product) is taken with the vector $\mathbf{y}$ whose ith component is the partial derivative of the objective function with respect to the ith dependent variable. The result is the sought after value of $\frac{\partial O}{\partial(\bar{l}^2_{i_{\bar{o}}})}$, which is multiplied by $l_{i_{\bar{o}}}$ (the length of the member) to get the relative force on this constrained member.

Application of these operations to the first solution to the four-frequency diamond t-tetrahedron problem yielded the values in Table 7.1.

The first tendon is slightly in compression which is not an appropriate force for a tendon. Excluding that tendon constraint resulted in a new model in which the relative forces were correct (the relative force for the excluded tendon being zero). As expected, the resultant length of the excluded tendon was less than its permitted maximum value; so, all constraints were satisfied.

Eliminating a tendon is not the best way to deal with an inappropriate force since it tends to make the structure less rigid.

Member #	Member ID	Relative Force
1	t_{12}	-0.075081
2	t_{13}	1.193570
3	t_{23}	0.647498
4	t_{47}	0.492239
5	s_{ab}	-1.452650
6	s_{bb}	-1.089917
7	t_{ab1}	0.940409
8	t_{ab2}	0.448489
9	t_{bb1}	0.455651
10	t_{bb2}	0.601166

Table 7.1: 4ν Diamond T-Tetrahedron: Preliminary Relative Forces

7.2.5 Endogenous Force Analysis: Calculations for the Penalty Formulation

Calculating endogenous forces is simpler when the penalty formulation is being used. In this case, Luenberger's proposition regarding Lagrange multipliers[8] provides a simple formula for calculating $\frac{\partial \mathrm{O}}{\partial(\bar{l}^2_{i_{\bar{o}}})}$. Since in the penalty formulation used here (see Section 3.2) $\overline{\mu}(l^2_{i_{\bar{o}}} - \bar{l}^2_{i_{\bar{o}}})^2$ appears in the penalty function, that proposition yields:

$$\frac{\partial \mathrm{o}}{\partial(\bar{l}^2_{i_{\bar{o}}})} = -2\overline{\mu}(l^2_{i_{\bar{o}}} - \bar{l}^2_{i_{\bar{o}}})$$

where $\overline{\mu}$ is the penalty value. As with the exact formulation, multiplying this value by the length of the $i_{\bar{o}}$th constrained member yields the relative force for that member.

7.2.6 Generality of Weighted Models

These results on endogenous forces can be used to illustrate the generality of weighted models in tensegrity design. Namely, it can be demonstrated that, with an appropriate selection of weights, any valid tensegrity structure can be obtained as the solution of a weighted model.

Let $\bar{l}_1, \ldots, \bar{l}_{n_m}$ be a valid tensegrity solution. For a valid solution, any tension member must be at its minimum length given the lengths of all the other members and any compression

[8] *Luenberger73,* pp. 284-285.

member must be at its maximum length given the lengths of all the other members. Therefore, for the jth tension member, the model must be a solution to the problem:

$$\begin{array}{ccccc} \underset{P_1,...,P_{n_h},V_1,...,V_{n_v}}{\text{minimize}} & & \text{o} & \equiv & l_j^2 \\ \text{subject to} & \text{Member constraints:} & & & \\ & & \pm\bar{l}_1^2 & \geq & \pm l_1^2 \\ & & & \cdots & \\ & & \pm\bar{l}_{j-1}^2 & \geq & \pm l_{j-1}^2 \\ & & \pm\bar{l}_{j+1}^2 & \geq & \pm l_{j+1}^2 \\ & & & \cdots & \\ & & \pm\bar{l}_{n_m}^2 & \geq & \pm l_{n_m}^2 \\ & \text{Symmetry constraints:} & & & \\ & & \overline{s}_1 & = & s_1(\cdots) \\ & & & \cdots & \\ & & \overline{s}_{n_s} & = & s_{n_s}(\cdots) \\ & \text{Point constraints:} & & & \\ & & \overline{d}_1 & = & \overline{W}_1 \cdot P_{d_1} \\ & & & \cdots & \\ & & \overline{d}_{n_d} & = & \overline{W}_{n_d} \cdot P_{d_{n_d}} \\ & \text{Vector constraints:} & & & \\ & & \overline{c}_1 & = & c_1(\cdots) \\ & & & \cdots & \\ & & \overline{c}_{n_c} & = & c_{n_c}(\cdots) \end{array}$$

Let $\overline{\frac{\partial \text{o}}{\partial(\bar{l}_1^2)}}, \ldots, \overline{\frac{\partial \text{o}}{\partial(\bar{l}_{j-1}^2)}}, \overline{\frac{\partial \text{o}}{\partial(\bar{l}_{j+1}^2)}}, \ldots, \overline{\frac{\partial \text{o}}{\partial(\bar{l}_{nm}^2)}}$ be the values for $\frac{\partial \text{o}}{\partial(\bar{l}_1^2)}, \ldots, \frac{\partial \text{o}}{\partial(\bar{l}_{j-1}^2)}, \frac{\partial \text{o}}{\partial(\bar{l}_{j+1}^2)}, \ldots, \frac{\partial \text{o}}{\partial(\bar{l}_{nm}^2)}$ for this solution.

Now look at the problem:

$$\underset{P_1,...,P_{n_h},V_1,...,V_{n_v}}{\text{minimize}} \quad o \equiv \overline{w}_1 l_1^2 + \cdots + \overline{w}_{n_m} l_{n_m}^2$$

subject to Symmetry constraints:

$$\begin{aligned} \overline{s}_1 &= s_1(\cdots) \\ &\cdots \\ \overline{s}_{n_s} &= s_{n_s}(\cdots) \end{aligned}$$

Point constraints:

$$\begin{aligned} \overline{d}_1 &= \overline{W}_1 \cdot P_{d_1} \\ &\cdots \\ \overline{d}_{n_d} &= \overline{W}_{n_d} \cdot P_{d_{n_d}} \end{aligned}$$

Vector constraints:

$$\begin{aligned} \overline{c}_1 &= c_1(\cdots) \\ &\cdots \\ \overline{c}_{n_c} &= c_{n_c}(\cdots) \end{aligned}$$

If $\overline{w}_j$ is chosen to be 1 and $\overline{w}_{i_m}$ is chosen to be $-\overline{\frac{\partial o}{\partial(\bar{l}_{i_m}^2)}}$ for $i_m \neq j$, $\overline{l}_1, \ldots, \overline{l}_{n_m}$ will also be a solution to this problem. This is so since for any feasible change in the l_{i_m}'s, a minimizing solution must have l_j correspondingly at the minimizing value it would have taken on in the first problem with the l_{i_m}'s constrained at these values. With the chosen weights, the effect to the objective function of the change of the l_{i_m}'s will be exactly offset by the effect of the change in the corresponding minimizing value of l_j. So, with the chosen weights, there is no feasible change at that point which can improve the objective function. So it must be a minimum point.

This shows that any valid tensegrity structure can be viewed as a solution to a weighted model. This is not to say that a given weighted model has only one tensegrity structure as a solution. Some models have more than one solution, each of which is a valid tensegrity structure. In some situations, it may be of interest to probe a given weighted model with different initial values to find alternative solutions.

7.3 Exogenous Member Forces

7.3.1 Exogenous Force Analysis: Method

The analysis of the response of a tensegrity structure to exogenous forces is achieved with a change of conceptual framework. A structure is now viewed as a flexibly-jointed set of

elastic and fixed-length members: the tendons being the elastic components, and the struts being the fixed-length components. Initially it will be assumed that the hub is a single point. Later, in Section 7.3.5, this last assumption will be relaxed.

The solution of the tensegrity programming problem and the subsequent endogenous force analysis provide a valid initial unloaded configuration for these members, a valid configuration being one in which the net force at each hub is zero. The unloaded forces at each hub are tendons pulling in various directions, a single pushing strut and pulling or pushing reactions due to any point constraints. The reaction due to a point constraint is in the direction of the determining vector of the constraint.

An exogenous load is introduced at selected hubs by adding an independent force vector to the forces present at a hub. In the initial configuration, the net force at these hubs is no longer zero, and a new configuration of the structure must now be found in which the net force at each hub is again restored to zero. A new configuration is derived by solving a system of equations rather than by solving an extremal problem as before. There is one equation each for the x, y and z component of the net force at each hub. This value must be equated to zero. Then there is one equation each for the length of each fixed-length member. This length must not change in the new configuration.

These equations are non-linear in their variables. The variables are the coordinate values, the forces in the fixed-length members and the scalings for the reactions due to the point constraints. (The force in an elastic member is determined by the coordinates of its end points and the elasticity equations which govern the member; so, it is not an equation variable.) The system is solved using the standard Newton method. The exogenous load forces may need to be introduced in an incremental way in order for the Newton method to converge.

7.3.2 Exogenous Force Analysis: Mathematical Framework

Two sets of equations must be satisfied for any tensegrity configuration. The first set of equations constrains the forces at the hubs to balance to zero. The net force at a hub is the sum of the forces in the members that meet at that hub, plus the sum of the reactions due to point constraints which impact the hub plus any exogenous force at the hub. The force due to a member will have a magnitude corresponding to the force in the member and a direction corresponding to the orientation of the member. The reaction force due to a point constraint will be the determining vector of the constraint multiplied by a scaling factor which is a variable of the analysis. For a strut, the force will be into the hub along the length of the member; for a tendon, the force will be out of the hub along the length of the member. So the first set of equations is:

$$\begin{bmatrix} 0 \\ \\ 0 \\ \\ 0 \end{bmatrix} = \sum_{j=1}^{m_i} F_{ij}^m + \sum_{j=1}^{q_i} F_{ij}^d + \overline{F}_i^e$$

$$i = 1, \ldots, n_h$$

where

n_h = number of hubs
m_i = number of members meeting at hub i
q_i = number of point constraints impacting hub i
F_{ij}^m = force at hub i due to member m_{ij} (vector)
m_{ij} = index of the jth member meeting at hub i
F_{ij}^d = force at hub i due to point constraint d_{ij} (vector)
d_{ij} = index of the jth point constraint impacting hub i
$\overline{F}_i^e$ = exogenous force at hub i (fixed vector)

The formula for F_{ij}^m is:

$$F_{ij}^m = f_{ij}^m \frac{D_{ij}}{|D_{ij}|}$$

where

f_{ij}^m = signed magnitude of force at hub i due to member m_{ij}
$D_{ij} = \tilde{P}_{ij} - P_i$ (vector)
P_i = point corresponding to hub i
$\tilde{P}_{ij}$ = end point of member m_{ij} away from hub i

If member m_{ij} is fixed-length (i.e. a strut), then f_{ij}^m is a negative variable whose value is adjusted to obtain a solution. If member m_{ij} is elastic (i.e. a tendon), then

$$f_{ij}^m = \overline{\epsilon}_{m_{ij}} \frac{|D_{ij}| - \overline{l}_{m_{ij}}}{\overline{l}_{m_{ij}}}$$

when $|D_{ij}| > \overline{l}_{m_{ij}}$ and $f_{ij}^m = 0$ otherwise, where

$\overline{\epsilon}_{m_{ij}}$ = proportional elasticity coefficient for member m_{ij}[9]

[9]If the member is of uniform cross section along its length, then $\overline{\epsilon}_{m_{ij}}$ is Young's modulus of elasticity of the material composing the member multiplied by the cross-sectional area of the member. See *Vilnay90*, p. 27. For materials where Young's modulus is variable, a more complex equation, or lookup table, for determining f_{ij}^m as a function of deviation of the member length, $|D_{ij}|$, from the reference length, $\overline{l}_{m_{ij}}$, may be necessary.

$\overline{l}_{m_{ij}}$ = reference length for member m_{ij}

The formula for F_{ij}^d is:

$$F_{ij}^d = \beta_{ij}\overline{W}_{ij}$$

where

β_{ij} = scaling value for reaction force at hub i due to point constraint d_{ij}
$\overline{W}_{ij}$ = determining vector for point constraint d_{ij}

β_{ij} is a variable whose value is adjusted to obtain a solution.

The second set of equations is just the point constraints.

The third and last set of equations constrains the lengths of the struts to remain constant:

$$|D_i| = \overline{l}_{f_i}$$

$$i = 1, \ldots, n_f$$

where

n_f = total number of struts = $\frac{n_h}{2}$
f_i = index of the ith strut
D_i = difference vector for the endpoints of member f_i (order of subtraction not important)

Thus, there are $3n_h + n_d + n_f$ equations which must be solved for the coordinate values of the hub points, the scaling values for the reaction forces corresponding to the point constraints and the magnitudes of the forces in the struts.

7.3.3 Exogenous Force Analysis: Initialization

An initial solution for these equations in the absence of exogenous loads can be obtained from coordinate values and endogenous forces computed using the methods described in Sections 7.2.3 and 7.2.4. The hubs are positioned according to the coordinate values. For the struts and point constraints, the force values obtained from the endogenous analysis are used to initialize f_{ij}^m and β_{ij}. For each tendon, a value for $\overline{\epsilon}_{m_{ij}}$ is chosen in accordance with the material being used for the tendon. $\overline{l}_{m_{ij}}$ is then chosen to be sufficiently smaller than the minimizing length of the tendon so that the value of f_{ij}^m is equal to the force for the tendon obtained from the endogenous analysis. Once this initial solution is obtained, values for F_i^e are incrementally introduced at the appropriate hubs, and the system is

solved using Newton's method at each increment. If the Newton iterations diverge at any point, a smaller increment can be chosen until the iterations converge.

7.3.4 Exogenous Force Analysis: A Sample Calculation

This methodology can be used to analyze the response of the 6ν t-octahedron dome (designed in Section 6.2) to an exogenous load. To reduce the computation required, the load will be applied symmetrically to the structure. The hub corresponding to P_2 and the two hubs symmetric to it will be loaded with a relative value of (-3, -3, -3). This is a force vector pointed toward the base of the structure. It is diagrammed in Figure 7.1.

The first step is to choose suitable values for the $\overline{\epsilon}_{m_{ij}}$ and $\overline{l}_{m_{ij}}$ parameters. $\overline{\epsilon}_{m_{ij}}$ is chosen to be the same for all tendons, and so that, when an average-valued force is applied to a tendon, it elongates by 2%. The average value for the force over all the tendons is 3.1294. This is computed from Tables 6.27 to 6.29. Therefore, $\overline{\epsilon}$ (the common value of all the $\overline{\epsilon}_{m_{ij}}$ parameters) was chosen to be $\frac{3.1294}{0.02}$ or 156.47.

Note that, for this sample calculation, all forces are posed in relative terms. To get real values, everything would need to be scaled. For example, if the tendons for the 6ν t-octahedron dome were composed of a material such that a force of 20 pounds (89 Newtons) was required to elongate a tendon by 2%, all force values would be scaled by $\frac{20}{3.1294} = 6.391$. This would make the magnitude of the exogenous load $6.391 \cdot (3^2 + 3^2 + 3^2)^0.5 = 33.21$ pounds (147.7 Newtons). The scale factor would also be applied to Tables 7.6 to 7.10 to get values in pounds.

Given the value for $\overline{\epsilon}$, the values for the $\overline{l}_{m_{ij}}$ parameters are chosen so the initial tendon forces match those from the unloaded length computation model. Tables 7.2 to 7.5 summarize the values used. As always, excluded members are marked with ‡.

The system is solved using the numerical version of the Newton method with a value of 0.001 for the double-sided numerical differentiation differential. Iterations were done until equations were solved within 10^{-8}. This required 21 iterations.

Figure 7.1 shows the positions and effect of the exogenous loads on the dome. Table 7.6 summarizes the resultant forces in the struts. Tables 7.7 to 7.10 summarize the resultant lengths and forces for the tendons. Tables 7.11 and 7.12 summarize the resultant coordinate values. Tables 7.13 and 7.14 summarize the resultant force vectors at the fixed base hubs before and after the load is applied. For the guy attachment points (P'_{30}, P'_{31} and P'_{32}), the sum of the component values of the force vectors at each point is positive. This means a force upward from the base is being exerted at those points. This is as expected since only tendons from above the base are attached at those points. P_2 descends by 0.66659 model units from 5.60914 units above the base of the structure to 4.94255 units as a result of the exogenous load. Notice also that in Table 7.9 a number of the binding tendons have gone slack. It might also be worthwhile to check clearances to see if any of

Member #	$\bar{l}$	Member #	$\bar{l}$
25	2.15428	49	1.99907
26	2.15461	50	2.00880
27	2.16971	51	2.01560
28	2.27822	52	2.07598
29	2.31555	53	2.04503
30	2.41331	54	2.10521
31	2.21302	55	2.01211
32	2.22800	56	2.00000
33	2.25652	57	1.64203
34	2.31157	58	2.02851
35	2.42218	59	2.11034
36	2.30228	60	2.07282
37	2.20050	61	1.99776
38	2.23024	62	1.62387
39	2.20572	63	1.99957
40	2.19539	64‡	N/A
41	2.18635	65	1.99624
42	2.17335	66	2.01033
43	2.19548	67‡	N/A
44	2.17859	68	2.00619
45	2.18847	69	1.99802
46	2.15907	70‡	N/A
47	2.17250	71	2.00545
48	2.15821	72	1.99592

Table 7.2: 6ν T-Octahedron Dome: Primary and Secondary Interlayer Tendon Reference Lengths

Member #	$\bar{l}$	Member #	$\bar{l}$
73	0.96937	97	0.97019
74	0.96743	98	0.96821
75	0.96803	99	0.96542
76	0.96904	100	0.97406
77	0.97113	101	0.96959
78	0.97664	102	0.97495
79	0.96791	103	0.96903
80	0.96884	104	0.96996
81	1.45412	105	0.96742
82	0.96814	106	0.96982
83	0.97680	107	0.97578
84	0.96977	108	0.97363
85	0.96880	109	0.96743
86	1.45285	110	0.96706
87	0.96804	111	0.96947
88‡	N/A	112	0.97145
89	0.96895	113	0.96856
90	0.96624	114	0.96435
91‡	N/A	115	0.96848
92	0.97332	116	0.97020
93	0.97148	117	0.96738
94‡	N/A	118	0.97068
95	0.97088	119	0.96875
96	0.96946	120	0.96645

Table 7.3: 6ν T-Octahedron Dome: Inner and Outer Convergence Tendon Reference Lengths

Member #	$\bar{l}$	Member #	$\bar{l}$
121	2.70032	145	1.87898
122	2.61972	146	1.82018
123	2.64847	147	1.99391
124	1.82857	148	1.20838
125	2.45745	149	1.27578
126	2.28837	150	1.27547
127	2.53689	151	1.28003
128	2.60341	152	1.64465
129	2.57646	153	1.27623
130	2.55666	154	1.24420
131	2.17235	155	1.26135
132	1.84061	156	1.21316
133	2.61640	157	1.73770
134	2.59125	158	1.31872
135	2.71977	159	1.38787
136‡	N/A	160	2.88421
137	2.68053	161	2.52592
138	2.70945	162	1.83510
139‡	N/A	163	2.93217
140	2.52263	164	2.51409
141	2.67634	165	1.78025
142‡	N/A	166	2.85398
143	2.65028	167	2.66071
144	2.66690	168	1.88192

Table 7.4: 6ν T-Octahedron Dome: Outer and Inner Binding Tendon Reference Lengths

Member #	$\bar{l}$
175	2.12793
176	2.02718
177	2.19077
178	2.05342
179	2.22276
180	1.99197

Table 7.5: 6ν T-Octahedron Dome: Guy Reference Lengths

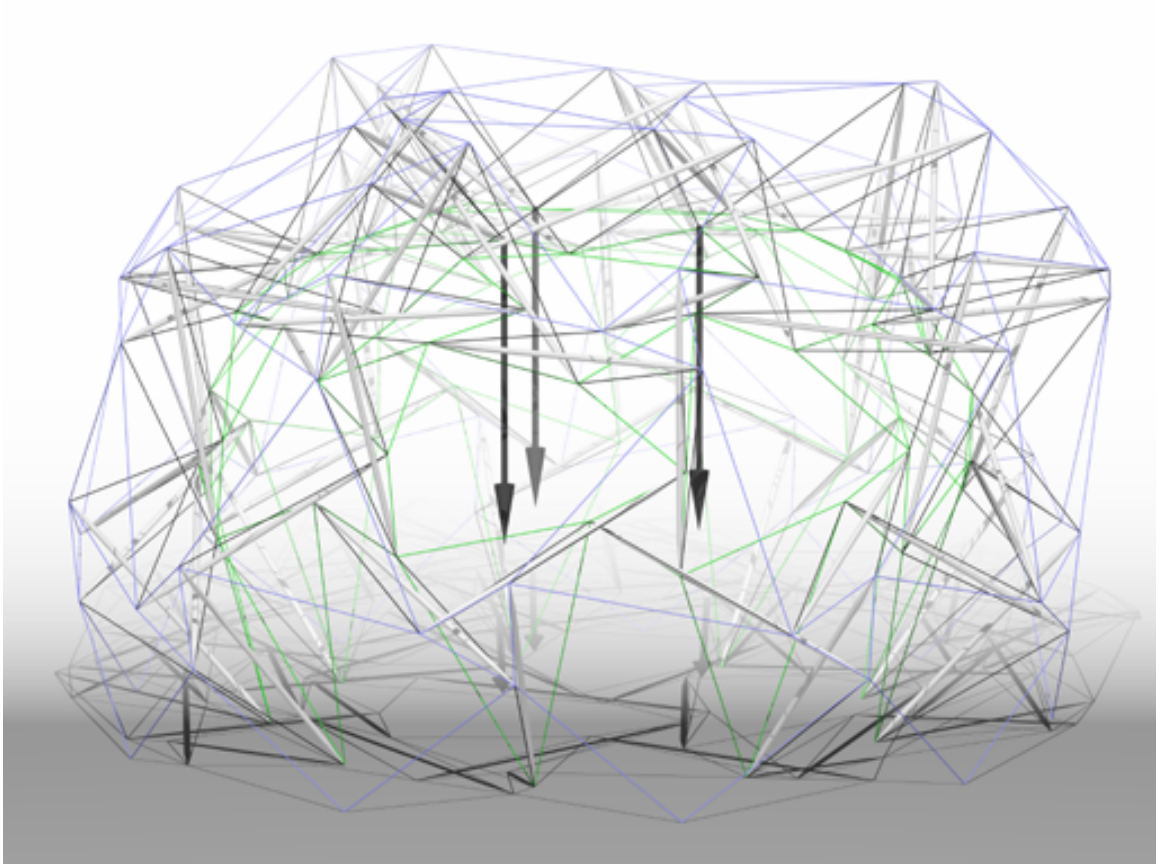

Figure 7.1: 6ν T-Octahedron Dome: Positions and Effect of Exogenous Loads

them have been affected adversely by the load. The assumptions of these calculations would be violated if the load drove one member into or through another.

7.3.5 Exogenous Force Analysis: Complex Hubs

The previously-outlined technique for exogenous force analysis works when vector constraints are not being used and the simple assumption that the hubs of the tensegrity are single points is being made. When hubs are complex and thus vector constraints are introduced, torque considerations must also be introduced. For this latter situation, the model which follows is proposed.

In the new model, corresponding to every strut is a strut envelope. The strut envelope is a single rigid body to which tendons are attached and which also may be impacted by point constraints and exogenous forces. Tendons, point constraints and exogenous forces are all assumed to impact the strut envelope at single points distributed over the envelope. These points are referred to as attachment points. The shape of the strut envelope is determined by the strut equations and the vector constraints. The strut equations are incorporated as constraints which maintain the struts at fixed lengths. There must be a sufficient number

Member #	Relative Force	Member #	Relative Force
1	-10.7566	13	-10.9204
2	-11.7166	14	-9.8635
3	-14.1718	15	-12.2574
4	-13.4791	16	-6.6828
5	-11.3231	17	-9.8881
6	-13.1420	18	-11.2389
7	-11.8063	19	-7.0818
8	-11.3412	20	-10.0929
9	-9.7997	21	-10.5841
10	-10.2812	22	-6.5853
11	-11.3834	23	-9.0954
12	-12.8010	24	-10.5933

Table 7.6: 6ν T-Octahedron Dome: Strut Loaded Forces

of strut and vector constraints so that the strut envelope is rigidly determined.

In contrast to the previous model where tendons were only attached at one of two points on the strut, now each tendon can have a unique attachment point on the strut envelope. It is possible that tendons share attachment points, but they don't need to. All the attachment points, including those for point constraints and exogenous forces, are assumed to cluster at two hubs. Each hub has a corresponding reference point which is referred to as an end point of the strut though the physical strut may extend considerably past it and perhaps not even through it. There must be more than one attachment point at each hub. Joints are still assumed to be flexible, so torque must only be considered for the strut envelope and can be neglected as far as the tendons are concerned.

Forces must still sum to zero in this new model, but only for the strut envelope as a whole rather than for each of the two hubs. In addition, the sum of the torque moments on the strut envelope exerted by all the forces must be zero.[10] A force and a torque moment vector can be derived for each strut envelope from the results of the exogenous analysis. These vectors will most likely approximate the axis of the strut, but in many cases will not coincide with it.

The equations representing the requirement that forces sum to zero are now:

[10]See, for example, *Hibbeler98,* pp. 193-194, for a statement of the conditions for rigid-body equilibrium.

Member #	Length	Relative Force	Member #	Length	Relative Force
25	2.20326	3.55741	49	2.03415	2.74632
26	2.20680	3.78963	50	2.07711	5.32121
27	2.24049	5.10497	51	2.10845	7.20793
28	2.35786	5.47004	52	2.10820	2.42796
29	2.43895	8.33865	53	2.09795	4.04919
30	2.51493	6.58847	54	2.14628	3.05190
31	2.29341	5.68381	55	2.04701	2.71396
32	2.29322	4.58086	56	2.03510	2.74633
33	2.34671	6.25362	57	1.66710	2.38867
34	2.38640	5.06486	58	2.05984	2.41664
35	2.51846	6.21956	59	2.15698	3.45785
36	2.38028	5.30160	60	2.11407	3.11398
37	2.27067	4.98962	61	2.03192	2.67516
38	2.31398	5.87477	62	1.64568	2.10171
39	2.27982	5.25673	63	2.03915	3.09712
40	2.27003	5.31957	64‡	N/A	N/A
41	2.24545	4.22960	65	2.02524	2.27278
42	2.23093	4.14557	66	2.04974	3.06680
43	2.27054	5.34933	67‡	N/A	N/A
44	2.23906	4.34314	68	2.03455	2.21201
45	2.25109	4.47740	69	2.03970	3.26448
46	2.22165	4.53522	70‡	N/A	N/A
47	2.23087	4.20444	71	2.03829	2.56217
48	2.21661	4.23362	72	2.03720	3.23582

Table 7.7: 6ν T-Octahedron Dome: Primary and Secondary Interlayer Tendon Loaded Lengths and Forces

Member #	Length	Relative Force	Member #	Length	Relative Force
73	0.99329	3.85972	97	0.99965	4.75017
74	1.01663	7.95780	98	0.99331	4.05643
75	1.01540	7.65689	99	1.00173	5.88465
76	0.99478	4.15546	100	0.99955	4.09540
77	0.99376	3.64598	101	1.00137	5.12947
78	0.99695	3.25321	102	1.01283	6.07944
79	0.99017	3.59783	103	1.00467	5.75433
80	1.00933	6.54029	104	1.00218	5.19817
81	1.50361	5.32548	105	0.99971	5.22217
82	0.99082	3.66633	106	1.00556	5.76645
83	1.00948	5.23566	107	1.00406	4.53408
84	0.99642	4.29989	108	1.00088	4.37907
85	0.98806	3.11137	109	0.99816	4.97036
86	1.51233	6.40604	110	1.00551	6.22156
87	1.00441	5.87963	111	1.00612	5.91662
88‡	N/A	N/A	112	0.99576	3.91605
89	1.00637	6.04386	113	1.00470	5.83896
90	1.00765	6.70593	114	1.00230	6.15694
91‡	N/A	N/A	115	1.00015	5.11714
92	1.00464	5.03427	116	1.00086	4.94495
93	1.00265	5.02001	117	1.00334	5.81591
94‡	N/A	N/A	118	0.99407	3.77070
95	1.00567	5.60734	119	1.00398	5.69160
96	1.00674	6.01624	120	0.99996	5.42603

Table 7.8: 6ν T-Octahedron Dome: Inner and Outer Convergence Tendon Loaded Lengths and Forces

Member #	Length	Relative Force	Member #	Length	Relative Force
121	2.70947	0.52980	145	1.87496	0.00000
122	2.53218	0.00000	146	1.83291	1.09459
123	2.44184	0.00000	147	2.01356	1.54175
124	1.84404	1.32367	148	1.23443	3.37263
125	2.30039	0.00000	149	1.08359	0.00000
126	2.30359	1.04060	150	1.14127	0.00000
127	2.54516	0.51011	151	1.28069	0.08096
128	2.62350	1.20781	152	1.62424	0.00000
129	2.57895	0.15158	153	1.29686	2.52944
130	2.57928	1.38453	154	1.14619	0.00000
131	2.17666	0.31057	155	1.27222	1.34780
132	1.86323	1.92369	156	1.24194	3.71146
133	2.64081	1.45944	157	1.64919	0.00000
134	2.59995	0.52518	158	1.31804	0.00000
135	2.73317	0.77089	159	1.40527	1.96143
136‡	N/A	N/A	160	2.88836	0.22524
137	2.70689	1.53865	161	2.51456	0.00000
138	2.72797	1.06931	162	1.86892	2.88352
139‡	N/A	N/A	163	2.90433	0.00000
140	2.55151	1.79147	164	2.50274	0.00000
141	2.70008	1.38773	165	1.80955	2.57487
142‡	N/A	N/A	166	2.86090	0.37926
143	2.66620	0.94011	167	2.65589	0.00000
144	2.67084	0.23110	168	1.91684	2.90318

Table 7.9: 6ν T-Octahedron Dome: Outer and Inner Binding Tendon Loaded Lengths and Forces

Member #	Length	Relative Force
175	2.13419	0.459938
176	2.02801	0.064638
177	2.19309	0.165828
178	2.06349	0.767356
179	2.22285	0.005841
180	1.99408	0.165191

Table 7.10: 6ν T-Octahedron Dome: Guy Loaded Lengths and Forces

	Coordinates		
Point	x	y	z
P_1	1.50456	0.40995	2.85399
P_2	1.00233	1.23867	2.55063
P_3	-0.59661	2.16366	2.87199
P_4	0.66472	0.72576	3.33198
P_5	0.96159	-0.35998	3.52049
P_6	-0.09865	0.17065	3.86423
P_7	-1.58666	2.20740	2.80497
P_8	-1.12115	1.20549	3.48417
P_9	-1.07951	0.22167	3.70649
P_{10}	0.03607	-0.29452	3.88378
P_{11}	1.01184	-1.34989	3.41346
P_{12}	2.24377	-1.01815	2.82434
P_{13}	-2.26128	0.76098	3.10646
P_{14}	-0.83994	-1.02583	3.77637
P_{15}	1.37853	-2.41936	2.73598
P_{16}	-2.70685	1.28850	2.37261
P_{17}	-2.88612	0.30664	2.48711
P_{18}	-1.72821	-0.71532	3.43013
P_{19}	-1.34254	-1.59864	3.14311
P_{20}	0.38935	-2.38946	2.92076
P_{21}	0.76841	-2.98729	2.20544
P_{22}	-3.73094	-0.08603	0.04784
P_{23}	-3.10232	-1.76219	1.09539
P_{24}	-1.60996	-3.20168	1.04252

Table 7.11: 6ν T-Octahedron Dome: Loaded Inner Coordinate Values

Point	Coordinates		
	x	y	z
P'_1	2.87120	0.70422	3.30117
P'_2	1.35842	2.61844	3.20190
P'_3	0.43034	2.65244	3.57177
P'_4	1.05048	1.20289	4.98885
P'_5	1.50968	0.32968	5.21792
P'_6	0.53617	0.45294	5.40814
P'_7	-2.19505	2.29874	4.14049
P'_8	-1.55397	1.79921	4.72264
P'_9	-1.19245	-0.16017	5.59900
P'_{10}	-0.20174	-0.30239	5.59633
P'_{11}	1.58750	-1.87493	4.55447
P'_{12}	2.46471	-1.52851	4.20406
P'_{13}	-2.42845	1.37874	4.46217
P'_{14}	-0.82003	-1.07359	5.41164
P'_{15}	2.14157	-2.43112	3.92621
P'_{16}	-4.02302	1.86969	2.30391
P'_{17}	-3.74810	-0.46244	3.30181
P'_{18}	-3.07624	-0.83364	3.94795
P'_{19}	-1.41976	-2.90815	3.70067
P'_{20}	-0.44273	-3.09431	3.80405
P'_{21}	1.38238	-4.26313	2.18230
P'_{22}	-4.52297	1.26281	1.69294
P'_{23}	-3.53726	-1.44084	3.30058
P'_{24}	-0.97004	-3.60258	3.13190
P'_{30}	-4.79594	-0.71196	1.73878
P'_{31}	-3.05833	-3.26445	2.55366
P'_{32}	-0.47757	-4.87734	1.58579

Table 7.12: 6ν T-Octahedron Dome: Loaded Outer Coordinate Values

Point	Force Vector		
	x	y	z
P_{22}	-0.23825	-0.44848	-0.74095
P_{23}	-0.47160	-0.56638	-1.08428
P_{24}	-0.63563	-0.30815	-0.89948
P'_{30}	0.64444	0.50802	0.60475
P'_{31}	0.66222	0.60749	0.52500
P'_{32}	0.67850	0.67438	0.48840

Table 7.13: 6ν T-Octahedron Dome: Base Point Unloaded Force Vectors

	Force Vector		
Point	x	y	z
P_{22}	-1.12554	-1.08852	-0.98920
P_{23}	-1.08628	-1.43482	-1.53837
P_{24}	-0.99081	-0.94641	-1.54760
P'_{30}	0.29387	0.00651	0.33279
P'_{31}	0.14264	0.03256	0.06753
P'_{32}	-0.17743	0.47498	0.57411

Table 7.14: 6ν T-Octahedron Dome: Base Point Loaded Force Vectors

$$\begin{bmatrix} 0 \\ \\ 0 \\ \\ 0 \end{bmatrix} = \sum_{j=1}^{m_i} F_{ij}^m + \sum_{j=1}^{q_i} F_{ij}^d + \sum_{j=1}^{u_i} \overline{F}_{ij}^e$$

$$i = 1, \ldots, n_f$$

where

n_f = number of struts = $\frac{n_h}{2}$
m_i = number of tendons attached to strut envelope i
q_i = number of point constraints impacting strut envelope i
u_i = number of exogenous forces impacting strut envelope i
F_{ij}^m = force at strut envelope i due to tendon m_{ij} (vector)
m_{ij} = index of the jth tendon attached to strut envelope i
F_{ij}^d = force at strut envelope i due to point constraint d_{ij} (vector)
d_{ij} = index of the jth point constraint impacting strut envelope i
$\overline{F}_{ij}^e$ = jth exogenous force impacting strut envelope i (fixed vector)

The formula for F_{ij}^m is:

$$F_{ij}^m = f_{ij}^m \frac{D_{ij}}{|D_{ij}|}$$

where

f_{ij}^m = signed magnitude of force at strut envelope i due to tendon m_{ij}
$D_{ij} = \tilde{P}_{ij}^m - P_{ij}^m$ (vector)
P_{ij}^m = point where tendon m_{ij} is attached to strut envelope i
$\tilde{P}_{ij}^m$ = far attachment point of tendon m_{ij}

The value of f_{ij}^m for tendons is derived as before. The value for struts is not relevant since

they are not included here. The formula for F_{ij}^d remains the same and the β_{ij} values are again one portion of the values which are adjusted to solve the system of equations.

The equations representing the requirement that torques sum to zero are:

$$\begin{bmatrix} 0 \\ 0 \\ 0 \end{bmatrix} = \sum_{j=1}^{m_i} F_{ij}^m \times (P_{ij}^m - P_i^c) + \sum_{j=1}^{q_i} F_{ij}^d \times (P_{ij}^d - P_i^c) + \sum_{j=1}^{u_i} \overline{F}_{ij}^e \times (P_{ij}^e - P_i^c)$$

$$i = 1, \ldots, n_f$$

where

P_{ij}^d = point on strut envelope i constrained by point constraint d_{ij}
P_{ij}^e = point on strut envelope i where the jth exogenous force is applied
$P_i^c = \frac{1}{m_i+q_i}(\sum_{j=1}^{m_i} P_{ij}^m + \sum_{j=1}^{q_i} P_{ij}^d)$ = center point of strut envelope i

The point constraints must also be met and are now joined by the vector constraints. The the set of equations constraining the lengths of the struts to remain constant are retained as well. Thus, there are $6n_f + n_d + n_c + n_f$ equations which must be solved for the coordinate values of $P_1, ..., P_{n_h}, V_1, ..., V_{n_v}$ and the scaling values, β_{ij}, for the reaction forces corresponding to the point constraints. A necessary condition for this to be possible is that $6n_f + n_d + n_c + n_f = 3(n_h + n_v) + n_d$. Since $2n_f = n_h$, this necessary condition can be expressed as $n_c + n_f = 3n_v$.

Actually, it is more pertinent to examine this last condition for each strut envelope. For an individual strut envelope, the condition can be expressed as $n_{c_i} + 1 = 3n_{v_i}$ where n_{c_i} is the number of vector constraints pertaining to strut i and n_{v_i} is the number of vectors used to model its hubs. If there are sufficient vector constraints to rigidly determine the strut envelope, this condition should obtain; otherwise, additional vector constraints will need to be added. It is possible that some vector constraints will only be used for the analysis of exogenous loads and will be ignored during the solution of the mathematical programming problem corresponding to the structure.

Once the equations have been solved, characteristic member forces can be computed for the strut envelopes. For each strut envelope, the attachments are separated into two groups corresponding to the two hubs. This is done using the center point of the strut envelope. First, the dot product of the center point is taken with the vector corresponding to the difference of the end points of the strut. Then, the dot product of the strut vector with each attachment point is taken. If the dot product for an attachment point is less than the dot product for the center point, then the attachments corresponding to the point go in one group; if not, they go in the other group. The characteristic member force for the strut envelope is found by summing the forces for one of the two groups of attachments. Since

the sum of the forces for all the attachments to the strut envelope is zero, the sum for one group will be the additive inverse of the other group.

In addition, a torque moment can be computed for each strut to estimate the twisting force it is subjected to. This computation uses the standard procedures for computing the moment of forces about a specified axis.[11] Using the same procedure as that described for the characteristic member-force computation for the strut envelopes, the attachments are separated into groups corresponding to the hubs. The signed magnitude of the moments corresponding to each hub are then computed using the following triple scalar products:

$$\frac{D_i}{|D_i|} \cdot \left(\sum_{j=1}^{m_i} F_{ij}^m \times (P_{ij}^m - P_i^m) + \sum_{j=1}^{q_i} F_{ij}^d \times (P_{ij}^d - P_i^m) + \sum_{j=1}^{u_i} \overline{F}_{ij}^e \times (P_{ij}^e - P_i^m)\right)$$
$$i = 1, \ldots, n_h$$

where

$D_i = \tilde{P}_i^m - P_i^m$ (vector)
P_i^m = point where strut is attached to hub i
$\tilde{P}_i^m$ = far attachment point of strut attached to hub i
m_i = number of tendons attached to hub i
q_i = number of point constraints impacting hub i
u_i = number of exogenous forces impacting hub i
F_{ij}^m = force at hub i due to tendon m_{ij} (vector)
m_{ij} = index of the jth tendon attached to hub i
P_{ij}^m = point where tendon m_{ij} is attached to hub i
F_{ij}^d = force at hub i due to point constraint d_{ij} (vector)
d_{ij} = index of the jth point constraint impacting hub i
P_{ij}^d = point on hub i constrained by point constraint d_{ij}
$\overline{F}_{ij}^e$ = jth exogenous force impacting hub i (fixed vector)
P_{ij}^e = point on hub i where the jth exogenous force is applied

Since for the strut as a whole the sum of the moments is zero, the moments for each of the two hubs of a strut will be equal.

7.3.6 Exogenous Force Analysis: Another Sample Calculation

For an example of exogenous force analysis with non-point hubs, it is useful to turn back to the tensegrity prism of Section 2.2. In the course of the example, meta-constraints are also illustrated. Meta-constraints are a design tool which allow a tensegrity to meet certain geometric specifications which would be illegitimate if they appeared in the mathematical programming problem. In this case, the meta-constraint will be that the struts of the

[11] See, for example, *Hibbeler98,* pp. 138-141.

prism are at 90° to each other. This allows the prism to be used as a joint in a cubic lattice. If this constraint were imposed in the mathematical programming problem it would be illegitimate and lead to a structure with loose tendons most of the time; however, the desired geometry can be achieved if the constraint is applied at a higher level.

Since eventually an exogenous load will be applied asymmetrically, symmetry transformations will not be used in the model. For the struts, 14-inch (356 mm) lengths of one-inch (25 mm) square wood stock will be used. Holes for attaching the tendons to the strut will be drilled at one inch (25 mm) from either end of the strut, so these attachment points will be 12 inches (305 mm) apart. So, the model is:

$$\begin{array}{cll} \underset{\substack{A,B,C,A',B',C' \\ V_a,V_b,V_c}}{\text{minimize}} & t_a^2+t_b^2+t_c^2 & \\ \text{subject to} & \text{Member constraints:} & \\ & \overline{s}^2 = s_a^2 = s_b^2 = s_c^2 & \\ & \overline{u}^2 = u_a^2 = u_b^2 = u_c^2 & \\ & \overline{u}^2 = \tilde{u}_a^2 = \tilde{u}_b^2 = \tilde{u}_c^2 & \\ & \text{Point constraints:} & \\ & 0 = x_A = y_A = z_A & \\ & 0 = y_B = z_B = z_C & \\ & \text{Vector constraints:} & \\ & \overline{v}^2 = |V_a|^2 = |V_b|^2 = |V_c|^2 & \\ & 0 = V_a\cdot(A'-A) = V_b\cdot(B'-B) = V_c\cdot(C'-C) & \end{array}$$

where

$s_a = |\overline{AA'}|$; $s_b = |\overline{BB'}|$; $s_c = |\overline{CC'}|$
$t_a = |\overline{\dot{A}\ddot{C}'}|$; $t_b = |\overline{\dot{B}\ddot{A}'}|$; $t_c = |\overline{\dot{C}\ddot{B}'}|$
$u_a = |\overline{\ddot{A}\ddot{B}}|$; $u_b = |\overline{\ddot{B}\ddot{C}}|$; $u_c = |\overline{\ddot{C}\ddot{A}}|$
$\tilde{u}_a = |\overline{\dot{A}'\dot{B}'}|$; $\tilde{u}_b = |\overline{\dot{B}'\dot{C}'}|$; $\tilde{u}_c = |\overline{\dot{C}'\dot{A}'}|$
$\dot{A} = A + V_a$; $\dot{B} = B + V_b$; $\dot{C} = C + V_c$
$\ddot{A} = A - V_a$; $\ddot{B} = B - V_b$; $\ddot{C} = C - V_c$
$\dot{A}' = A' + V_a$; $\dot{B}' = B' + V_b$; $\dot{C}' = C' + V_c$
$\ddot{A}' = A' - V_a$; $\ddot{B}' = B' - V_b$; $\ddot{C}' = C' - V_c$

$\overline{v} = 0.5$ inches (13 mm) since it represents half the length of the holes drilled through the wooden struts. The vectors used to construct the offsets from the strut end points to where the tendons are connected to the strut are restricted to be orthogonal to their corresponding struts since the holes are drilled orthogonal to the strut. Note that for each strut the same vector is used to construct all four offsets at the two hubs. This is appropriate since the holes drilled through the struts are aligned with each other. In

another situation, a different independently-adjustable vector might be used to construct each offset.

$\overline{s} = 12$ inches (305 mm) since it represents the distance between the two holes drilled through each wooden strut. $\overline{u}$ will start out at $\frac{3 \cdot 12}{7} = 5.14$ inches (130 mm) and will be adjusted between successive solutions to the mathematical programming problem to obtain a structure with orthogonal struts. It is scaled up from the value of 3 used in Section 2.2.2 to account for the fact that the strut length is now 12 inches (305 mm) rather than 7 inches (178 mm).

Though the model used is more in the vein of the Cartesian version of the tensegrity prism presented in Section 2.2.3, initial data for the mathematical programming problem can be obtained from the results of Section 2.2.2. First the base triangle is placed in a way to satisfy the point constraints. The other end triangle is obtained by rotating the first by 150° about its center and raising it by the appropriate height. The height, which represents the value for z in this model, is found by solving the formula for s^2 of Section 2.2.2 for h and using the fact that $\overline{r}^2 = 3(\frac{12}{7})^2$:

$$h = (\overline{s}^2 - 2\overline{r}^2 + 2\overline{r}^2 cos\theta)^{\frac{1}{2}} = (12^2 - 2 \cdot 3(\frac{12}{7})^2 + 2 \cdot 3(\frac{12}{7})^2 \cos(150^\circ))^{\frac{1}{2}} = 10.54 \text{ inches (268 mm)}$$

Table 7.15 summarizes the initial values. The initial data fit the constraints closely enough that no penalty iterations were necessary to reach a point so that the equation system could be solved for the dependent in terms of the independent variables. The initial iterations were rough in that the step size and the partitioning had to constantly be adjusted to make progress. Initially eight steepest-descent iterations were done and the variables were repartitioned at each step. Then eight Fletcher-Reeves iterations were done with no repartitioning necessary. Finally a Newton iteration was done to enhance the accuracy of the solution.

To track the angle between adjacent struts, a dot product was taken of their corresponding vectors. A value of zero would indicate that the desired orthogonality was reached. For this first solution, the value was 80.7266. Increasing the value of $\overline{u}$ by 0.01 decreased the dot product to 80.5217. Using the usual Newton technique, this result was used to extrapolate the increase to $0.01 \cdot \frac{80.7266}{80.7266 - 80.5217} = 3.93980$ which added to the original value of $\overline{u}$ yielded 9.08266.

This new value for $\overline{u}$ was a large enough change that the equation system could no longer be solved for the dependent variables in terms of the independent ones, so ten Fletcher-Reeves iterations were done using the penalty method. This resulted in a solvable system, but again one in which the initial iterations were rough. A solution was reached which yielded a value of -20.2664 for the dot product of the struts. The Newton meta-iterations were continued until a dot product close to zero was reached. Table 7.16 summarizes the sequence of values. None of the changes after the first large one was large

Point/ Vector	Coordinates (inches) x	y	z
A	0	0	0
B	5.14	0	0
C	2.57	4.45	0
A'	5.54	1.48	10.54
B'	1.09	4.06	10.54
C'	1.09	-1.09	10.54
V_a	0	0.5	0
V_b	0	0.5	0
V_c	0	0.5	0

Table 7.15: T-Prism: Initial Cartesian Coordinates

$\overline{u}$	Strut Dot Product
5.14286	80.7266
5.15286	80.5217
9.08266	-20.2664
9.07266	-19.9746
8.38813	-0.150138
8.37813	0.135670
8.38288	-0.000073
8.38287	0.000213

Table 7.16: T-Prism: Meta-Iteration Values

enough that the equation system became unsolvable, so the exact technique could be used throughout rather than resorting to the penalty method. The final value for $\overline{u}$ was 8.38288, and that for t_a, t_b and t_c was 6.65618.

The meta-solution values for the control variables are summarized in Table 7.17, and the resulting structure is shown in Figure 7.2. The orthogonal configuration gives the struts their maximum clearance per unit length with respect to each other. Each strut has an edge which is exactly flush with the supporting surface, though this is not peculiar to the orthogonal configuration.

Table 7.18 summarizes the prestress forces. The prestress forces are scaled so the average tendon force is 20 pounds (89 Newtons). This results in a torque on the strut of 0.75 foot-pounds (1.01 Newton-meters).

As an example of an exogenous load, a sign weighing 10 pounds (44 Newtons) is suspended from two corners of the prism, $A' - V_a + \frac{1}{12}(A' - A) - V_a \times \frac{1}{12}(A' - A)$ and

Point/ Vector	Coordinates (inches)		
	x	y	z
A	0	0	0
B	8.86046	0	0
C	4.43023	7.67339	0
A'	9.53646	2.24850	6.92821
B'	2.14498	7.13457	6.92821
C'	1.60925	-1.70968	6.92821
V_a	-0.280971	-0.066247	0.408248
V_b	0.197857	-0.210205	0.408248
V_c	0.083114	0.276452	0.408248

Table 7.17: Orthogonal T-Prism: Cartesian Coordinates

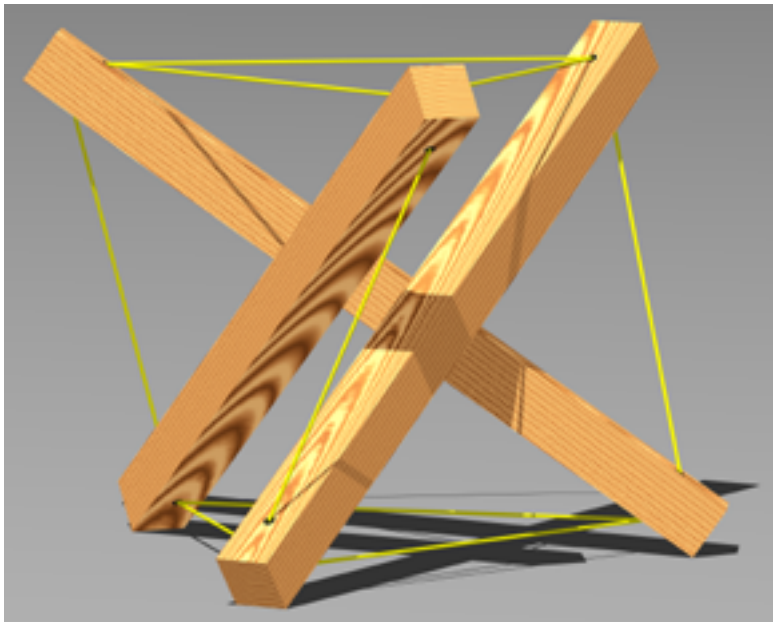

Figure 7.2: Orthogonal Tensegrity Prism

Member Labels	Member Force (pounds)
s_a, s_b, s_c	-41
t_a, t_b, t_c	26
u_a, u_b, u_c	17
$\tilde{u}_a$, $\tilde{u}_b$, $\tilde{u}_c$	17

Table 7.18: Orthogonal T-Prism: Prestress Member Forces

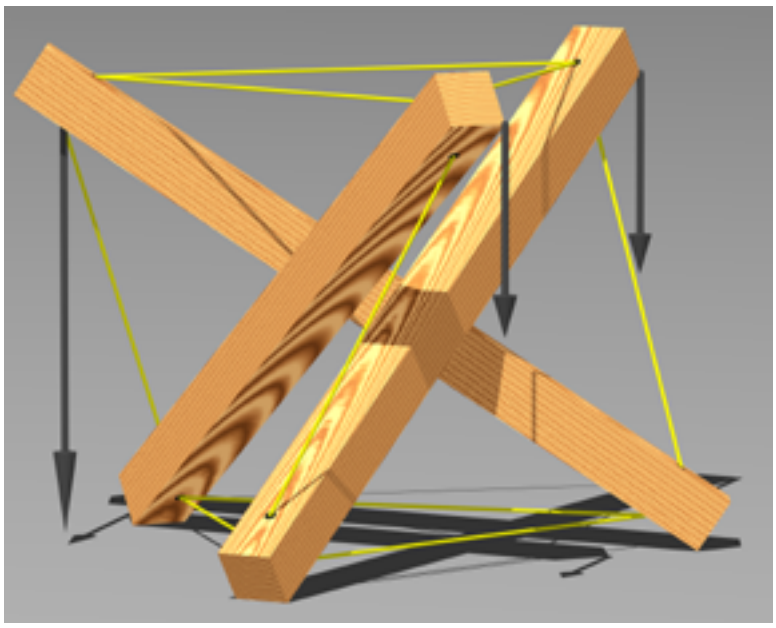

Figure 7.3: Orthogonal T-Prism: Positions and Effect of Exogenous Loads

Point	Displacement (z difference) (inches)
$A' - V_a + \frac{1}{12}(A' - A) - V_a \times \frac{1}{12}(A' - A)$	-0.205
$C' - V_c + \frac{1}{12}(C' - C) + V_c \times \frac{1}{12}(C' - C)$	-0.280
$\ddot{B}'$	-0.207

Table 7.19: Orthogonal T-Prism: Displacements due to Exogenous Loads

$C' - V_c + \frac{1}{12}(C' - C) + V_c \times \frac{1}{12}(C' - C)$. Along with the sign, a counterweight of 10 pounds (44 Newtons) is suspended from the tendon attachment point $\ddot{B}'$. This load and its effect on the prism are diagrammed in Figure 7.3. The tendons of the prism are linearly elastic, and a load of 20 pounds (89 Newtons) extends a tendon by 2%. The prism is supported at five of the six strut corners it rests on. One corner is excluded since it pulls away from the support surface by about 0.01 inch (250 μm) when the load is applied.

A two-sided numerical differentiation differential of 0.00001 (inches or pounds as appropriate) resulted in convergence in four iterations to a solution with a tolerance of 0.0001 (again inches or pounds as appropriate). Table 7.19 gives the displacements of the points where the exogenous loads are applied. Table 7.20 gives the reaction forces corresponding to the five corners where the prism is supported. Table 7.21 gives the forces and torques corresponding to each strut. Table 7.22 gives the forces and lengths corresponding to each tendon. And Table 7.23 gives the new coordinate values for the strut end points and the vector offsets to the tendon attachment points.

Point	Reaction Force (pounds)
$A - V_a - \frac{1}{12}(A' - A) + V_a \times \frac{1}{12}(A' - A)$	2.43649
$A - V_a - \frac{1}{12}(A' - A) - V_a \times \frac{1}{12}(A' - A)$	4.76605
$B - V_b - \frac{1}{12}(B' - B) + V_b \times \frac{1}{12}(B' - B)$	Excluded
$B - V_b - \frac{1}{12}(B' - B) - V_b \times \frac{1}{12}(B' - B)$	4.05988
$C - V_c - \frac{1}{12}(C' - C) + V_c \times \frac{1}{12}(C' - C)$	8.34852
$C - V_c - \frac{1}{12}(C' - C) - V_c \times \frac{1}{12}(C' - C)$	0.389018
Sum	20.0000

Table 7.20: Orthogonal T-Prism: Support Reaction Forces due to Exogenous Loads

Strut	Force (pounds)	Torque (foot-pounds)
s_a	-50.5422	0.704414
s_b	-48.5601	0.707202
s_c	-47.0621	0.963006

Table 7.21: Orthogonal T-Prism: Strut Forces and Torques with Exogenous Loads

Tendon	Force (pounds)	Length (inches)
t_a	24.0531	6.64310
t_b	26.3338	6.65790
t_c	20.3017	6.61877
u_a	21.8590	8.42320
u_b	19.0996	8.40046
u_c	21.3238	8.41879
$\tilde{u}_a$	22.2399	8.42634
$\tilde{u}_b$	19.3835	8.40280
$\tilde{u}_c$	20.7480	8.41405

Table 7.22: Orthogonal T-Prism: Tendon Forces and Lengths with Exogenous Loads

Point/ Vector	Coordinates (inches)		
	x	y	z
A	0.0318724	0.0318693	-0.00958155
B	8.92941	0.0256662	-0.00839036
C	4.51264	7.71161	-0.00965609
A'	9.58138	2.71797	6.74258
B'	1.77471	6.98253	6.65587
C'	1.97666	-1.87981	6.74115
V_a	-0.27083	-0.0761796	0.413337
V_b	0.204166	-0.188303	0.415762
V_c	0.0719009	0.271939	0.413376

Table 7.23: Orthogonal T-Prism: Coordinates with Exogenous Loads

Chapter 8

Analyzing Clearances in Tensegrities

8.1 Clearance Analysis: Introduction

A practical factor which must be taken into account in analyzing the outcome of a tensegrity mathematical programming problem is the clearance between (in other words, the distance separating) one member and another. Especially with truss tensegrities, solutions to a problem can very easily have clearances which would result in one member inadvertently intersecting another if the model were implemented. If this is the case, adjustments must be made using length constraints, objective function weights and/or model configuration until satisfactory clearances are obtained.

8.2 Clearance Analysis: Formulas

Two members can be modeled mathematically as two line segments in space. When neither endpoint of the two line segments coincides, the parameter of interest is the minimum distance between the two line segments. The position of the points on the two segments where this minimum is attained may also be of interest. When the two segments coincide at one endpoint, the angle between the two segments may be of concern.

8.2.1 Clearance Formulas: Distance Between Two Line Segments

Let $\overline{AB}$ and $\overline{CD}$ be two line segments. An arbitrary point, call it P_{AB}, on the line obtained by extending the segment $\overline{AB}$ can be generated as a function of a scalar multiplier, call it λ_{AB}, using the formula

$$P_{AB} \equiv A + \lambda_{AB}(B - A).$$

If λ_{AB} is between 0 and 1, this point will lie on the segment $\overline{AB}$. Similarly, a point on the line coinciding with $\overline{CD}$ can be generated using the formula

$$P_{CD} \equiv C + \lambda_{CD}(D - C).$$

To find the minimum distance between these two **lines** (which is not necessarily the distance between the two line segments), values for λ_{AB} and λ_{CD} can be found which minimize the distance between P_{AB} and P_{CD}. Thus, the following unconstrained programming problem is arrived at:

$$\begin{array}{ll} \text{minimize} & |P_{AB} - P_{CD}|^2 \equiv (P_{AB} - P_{CD}) \cdot (P_{AB} - P_{CD}) \\ \lambda_{AB}, \lambda_{CD} & \end{array}$$

This problem can be solved by differentiating the objective function with respect to λ_{AB} and λ_{CD}, setting the two resulting equations equal to zero and solving the implied system for λ_{AB} and λ_{CD}.

Substituting using

$$\begin{aligned} P_{AB} - P_{CD} &= A + \lambda_{AB}(B - A) - (C + \lambda_{CD}(D - C)) \\ &= (A - C) + \lambda_{AB}(B - A) - \lambda_{CD}(D - C) \end{aligned}$$

and differentiating results in the system:

$$\begin{aligned} 2\lambda_{AB}|\overline{AB}|^2 - 2\lambda_{CD}(B - A) \cdot (D - C) + 2(A - C) \cdot (B - A) &= 0 \\ -2\lambda_{AB}(B - A) \cdot (D - C) + 2\lambda_{CD}|\overline{CD}|^2 - 2(A - C) \cdot (D - C) &= 0 \end{aligned}$$

Since

$$(B - A) \cdot (P_{AB} - P_{CD}) = \lambda_{AB}|\overline{AB}|^2 - \lambda_{CD}(B - A) \cdot (D - C) + (B - A) \cdot (A - C)$$

and

$$(D - C) \cdot (P_{AB} - P_{CD}) = -\lambda_{CD}|\overline{CD}|^2 + \lambda_{AB}(D - C) \cdot (B - A) + (D - C) \cdot (A - C)$$

this system implies

$$\begin{aligned} 0 &= (B - A) \cdot (P_{AB} - P_{CD}) \\ 0 &= (D - C) \cdot (P_{AB} - P_{CD}) \end{aligned}$$

In other words, the line segment connecting the two closest points on the lines is orthogonal to both lines.

This system can be solved to find values for λ_{AB} and λ_{CD}. If either of these values is outside the range $[0.0, 1.0]$, then this solution is not valid as the distance between the two line **segments** and boundary solutions must be searched.

The first sort of boundary solution which can be investigated is one in which the minimum distance is attained at one endpoint of one of the segments with the other minimum point being an interior point of the other segment. Calculating this distance involves another minimization problem. For example, to calculate the distance between A and $\overline{CD}$ the following minimization problem would need to be solved:

$$\underset{\lambda_{CD}}{\text{minimize}} \quad |A - P_{CD}|^2 \equiv (A - P_{CD}) \cdot (A - P_{CD})$$

This problem can be solved by differentiating the objective function with respect to λ_{CD}, setting the resulting equation equal to zero and solving the implied system for λ_{CD}.

Substituting using

$$\begin{aligned} A - P_{CD} &= A - (C + \lambda_{CD}(D - C)) \\ &= (A - C) - \lambda_{CD}(D - C)) \end{aligned}$$

and differentiating results in the equation

$$2\lambda_{CD}|\overline{CD}|^2 - 2(A - C) \cdot (D - C) = 0$$

or

$$\lambda_{CD} = \frac{(A - C) \cdot (D - C)}{|\overline{CD}|^2}$$

Since

$$(D - C) \cdot (A - P_{CD}) = -\lambda_{CD}|\overline{CD}|^2 + (D - C) \cdot (A - C)$$

the solution equation implies

$$(D - C) \cdot (A - P_{CD}) = 0$$

In other words, the line segment connecting A with the closest point on $\overline{CD}$ is orthogonal to $\overline{CD}$.

If λ_{CD} is outside the range $[0.0, 1.0]$, then again the value is not valid as a minimum distance to the line segment from the point, and the minimum of $|\overline{AC}|$ and $|\overline{AD}|$ should be selected as the value. $|\overline{AC}|$ is calculated using the Pythagorean distance formula $|\overline{AC}| = \sqrt{(A - C) \cdot (A - C)}$ and $|\overline{AD}|$ is computed similarly.

In searching for a boundary value for the minimum length between the two segments, all four boundary possibilities should be examined (A and $\overline{CD}$, B and $\overline{CD}$, $\overline{AB}$ and C, $\overline{AB}$ and D) and the minimum of these taken to be the solution.

8.2.2 Clearance Formulas: Angle Between Two Line Segments

The formula for the angle between two line segments coincident at a point is derived from the Schwarz inequality (see *Lang71,* p. 22). For example, the angle between the two line segments $\overline{AB}$ and $\overline{AC}$ is equal to

$$\arccos\left(\frac{(A - B) \cdot (A - C)}{|\overline{AB}||\overline{AC}|}\right).$$

8.2.3 Clearance Formulas: A Sample Application

The line segment formulas were used to look at the clearances of the struts and interlayer tendons of the 4ν t-octahedron spherical truss of Section 5.3. The planned realization in mind was a structure at a scale of 1 model unit = 90 mm using 8-mm-diameter wooden dowels for struts and fishing line for tendons. The clearance goal was one strut diameter between the outer surfaces of any two members. This reduced to 2 strut diameters between two strut center lines, 1.5 strut diameters between a strut center line and a tendon center line, and 0.5 strut diameter between two tendon center lines. The diameter of the tendon was regarded as negligible. In model units, these thresholds were $\frac{2 \cdot 8}{90} = 0.18$, $\frac{1.5 \cdot 8}{90} = 0.13$ and $\frac{1 \cdot 8}{90} = 0.09$ respectively.

It was found strut member #3 and a transformed[1] version of tendon member #5 had a

[1]The transformation was $(x,\ y,\ z) \Rightarrow (-x, -y,\ z)$.

poor clearance of 0.081 model units. In addition, at 0.17 model units the clearance between the two strut members #1 and #3 was marginally a problem. Increasing the constrained length of the highly-tensioned tendon member #28 from 1 to 1.4 model units increased the first clearance to 0.16 model units and the second clearance to 0.20 model units without creating clearance problems between other members. Table 8.1 shows the values for the lengths and relative member forces of the revised model. Table 8.2 shows the revised values for the coordinates of the basic points.

Member #	Length	Relative Force
1	3.000000	-12.309
2	3.000000	-11.701
3	3.000000	-11.604
4	3.000000	-11.265
5	2.357656	4.715
6	2.389582	4.779
7	2.437046	4.874
8	2.365863	4.732
9	2.030353	4.061
10	2.047569	4.095
11	2.040178	4.080
12	1.640244	3.280
13	1.000000	3.950
14	1.000000	5.618
15	1.000000	4.330
16	1.000000	5.030
17	2.498276	0.999
18	2.732085	1.093
19	2.745418	1.098
20	2.924998	1.170
21	1.382591	1.383
22	1.427206	1.427
23	1.500065	1.500
24	0.943181	0.943
25	1.000000	6.055
26	1.000000	6.400
27	1.000000	5.535
28	1.400000	6.260

Table 8.1: 4ν T-Octahedron: Revised Member Lengths and Forces

Point	Coordinates		
	x	y	z
P_1	1.092297	-0.280953	2.035248
P_2	-0.128883	0.310054	2.301681
P_3	0.820711	1.137818	1.630864
P_4	-1.029370	1.245104	1.777463
P'_1	1.578759	0.504378	3.382666
P'_2	0.618364	0.662396	3.612169
P'_3	1.160445	1.393792	3.198396
P'_4	-1.675120	2.090616	2.491573

Table 8.2: 4ν T-Octahedron: Revised Basic Point Coordinates

Appendix A

Other Double-Layer Technologies

Another approach to planar tensegrity truss design similar to Snelson's approach outlined in Chapter 5 has been independently developed by Georges David Emmerich,[1] Ariel Hanaor[2] and René Motro.[3] For the most part, the tendon network for the outer and inner layers of these structures is identical with the double-layer truss described in Chapter 5. However, the way the struts and tendons are connected between the layers is very different.

The starting point of Emmerich *et al.'s* system is a planar assembly of t-prisms.[4] Figure A.1 shows how such a planar assembly would appear.[5] As is evident in comparing Figures 2.1 and 5.1, the topological difference between a t-prism and a t-tripod is not great: the t-prism is topologically equivalent to a t-tripod with a tendon triangle connecting the struts at the t-tripod's base.[6] While the manner of Emmerich *et al.'s* assembly retains triangulation in the outer and inner tendon layers, the interlayer triangulation exhibited by individual prisms is broken up by the arrangement. In this situation a dome is induced by introducing curvature in the planar assembly of prisms transforming them into truncated pyramids.

To emphasize the contrast between the two systems, Figure A.2 shows how t-tripods would be arranged in a planar context. As seen in Chapter 5, the outer layer has been completed by interconnecting the t-tripod apexes with tendon triangles to yield an outer layer which is identical with that obtained in Emmerich *et al.'s* arrangement.

Each inner tendon triangle where the struts of three t-tripods converge is viewed as the

[1] *Emmerich88,* "reseaux antiprismatiques", p. 281.

[2] *Hanaor87* and *Hanaor92.*

[3] *Motro87* and *Motro92.*

[4] This is a typical application of the technique. It has various ways it can be applied, and is not limited to t-prisms.

[5] cf. *Hanaor87,* Figure 9.

[6] Hanaor might call the t-tripod a truncated pyramid with its larger end triangle removed. See *Hanaor92,* Fig. 3(f).

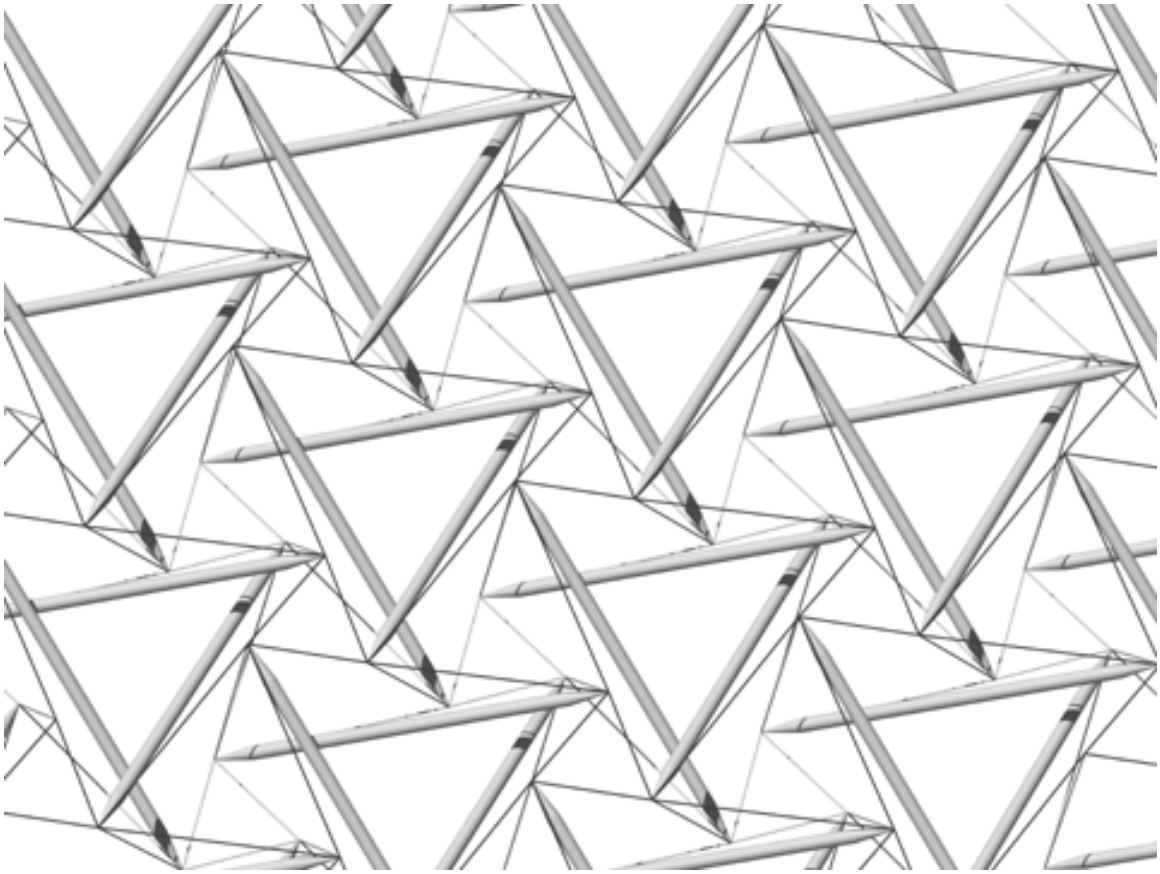

Figure A.1: Planar Assembly of T-Prisms

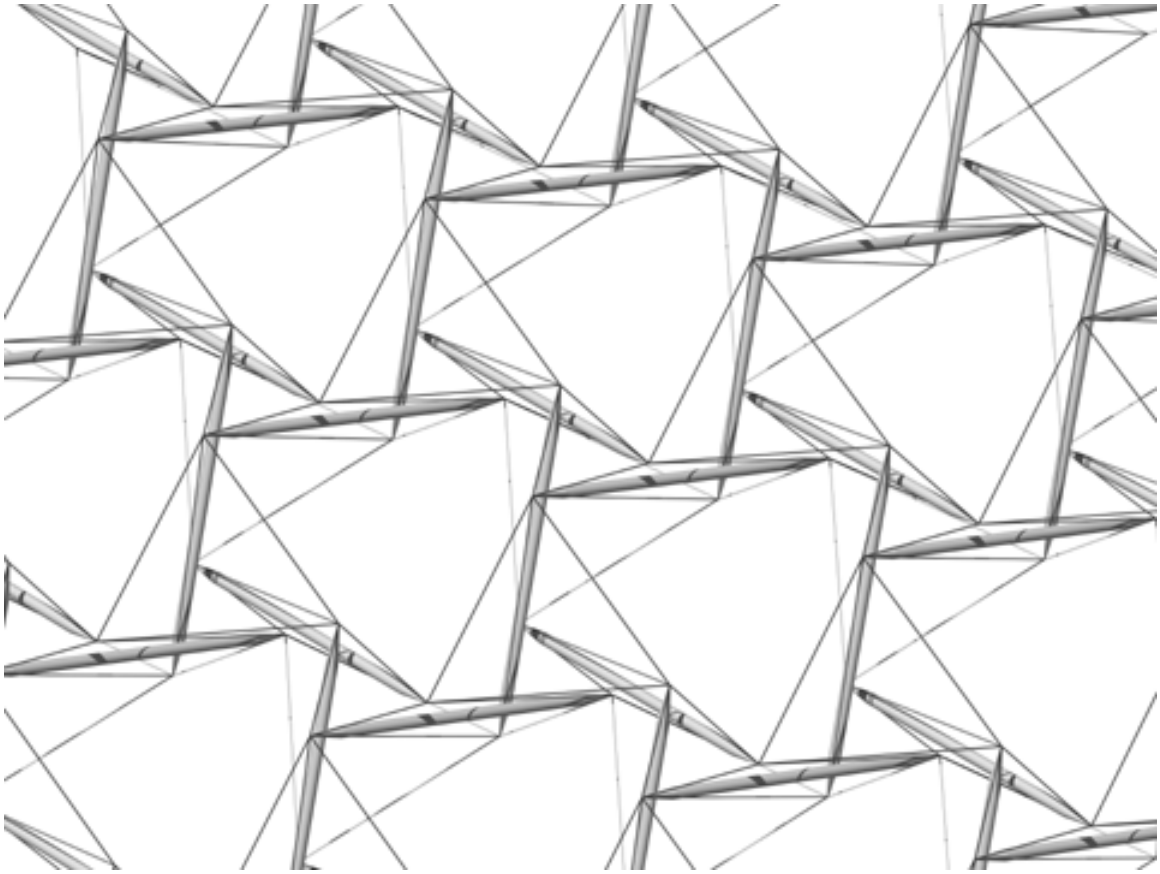

Figure A.2: Planar Assembly of T-Tripods

apex of an inward-pointing t-tripod. Adding the corresponding interlayer tendons to complete these t-tripods (the secondary interlayer tendons of Chapter 5) provides more interlayer triangulation, and thus more reinforcement of the structure. In this configuration, each strut is secured by 12 tendons. It is worth noting that this is precisely the minimum number of tendons Fuller has experimentally found to be necessary to rigidly fix one system in its relationship to a surrounding system.[7]

Hanaor's articles also present computations and models for several structures. Computations for both member lengths and forces are presented. All computations are based on a methodology presented in *Argyris72*. The relative performance of that methodology and the ones presented in this work is unknown.

[7] *Fuller75,* pp. 105-107.

Appendix B

Proof that the Constraint Region is Non-convex

In Section 3.2, the claim is made that the constraint region in the general tensegrity mathematical programming problem is not convex. A proof is given here.

The non-convexity is due to the strut constraints. To demonstrate this, let P_a and P_b be one set of endpoints for a strut which meet its length constraint with equality, and let $P_{a'}$ and $P_{b'}$ be another such set. Let $\overline{l}_n$ be the value of the corresponding constraint constant. By assumption:

$$\begin{aligned} |P_a - P_b|^2 &= \overline{l}_n^2 \\ |P_{a'} - P_{b'}|^2 &= \overline{l}_n^2 \end{aligned}$$

Let $P_{a''}$ and $P_{b''}$ be a convex combination of these two point sets. This means:

$$\begin{aligned} P_{a''} &\equiv \lambda P_a + (1-\lambda) P_{a'} \\ P_{b''} &\equiv \lambda P_b + (1-\lambda) P_{b'} \end{aligned}$$

where $\lambda \in (0,1)$. Therefore:

$$\begin{aligned} |P_{a''} - P_{b''}|^2 &= |\lambda(P_a - P_b) + (1-\lambda)(P_{a'} - P_{b'})|^2 \\ &= \lambda^2 |P_a - P_b|^2 + 2\lambda(1-\lambda)(P_a - P_b)\cdot(P_{a'} - P_{b'}) + (1-\lambda)^2 |P_{a'} - P_{b'}|^2 \end{aligned}$$

By the Schwarz inequality (see *Lang71*, p. 22):

$$(P_a - P_b)\cdot(P_{a'} - P_{b'}) < |P_a - P_b||P_{a'} - P_{b'}|$$

So:

$$\begin{aligned} |P_{a''} - P_{b''}|^2 &< \lambda^2 |P_a - P_b|^2 + 2\lambda(1-\lambda)|P_a - P_b||P_{a'} - P_{b'}| + (1-\lambda)^2 |P_{a'} - P_{b'}|^2 \\ &= (\lambda |P_a - P_b| + (1-\lambda)|P_{a'} - P_{b'}|)^2 \\ &= (\lambda \overline{l}_n + (1-\lambda)\overline{l}_n)^2 \\ &= \overline{l}_n^2 \end{aligned}$$

In summary:

$$\bar{l}_n^2 > |P_{a''} - P_{b''}|^2$$

This means the constraint is violated; hence, the constraint region is not convex.

Appendix C

References

Argyris72 Argyris, J. H. and D. W. Scharpf, "Large Deflection Analysis of Prestressed Networks," *Journal of the Structural Division, ASCE,* Vol. 98 (1972: ST3), pp. 633-654.

Chajes83 Chajes, Alexander, *Structural Analysis,* Englewood Cliffs, New Jersey: Prentice-Hall, Inc., 1983.

Coplans67 Coplans, John, "An Interview with Kenneth Snelson," *Artforum,* March 1967, pp. 46-49.

Emmerich88 Emmerich, David Georges, *Structures Tendues et Autotendantes,* Paris, France: Ecole d'Architecture de Paris la Villette, 1988.

Fuller92 Fuller, R. Buckminster with Kiyoshi Kuromiya, *Cosmography,* New York: MacMillan Publishing Co., Inc., 1992.

Fuller75 Fuller, R. Buckminster, *Synergetics: Explorations in the Geometry of Thinking,* New York: MacMillan Publishing Co., Inc., 1975.

Fuller73 Fuller, R. Buckminster and Robert W. Marks, *The Dymaxion World of Buckminster Fuller,* Garden City, New York: Anchor Books, 1973.

Fuller61 Fuller, R. Buckminster, "Tensegrity," *Portfolio and Art News Annual,* No. 4 (1961), pp. 112-127, 144, 148.

Gough98 Gough, Maria, "In the laboratory of constructivism: Karl Ioganson's cold structures," *October,* No. 84 (Spring 1998), pp. 90-117.

Hanaor92 Hanaor, Ariel, "Aspects of Design of Double-Layer Tensegrity Domes," *International Journal of Space Structures,* Vol. 7 (1992), pp. 101-113.

Hanaor87 Hanaor, Ariel, "Preliminary Investigation of Double-Layer Tensegrities," in H.V. Topping, ed., *Proceedings of International Conference on the*

Design and Construction of Non-conventional Structures (Vol. 2), Edinburgh, Scotland: Civil-Comp Press, 1987.

Hibbeler98 Hibbeler, R. C., *Engineering mechanics. Statics* (8th edition), Upper Saddle River, New Jersey: Prentice-Hall, Inc., 1998.

Hogben65 Hogben, Lancelot, *Mathematics for the Million,* New York: Pocket Books, Inc., 1965.

Ingber98 Ingber, Donald E., "The Architecture of Life", *Scientific American,* Vol. 278, No. 1 (January, 1998), pp. 48-57.

Johnston82 Johnston, R.L., *Numerical Methods: A Software Approach,* New York: John Wiley & Sons, 1982.

Kanchanasaratool02 Kanchanasaratool, Narongsak and Darrell Williamson, "Modelling and control of class NSP tensegrity structures", *International Journal of Control,* Vol. 75, No. 2 (January 20, 2002), pp. 123-139.

Kells42 Kells, Lyman M., et al., *Spherical Trigonometry with Naval and Military Applications,* New York: McGraw-Hill, 1942.

Kelly92 Kelly, K., "Biosphere 2 at One," *Whole Earth Review,* Winter 1992, pp. 90-105.

Kenner76 Kenner, Hugh, *Geodesic Math and How to Use It,* Berkeley, California: University of California Press, 1976.

Lalvani96 Lalvani, Haresh, ed., "Origins of Tensegrity: Views of Emmerich, Fuller and Snelson", *International Journal of Space Structures,* Vol. 11 (1996), Nos. 1 & 2, pp. 27-55.

Lang71 Lang, Serge, *Linear Algebra* (2nd edition), Reading, Massachusetts: Addison-Wesley Publishing Co., 1971.

Leithold72 Leithold, Louis, *The Calculus with Analytic Geometry* (2nd edition), New York: Harper & Row, 1972.

Luenberger73 Luenberger, David G., *Introduction to Linear and Nonlinear Programming,* Reading, Massachusetts: Addison-Wesley Publishing Co., 1973.

Makowski65 Makowski, Z.S., *Steel Space Structures,* London: Michael Joseph Ltd., 1965.

Motro92 Motro, R., "Tensegrity Systems: The State of the Art," *International Journal of Space Structures,* Vol. 7 (1992), pp. 75-84.

Motro87 Motro, R., "Tensegrity Systems for Double-Layer Space Structures," in H.V. Topping, ed., *Proceedings of International Conference on the Design and Construction of Non-conventional Structures* (Vol. 2), Edinburgh, Scotland: Civil-Comp Press, 1987.

Müller71 Müller, Grégoire, "Kenneth Snelson", *Arts Magazine,* Vol. 45, No. 7 (May, 1971), pp. 25-27.

Otto73 Otto, Frei, ed., *Tensile structures; design, structure, and calculation of buildings of cables, nets, and membranes,* Cambridge, Massachusetts: MIT Press, 1973.

Pugh76 Pugh, Anthony, *An Introduction to Tensegrity,* Berkeley, California: University of California Press, 1976.

Rogers76 Rogers, D.F. and J.A. Adams, *Mathematical Elements for Computer Graphics,* New York: McGraw-Hill, Inc., 1976.

Roth81 Roth, B. and W. Whiteley, "Tensegrity Frameworks," *Transactions of the American Mathematical Society,* Vol. 265 (1981), pp. 419-446.

Skelton97 Skelton, Robert E. and M. He, "Smart tensegrity structure for NESTOR," *Proceedings of SPIE – The International Society for Optical Engineering,* Vol. 3041 (1997), pp. 780-787.

Snelson81 Snelson, Kenneth and Douglas G. Schultz, *Kenneth Snelson, an exhibition,* Buffalo, New York: Albright-Knox Art Gallery, c1981.

Tauchert74 Tauchert, Theodore R., *Energy Principles in Structural Mechanics,* New York: McGraw-Hill, Inc., 1974.

Varian78 Varian, Hal, *Microeconomic Analysis,* New York: W. W. Norton & Co., 1978.

Vilnay90 Vilnay, Oren, *Cable Nets and Tensegric Shells: Analysis and Design Applications,* New York: Ellis Horwood Ltd., 1990.

Wang98 Wang, Bin-Bing, "Cable-strut systems: Part I - Tensegrity," *Journal of Constructional Steel Research,* Vol. 45 (1998), No. 3, pp. 281-289.

Wong99 Wong, Yunn Chii, *The Geodesic Works of Richard Buckminster Fuller, 1948-1968 (The Universe as a Home of Man),* PhD thesis, Cambridge, Massachusetts: Massachusetts Institute of Technology, Department of Architecture, 1999.